

Slider – Crank Mechanism for Demonstration and Experimentation

MQP

Advisor: Eben C. Cobb

ERIC BRIGHAM

CHRIS DESTEFANO

ZACHARY KILLOY

Date Submitted: April 25, 2013

Slider – Crank Mechanism for Demonstration and Experimentation

Abstract

The slider-crank mechanism is a particular four-bar linkage configuration that exhibits both linear and rotational motion simultaneously. This mechanism is frequently utilized in undergraduate engineering courses to investigate machine kinematics and resulting dynamic forces. The position, velocity, acceleration and shaking forces generated by a slider-crank mechanism during operation can be determined analytically. Certain factors are often neglected from analytical calculations, causing results to differ from experimental data. The study of these slight variances produces useful insight. The following report details the successful design, fabrication and testing of a pneumatically powered slider-crank mechanism for the purpose of classroom demonstration and experimentation. Transducers mounted to the mechanism record kinematic and dynamic force data during operation, which can then be compared to analytical values. The mechanism is capable of operating in balanced and unbalanced configurations so that the magnitude of shaking forces can be compared. The engine was successfully manufactured and operates as intended. Data recorded by the device's accelerometers is comparable to calculated values of acceleration and shaking force.

Slider – Crank Mechanism for Demonstration and Experimentation

Contents

ABSTRACT	I
CONTENTS.....	1
EXECUTIVE SUMMARY	3
DESIGN DESCRIPTION.....	4
OBJECTIVE.....	4
TASK SPECIFICATIONS.....	4
DECISION MATRIX	5
BACKGROUND.....	6
SOLID MODELING.....	7
DESIGN FOR MANUFACTURABILITY.....	9
TRANSDUCER SELECTION.....	11
ANALYSIS.....	13
KINEMATIC ANALYSIS.....	13
<i>POSITION ANALYSIS.....</i>	<i>13</i>
<i>VELOCITY ANALYSIS.....</i>	<i>15</i>
<i>ACCELERATION ANALYSIS.....</i>	<i>17</i>
<i>DYNAMIC FORCE ANALYSIS.....</i>	<i>19</i>
TORSIONAL STRESS ANALYSIS OF CRANKSHAFT	28
FINITE ELEMENT ANALYSIS OF CRANKSHAFT	32
TORSIONAL VIBRATION ANALYSIS OF CRANKSHAFT.....	41
CROSSHEAD GUIDE DEFLECTION ANALYSIS.....	42
CROSSHEAD GUIDE NATURAL FREQUENCY ANALYSIS.....	44
DAMPER SELECTION THROUGH VIBRATION ANALYSIS.....	45
PIN STRESS ANALYSIS.....	47
PRELIMINARY VALVE DESIGN.....	48
<i>CYLINDER PRESSURIZATION ANALYSIS.....</i>	<i>48</i>
<i>EXPERIMENTAL EVALUATION OF MASS FLOW THROUGH SYSTEM.....</i>	<i>48</i>
MANUFACTURING.....	50
LIMITATIONS AND VARIATIONS.....	50

Slider – Crank Mechanism for Demonstration and Experimentation

CRANKSHAFT OPERATIONS AND FOURTH AXIS MACHINING	51
MACHINING IMAGES	56
RESULTS OF INITIAL TESTING.....	62
SLIDER ACCELERATION AND CYLINDER PRESSURE.....	62
SHAKING FORCES.....	65
COMPARISON OF ANALYTICAL AND EXPERIMENTAL RESULTS.....	68
CONCLUSION.....	70
DISCUSSION.....	71
RECOMMENDATIONS FOR FUTURE MQPS.....	72
FIGURES.....	74
BIBLIOGRAPHY	77
APPENDICES.....	78

Slider – Crank Mechanism for Demonstration and Experimentation

Executive Summary

The slider-crank mechanism is a particular four-bar linkage configuration that converts linear motion to rotational, or vice versa. Internal combustion engines are a common example of this mechanism, where combustion in a cylinder creates pressure which drives a piston. The piston's linear motion is converted into rotational motion at the crank through a mutual link, referred to as the connecting rod. As the geometry of the crank forces the conversion of linear motion to rotational, shaking forces are generated and applied to the crank's housing. These shaking forces result in vibrations which impede the operation of the engine.

The slider-crank mechanism is frequently utilized in undergraduate engineering courses to investigate machine kinematics and resulting dynamic forces. The position, velocity, acceleration and shaking forces generated by a slider-crank mechanism during operation can be determined analytically. Certain factors are often neglected from analytical calculations, causing results to differ from experimental data. The assumption is frequently made that the crankshaft's angular velocity is constant. In reality, angular velocity is slightly higher on the power stroke than the return stroke. The study of these slight variances produces useful insight into the characteristics of piston driven engines.

The following report details the successful design, fabrication and testing of a pneumatically powered slider-crank mechanism for the purpose of classroom demonstration and experimentation. Complete analysis of the engine's kinematics was performed, assuming a constant angular acceleration.. Shaking forces of the unbalanced mechanism were calculated and balancing weights were designed for statically and dynamically balanced configurations at the same constant angular velocity. Transducers mounted to the mechanism were used to record kinematic and dynamic force data during operation, which was then compared to the analytical values.

The engine was successfully manufactured and operates as intended. Data recorded by the device's accelerometers is comparable to calculated values of acceleration and shaking force.. Satisfactory operation of the engine was achieved with minimal tuning. The engine is capable of operating at angular velocities ranging from 80 to 330 RPM, using a balancing weight optimized for 200RPM. Sustained motion is achievable with cylinder pressures as low as 4.5psi, with a loss of only 2 psi through the system. The reduction in shaking force achieved through use of the balance weights is apparent both visually and in recorded data. All experimental values were reasonable when compared with analytical calculations.

Slider – Crank Mechanism for Demonstration and Experimentation

Design Description

Objective

The objective of this MQP is to fabricate a working model of a slider crank mechanism that demonstrates the associated motion and provides means to measure kinematic properties, dynamic forces and cylinder pressure in various states of balance.

Task Specifications

1. The slider-crank mechanism's motion must be visible.
2. The mechanism must be able to sustain motion when acted on by a driving force.
3. Removable balance weights must be incorporated into the design.
4. The mechanism must be capable of operating in both balanced and unbalanced states.
5. A means of measuring and recording the kinematic and dynamic characteristics of the slider-crank mechanism's motion must be incorporated into the design.
6. All components of the mechanism must exhibit a safety factor of 5 in regards to static failure.
7. The mechanism, all equipment required for operation and data acquisition must be portable and self-contained.
8. The total width of the unit must not exceed 2.5 feet, to allow for transport through a doorway.
9. The mechanism must be operable by one individual.
10. All moving components must operate behind a safety shield.
11. The mechanism must be manufactured within the MQP's cost constraints.
12. Design, manufacturing and experimentation must be completed within the allotted time.

Slider – Crank Mechanism for Demonstration and Experimentation

Decision Matrix

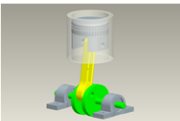
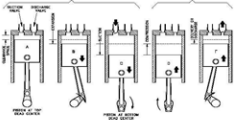



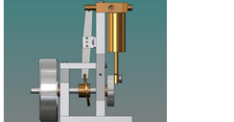
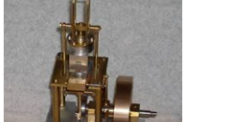
Slider-Crank MQP Decision Matrix														
	Weighting Factors (from 0 to 1, variants ranked 0 to 10)													
	Mechanism Visibility	Functionality	Amount of kinematic experimentation possible	Amount of cylinder pressure experimentation possible	Amount of dynamic force experimentation possible	Balancing experimentation opportunities / ease	Low leak chance / high tolerance allowances	Low cost	High portability	Valve train simplicity	Design challenge	High percentage of purchasable parts	Overall simplicity/manufacturability	TOTAL:
Slider-Crank Variants	0.7	0.6	1	0.6	0.85	0.85	0.2	0.35	0.4	0.4	0.4	0.3	0.8	
Crank-driven model, non-realistic cylinder pressure: 	10	2	8	0	8	10	10	10	10	10	2	10	10	56.8
Electric crank-driven pump, realistic cylinder pressure: 	7	5	8	7	8	7	5	8	9	4	4	6	8	50.85
Double-acting pneumatic steam locomotive engine / drive assembly, sliding valve, electric motor on crank 	5	10	10	0.67	8	7	5	6	6	6	10	3	6	56.652
Pneumatic engine, cam shaft / poppet valves, electric motor on crank 	5	10	10	10	8	7	5	6	6	4	8	6	4	53.55
Scaled up "Standby": single-acting pneumatic engine, no valve linkage (incorporated into crankshaft) electric motor on crank 	7	10	10	10	7	10	6	8	6	10	4	2	8	60.35
Single acting pneumatic engine, "wobble-plate" offset cam-follower valve linkage, electric motor on crank 	7	10	9	10	8	7	5	7	6	8	4	2	6	54.7
Double-acting pneumatic, mine engine model, mirrored connecting rods, electric motor on crank 	10	10	10	6	7	9	5	4	5	2	8	2	2	50.8

Figure 1: Decision Matrix used to rank proposed designs

Slider – Crank Mechanism for Demonstration and Experimentation

Background

The assembly of a piston, cylinder, connecting-rod and crankshaft is the classic form of the slider-crank mechanism. In general a slider crank transmits motion generated by the linear displacement of the piston by a working fluid to rotational motion of a shaft. There are many applications of slider cranks and among the most common are engines. The use of these mechanisms for power generation began with the steam engine in the late 18th century and has developed into possibly its most recognizable form as the current day internal combustion engine. A single piston engine model could serve as a functional, eye-catching example of a slider-crank.

Elmer's Standby Single-Acting, Single Piston Pneumatic Engine:

The "Standby" single acting, single piston pneumatic engine is one example of a slider crank mechanism. This engine utilizes a piston-wrist-pin-connecting rod construction that resembles an automotive engine. This type of engine provides a clear visual of the kinematics of a slider crank. The design can be powered by compressed air or steam and is driven by pressure applied to one side of the piston within the cylinder. The single acting nature of this engine also more closely resembles the operation of an internal combustion engine. The design is simpler than alternative pneumatic and steam engines based on its lack of external eccentric valve gear. The design uses grooves on the crankshaft to port air into and out of the cylinder at specific times in its rotation.

By attaching pressure transducers and accelerometers to this design it would be possible to relate cylinder pressures to the mechanism's kinematics. The crankshaft in this design would also be easily modified in order to create detachable balancing weights to demonstrate shaking forces for unbalanced, overbalanced and perfectly balanced situations.

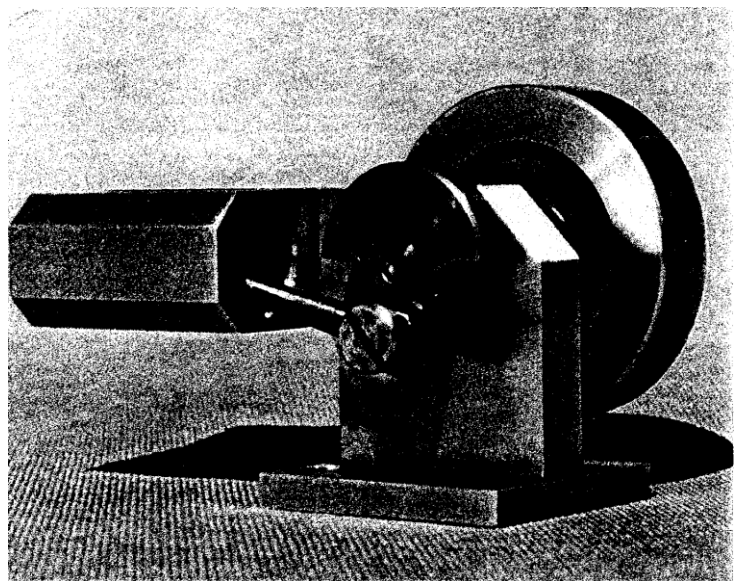


Figure 2: Elmer's Standby Model Engine

Slider – Crank Mechanism for Demonstration and Experimentation

Solid Modeling

The Standby engine utilizes a valve system which is integrated into the crankshaft. This design characteristic was incorporated into the demonstration device.

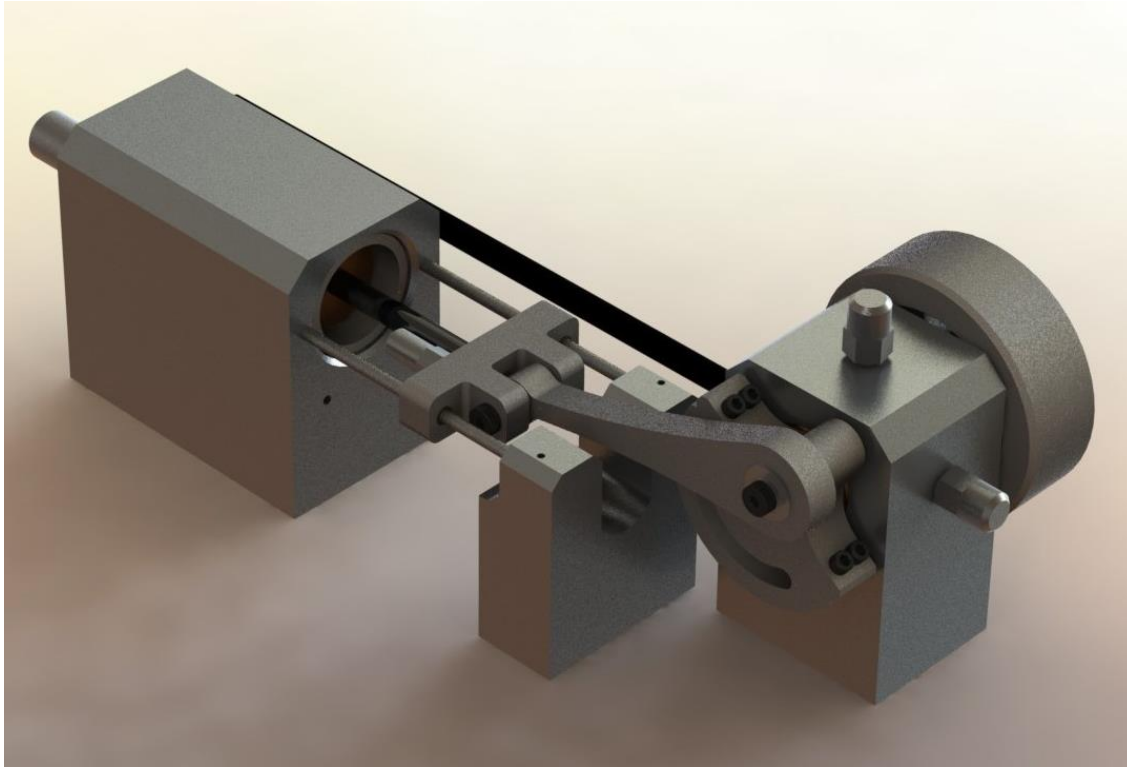


Figure 3: Isometric View Solid Model of Slider Crank Mechanism

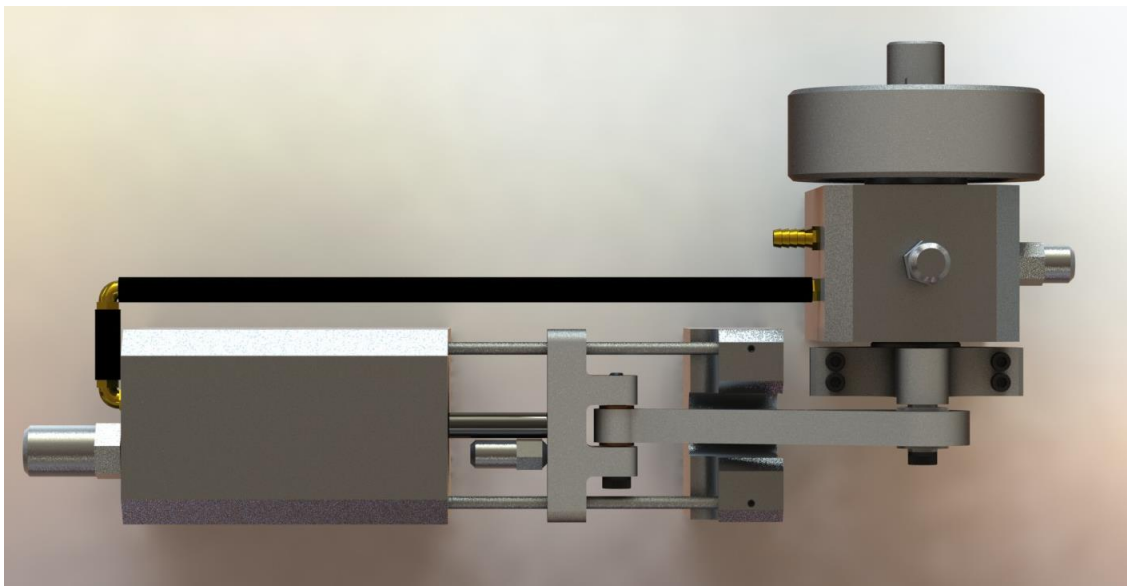


Figure 4: Top View Solid Model of Slider Crank Mechanism

Slider – Crank Mechanism for Demonstration and Experimentation

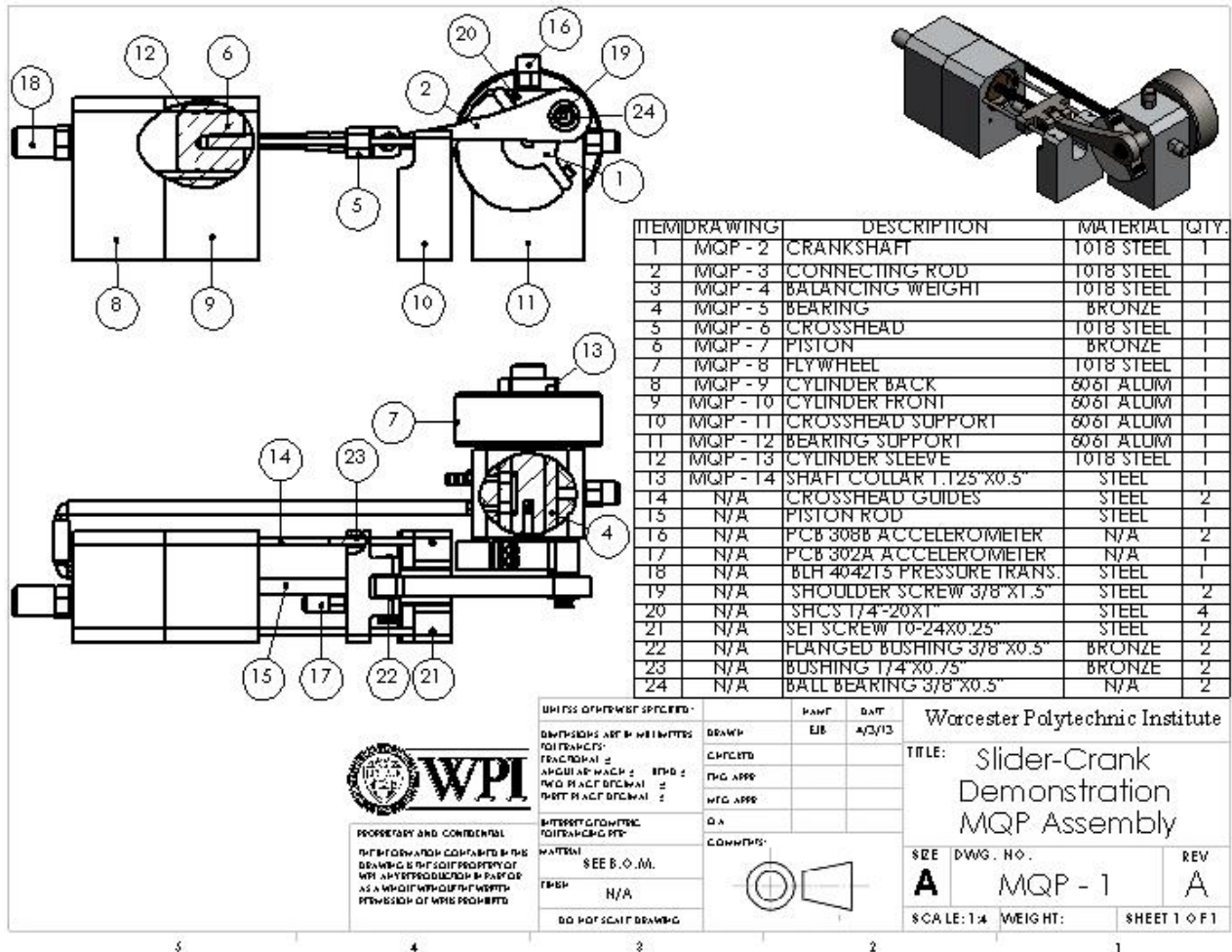


Figure 5: Assembly Drawing for Slider Crank Mechanism

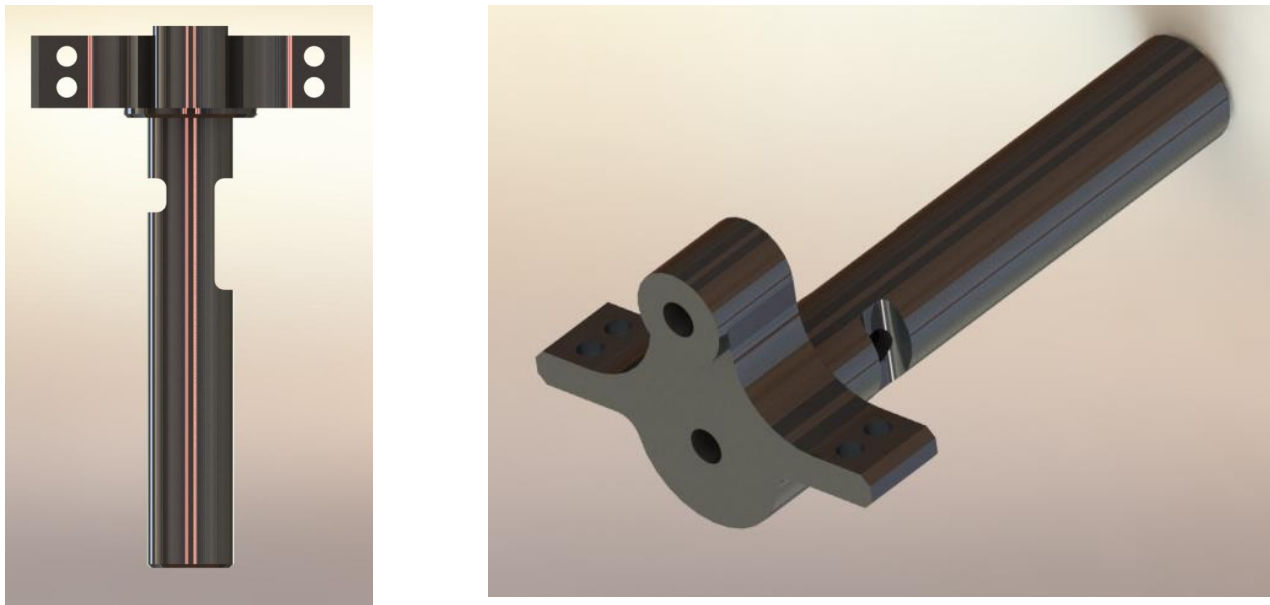


Figure 6: (Left) Solid Model of Crankshaft Top View; (Right) Solid Model of Crankshaft Isometric View

Slider – Crank Mechanism for Demonstration and Experimentation

Design for Manufacturability

When the group finalized the design there were some changes made in order to make the machining of the components both simpler and less time intensive. Some changes included removing certain features which did not generate any real benefit to the design. The group also designed the mechanism to be feasibly manufactured with the machines and standard tooling in the Washburn Shops. This included the use of CNC machining specifically using the HAAS VM-3 Mold Maker, the HAAS VF-4 Milling Center and the HAAS SL20 Lathe. Once the design had been finalized the group was able to apply tolerancing to sliding, press-fit and rotating parts.

In defining the dimensions of the parts the group had to account for certain limitations in tooling, machine capability as well as the errors which may be generated through measurements of the individual components. For parts such as the cylinder support, the slide-support and the crank support the exterior dimensions (that is to say dimensions other than the bores) were not critical for the functionality of the design. This was not the case, however, for parts such as the piston, the sleeve, the crank-shaft and the bearing. Each of these individual parts required extensive tolerancing, both in design and manufacture.

The group referred to the Machinery's Handbook (28th Edition) for much of the required fits. To generate a free rotating yet accurate fit between the crankshaft and the bearing the group referred to the American National Standard Running and Sliding Fits Table (ANSI B4.1-1967), and decided on using a RC3 Precision Running Fit. The use of this fit is chiefly applied to precision machinery where low to moderate surface speed is expected and light journal pressures are encountered without appreciable temperature change. The use of this fit was employed in order to maintain an airtight yet free-running fit between the shaft and the bearing. This fit for a shaft of the range 0.71-1.19 generates a range of clearance from 0.0008-0.0021". The crankshaft diameter was designed to be 1.125" so a value of 0.001" was chosen for the clearance. This clearance as dictated by the table could be produced by machining the shaft to a range of -0.0008 to -0.0013 of the nominal size while machining the bushing (hole) to a range of 0.0008 to the exact nominal size. The group used the table again to generate a design tolerance on the piston and cylinder but this time for the diameter range of 1.97-3.15. The piston and the cylinder were designed to have a diameter of 2". This generated a clearance in the range of 0.0012 to 0.0031 with the piston diameter ranging from -0.0012 to -0.0019 from its nominal size and the cylinder ranging from 0.0012 to its nominal size.

Slider – Crank Mechanism for Demonstration and Experimentation

In addition to the rotating and sliding fits certain parts required press and interference fits which were also determined using the Machinery's Handbook. These fits were required for the fit between the cylinder stands and cylinder sleeves, the bearings in the connecting-rod as well as the bushings for the slide and slide-rail interface. All of these fits fell within the FN1 Standard for Force and shrink fits. These fits range by the diameter of the "shaft" and "hole diameter and are listed below:

- Large Bearing Connecting Rod:
Hole: 0.8755"-0.8750"; Shaft: 0.8757"-0.8761"; Interference: 0.0002"-0.0011"
- Small Bearing Connection Rod:
Hole: 0.5004"-0.5000"; Shaft: 0.5005-0.5008"; Interference: 0.0001"-0.0008"
- Cylinder Sleeve/Cylinder Stand:
Hole: 2.5007"-2.5000"; Shaft: 2.5013"-2.5018"; Interference: 0.0006"-0.0018"
- Slide Bushing/Slide:
Hole: 0.3754"-0.3750"; Shaft: 0.3755"-0.37575"; Interference: 0.0001"-0.00075"

Slider – Crank Mechanism for Demonstration and Experimentation

Transducer Selection

PCB 302A piezoelectric uniaxial accelerometer:

Model (note options below)	Sensitivity (mV/g)	Frequency Range ($\pm 10\%$)	Amplitude Range ($\pm g$ pk)	Temp Range ($^{\circ}F$)	Connector Type/Location	Mounting	Mass (grams)
302A	10	0.7-10000	500	-65/250	10-32 top	10-32	25

The PCB 302A accelerometer is rigidly fixed to the crosshead. Linear acceleration data is recorded during operation to compare with calculated values of the slider’s acceleration. Position and velocity of the slider can be derived by integrating the recorded acceleration curve. A charge amplifier is required to operate the piezoelectric accelerometers used in this project. The PCB 482A16 four channel amplifier was selected because it can accommodate all accelerometers simultaneously. A data acquisition unit is utilized in conjunction with LabView programs to record and save data from all of the mechanism’s transducers.

PCB 308B piezoelectric uniaxial accelerometer:

Model (note options below)	Sensitivity (mV/g)	Frequency Range ($\pm 10\%$)	Amplitude Range ($\pm g$ pk)	Temp Range ($^{\circ}F$)	Connector Type/Location	Mounting	Mass (grams)
308B	100	1-5000	50	-65/250	10-32 side	10-32	50

The crankshaft is supported by the bearing, which is pressed inside the bearing support. Two PCB 308B accelerometers are rigidly fixed to the bearing support. One accelerometer is positioned along the slider’s axis of translation, while the other is perpendicular to it. During operation, linear acceleration data is recorded in both directions. This data is used to determine the shaking forces generated by the mechanism along both axes and will be compared to analytical values. The PCB 308B is ten times more sensitive than the PCB 302A and was selected for this scenario due to the comparatively low magnitude of acceleration experienced by the bearing support.

Slider – Crank Mechanism for Demonstration and Experimentation

BLH 404215 pressure transducer:

The BLH 404215 pressure transducer operates in the range of 0 to 100 psi. The required excitation voltage of 10 Vdc is supplied by a 2310 signal conditioning amplifier. This transducer is connected by rigid piping to the mechanism's cylinder and records variations in pressure during operation. The pressure curve generated by the device is similar to that of a single acting steam engine. This data may be used to determine the input pressure that results in maximum operational speed.

Slider – Crank Mechanism for Demonstration and Experimentation

Analysis

Kinematic Analysis

The kinematics of the slider-crank mechanism are evaluated at a rotational speed of 200rpm. All of the following kinematic and dynamic force equations are taken from Norton's *Design of Machinery*.

Angular Velocity $\eta := 200$ revolutions per minute

$$\omega := \frac{(2\pi \eta)}{60} \quad \omega = 20.944 \text{ radians per second}$$

Position Analysis

Slider Position

$$S(\theta) := L - \frac{R^2}{4L} + R \cdot \left(\sin(\theta) + \frac{R}{4L} \sin(2\theta) \right)$$

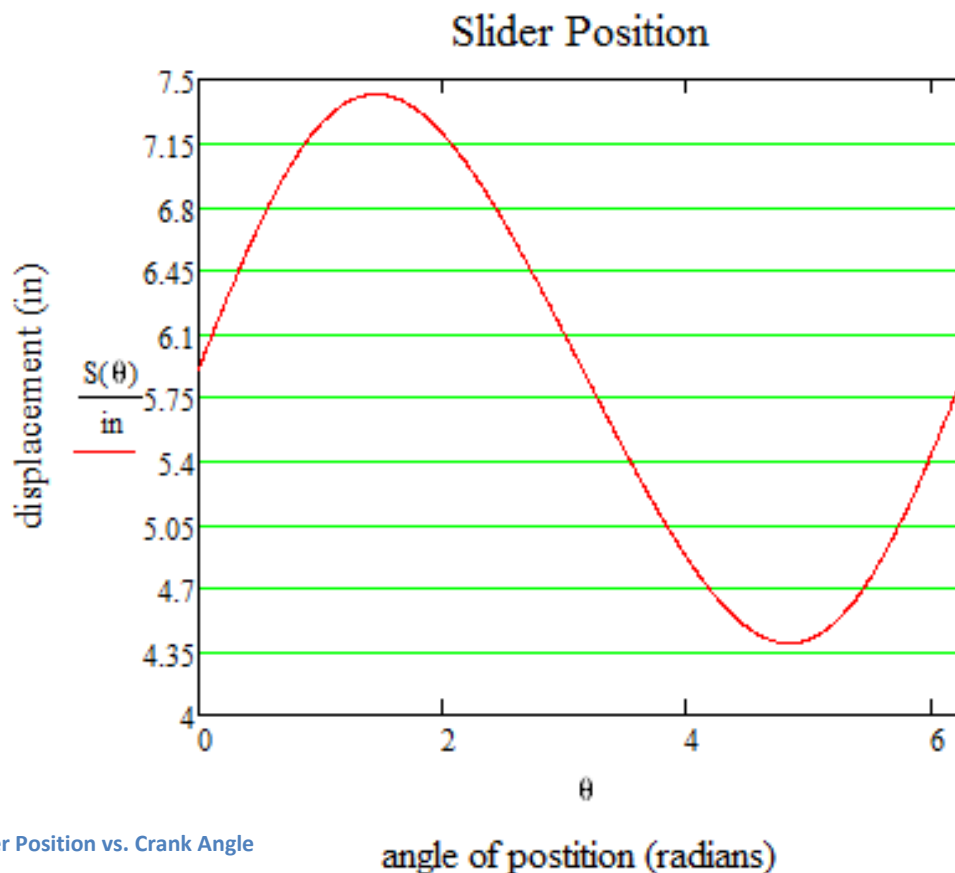


Figure 7: Slider Position vs. Crank Angle

Slider – Crank Mechanism for Demonstration and Experimentation

Crank Position

$$S_x(\theta) := R \cdot \sin(\theta)$$

$$S_y(\theta) := R \cdot \cos(\theta)$$

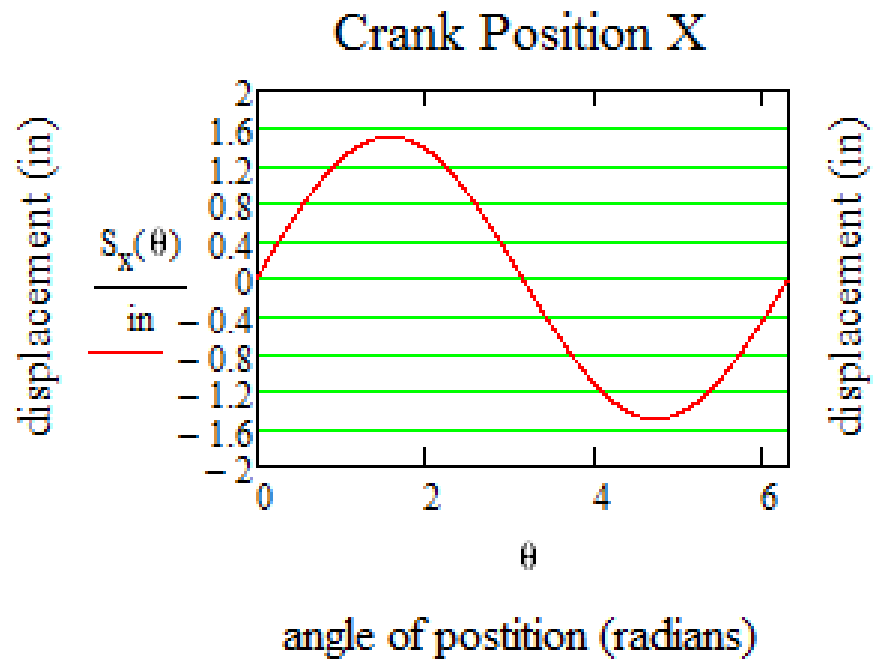


Figure 8: Crankshaft X Displacement vs. Crank Angle

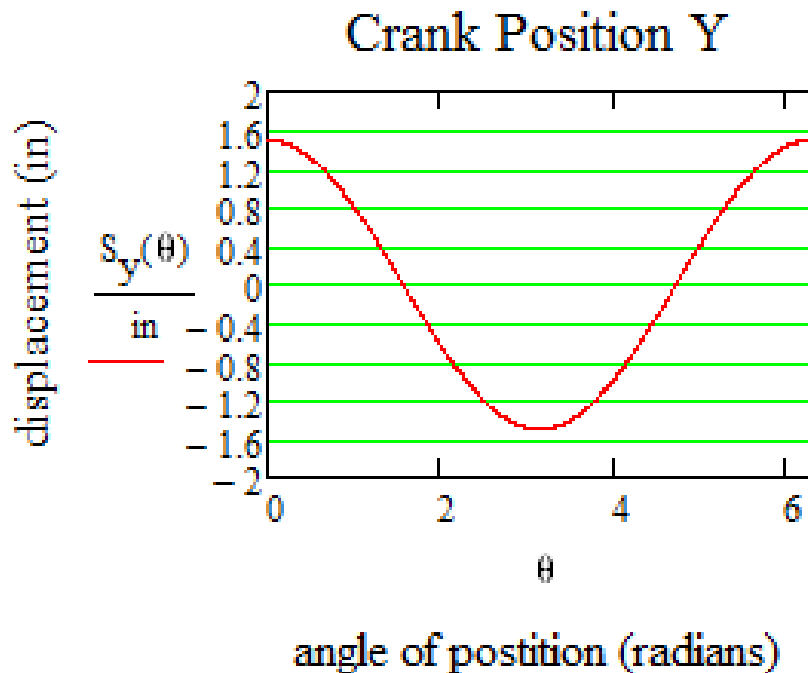


Figure 9: Crank Y Displacement vs. Crank Angle

Slider – Crank Mechanism for Demonstration and Experimentation

Velocity Analysis

Slider Velocity

$$V(\theta) := \omega \cdot R \cdot \left(\cos(\theta) + \frac{R}{2L} \cos(2\theta) \right)$$

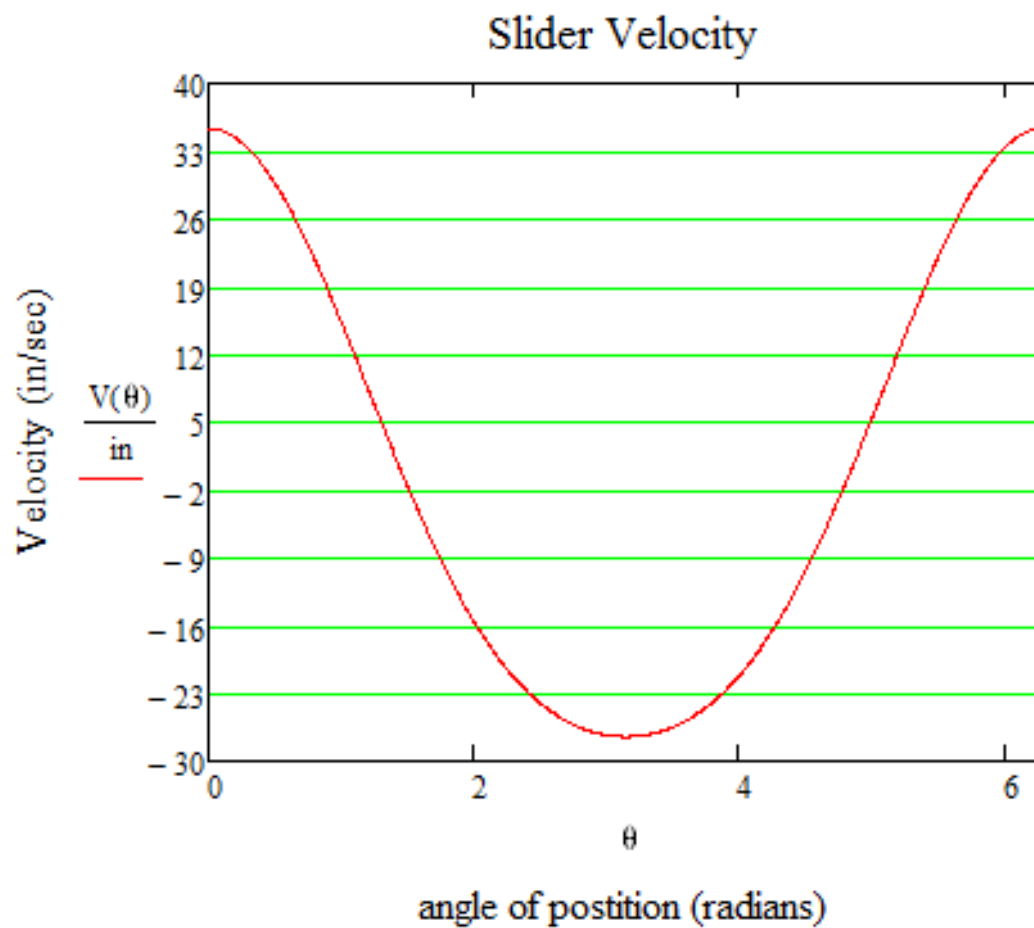


Figure 10: Slider Velocity vs. Crank Angle

Slider – Crank Mechanism for Demonstration and Experimentation

Crank Velocity

$$V_x(\theta) := \omega \cdot R \cdot \cos(\theta)$$

$$V_y(\theta) := -\omega \cdot R \cdot \sin(\theta)$$

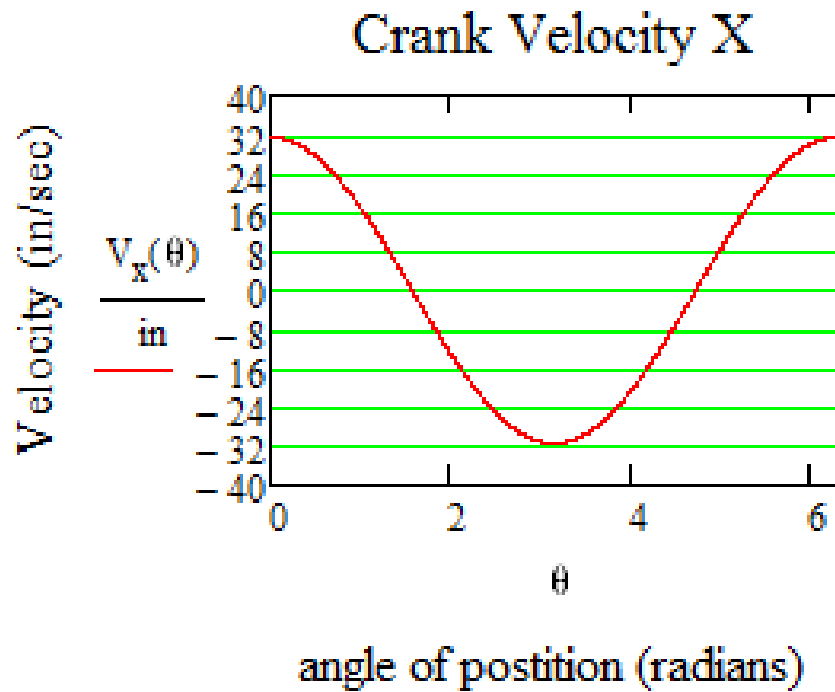


Figure 11: X Component of Crank Velocity vs. Crank Angle

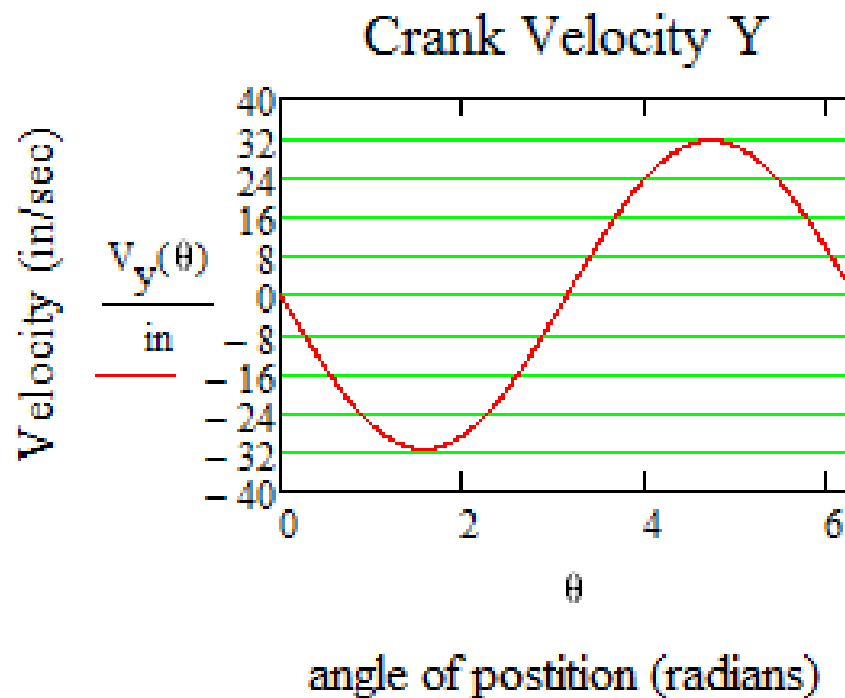


Figure 12: Y Component of Crank Velocity vs. Crank Angle

Slider – Crank Mechanism for Demonstration and Experimentation

Acceleration Analysis

Slider Acceleration

$$\ddot{A}(\theta) := \left[-R \cdot \omega^2 \left(\sin(\theta) + \frac{R}{L} \sin(2\theta) \right) \right]$$

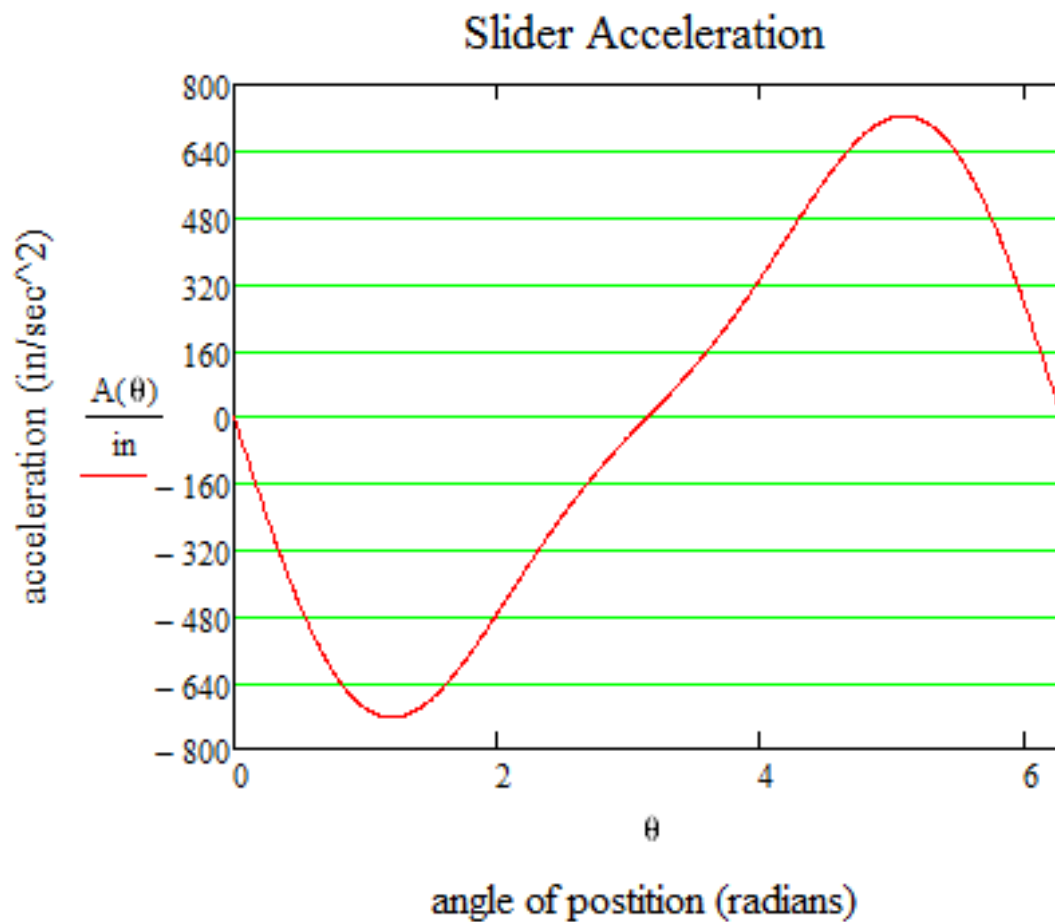


Figure 13: Slider Acceleration vs. Crank Angle

Slider – Crank Mechanism for Demonstration and Experimentation

Crank Acceleration

$$A_x(\theta) := -(\omega)^2 \cdot R \cdot \sin(\theta)$$

$$A_y(\theta) := -(\omega)^2 \cdot R \cdot \cos(\theta)$$

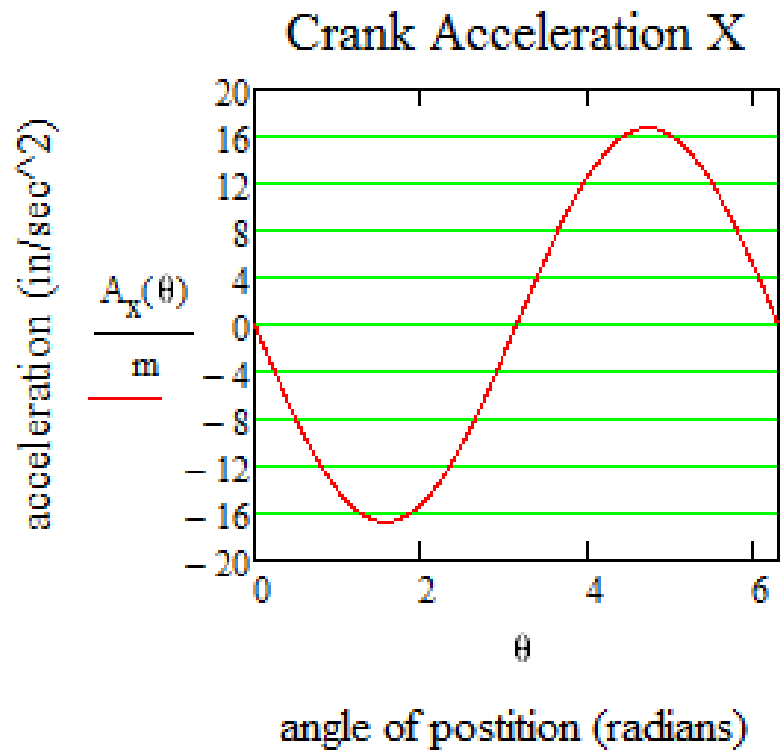


Figure 14: X-Component of Crank Acceleration vs. Crank Angle

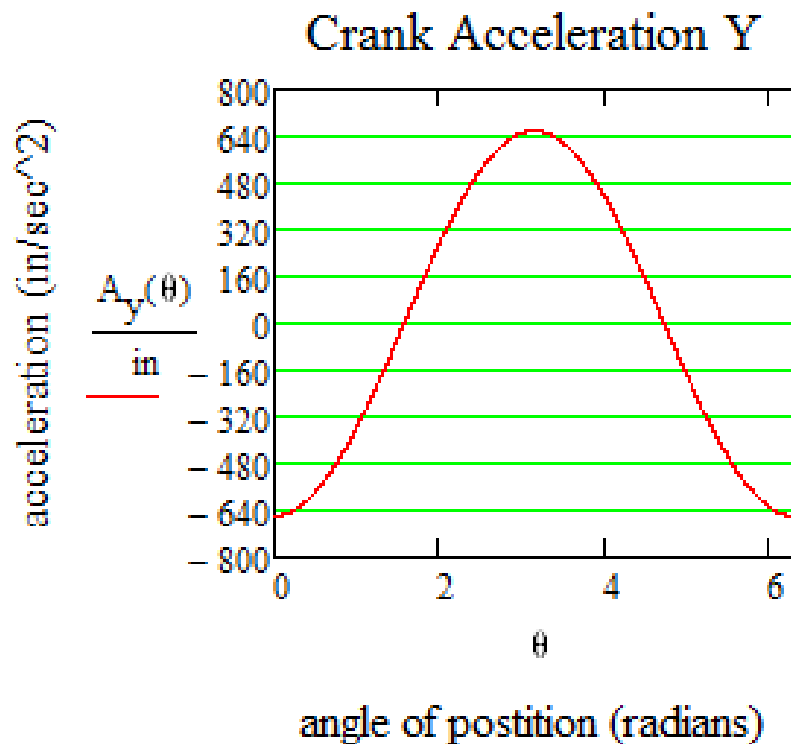


Figure 15: Y-Component of Crank Acceleration vs. Crank Angle

Slider – Crank Mechanism for Demonstration and Experimentation

Dynamic Force Analysis

Shaking Forces

Shaking force is defined as the sum of all forces acting on the ground plane of the system.

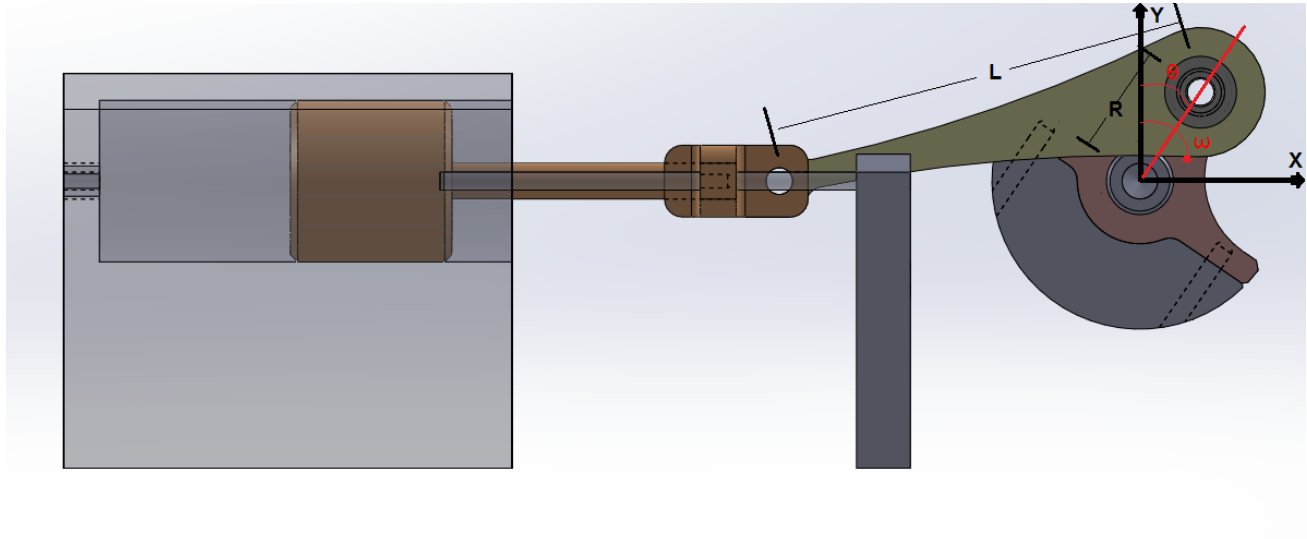


Figure 16: Slider-Crank Coordinate System and Variables

Unbalanced Configuration

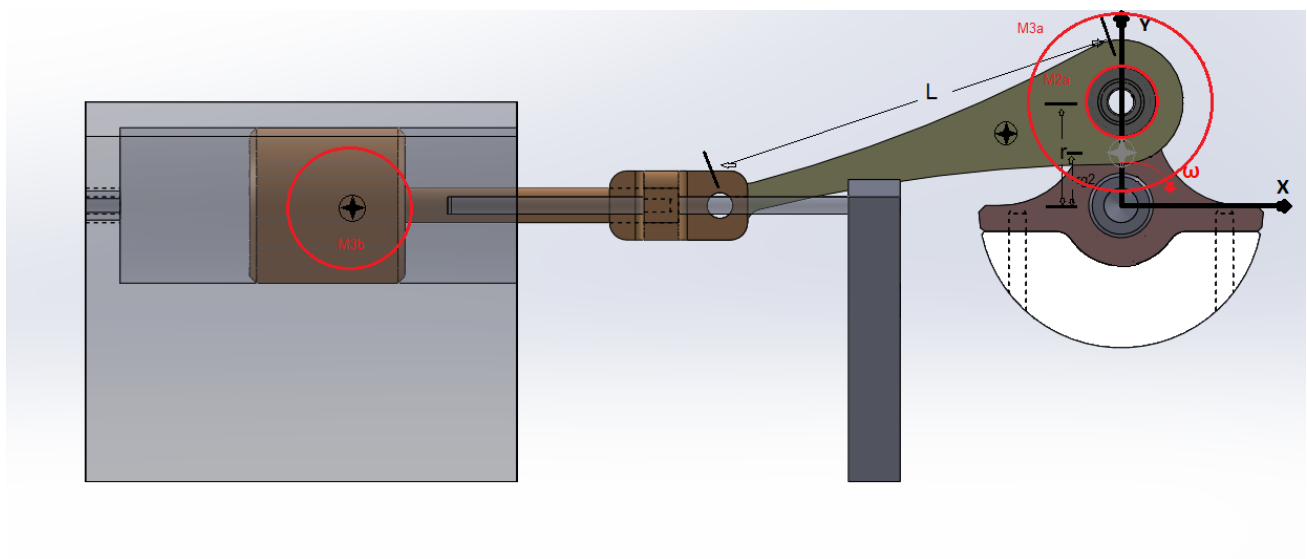


Figure 17: Unbalanced Slider-Crank model (see Norton Design of Machinery fig. 13-12 p.618)

Slider – Crank Mechanism for Demonstration and Experimentation

M2a has a mass*radius product equal to that of the unbalanced crank

M3a is equal to 2/3 the mass of the connecting rod

M3b is equal to 1/3 the mass of the connecting rod

Effective mass at crank (lumped mass A)

- $M_a = M_a$

Effective mass at slider (lumped mass B)

- $M_b = M_{3b} + (\text{slider mass})$

$$F_{sx}(\theta) := -M_a \cdot (R \cdot \omega^2 \cdot \cos(\theta)) - M_b \cdot \left[R \cdot \omega^2 \left(\cos(\theta) + \frac{R}{L} \cdot \cos(2\theta) \right) \right] \quad \text{Lumped Mass A} \quad M_a := 0.467\text{kg}$$

$$F_{sy}(\theta) := -M_a \cdot (R \cdot \omega^2 \cdot \sin(\theta)) \quad \text{Lumped Mass B} \quad M_b := 1.543\text{kg}$$

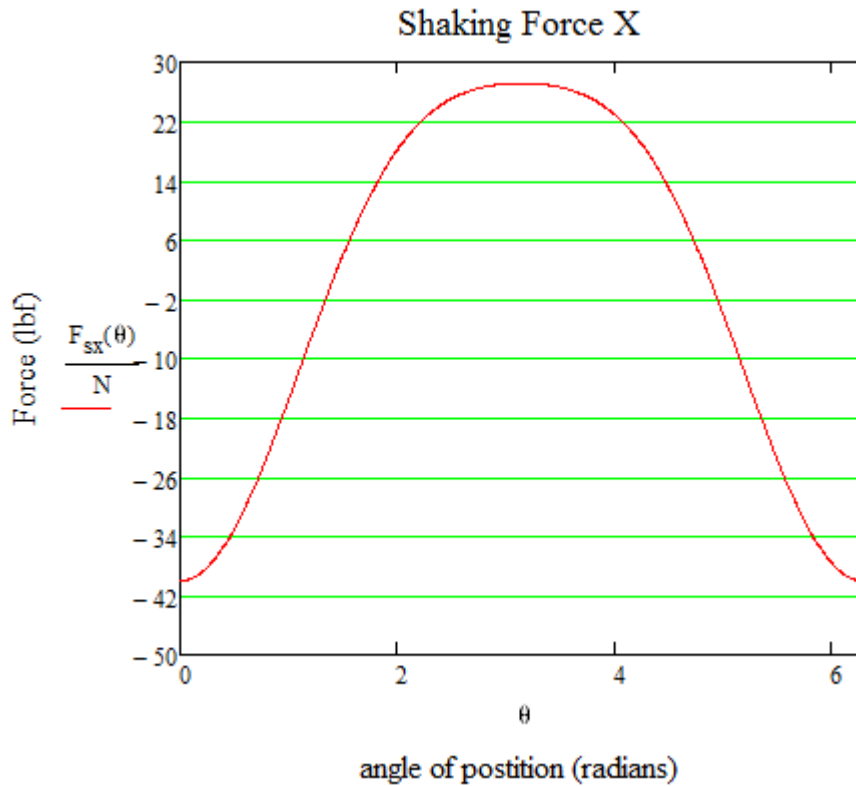


Figure 18: X-Component Shaking Force vs. Crank Angle (Unbalanced)

Slider – Crank Mechanism for Demonstration and Experimentation

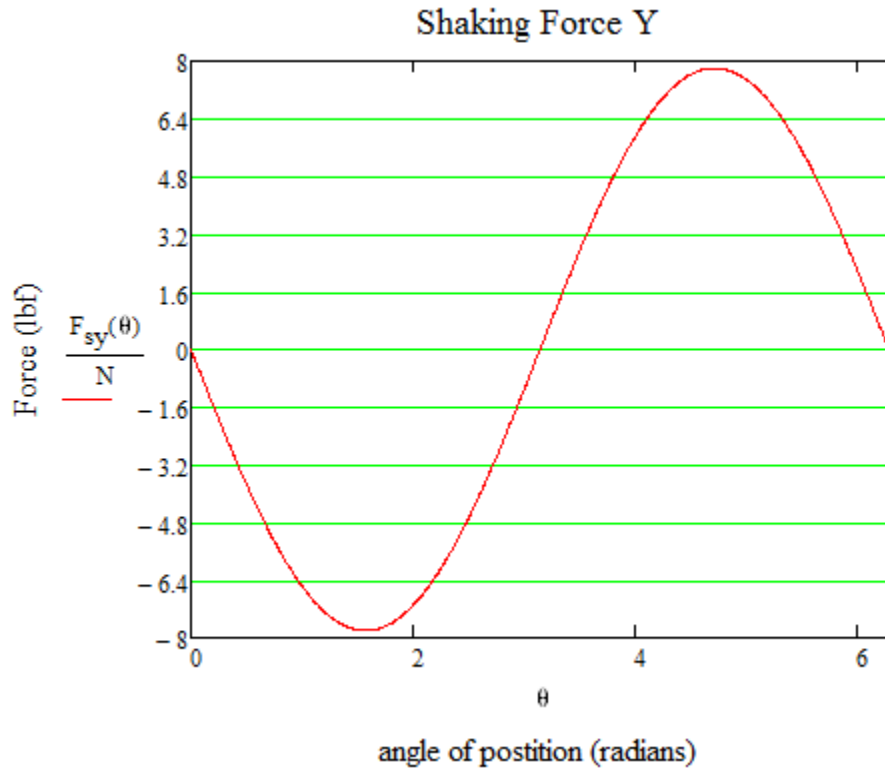


Figure 19: Y-Component Shaking Force vs. Crank Angle (Unbalanced)

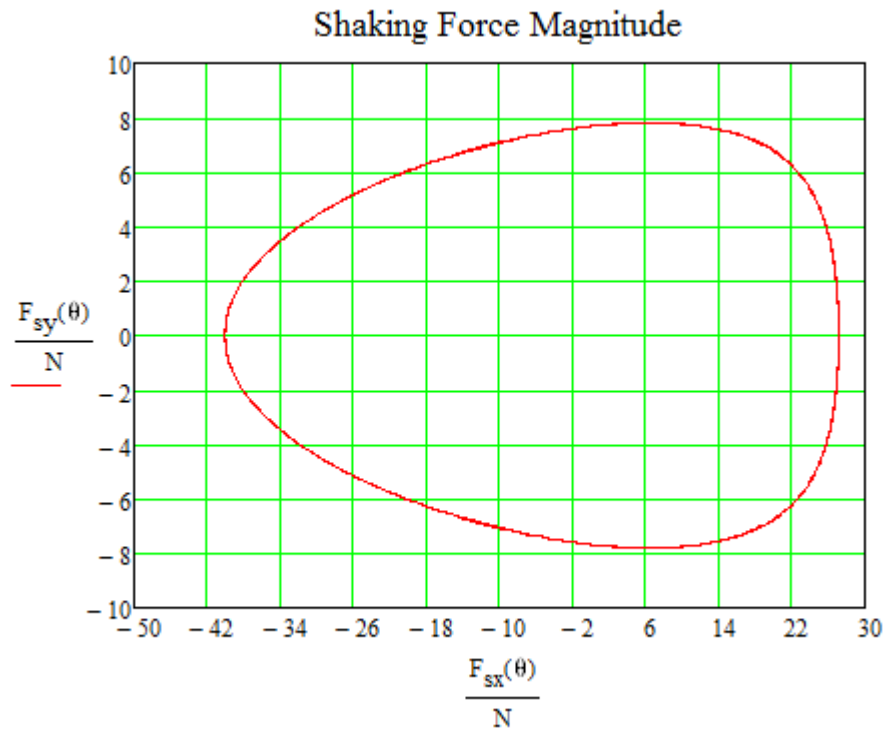


Figure 20: Total Magnitude of Shaking Force (Unbalanced)

Slider – Crank Mechanism for Demonstration and Experimentation

Statically Balanced Configuration

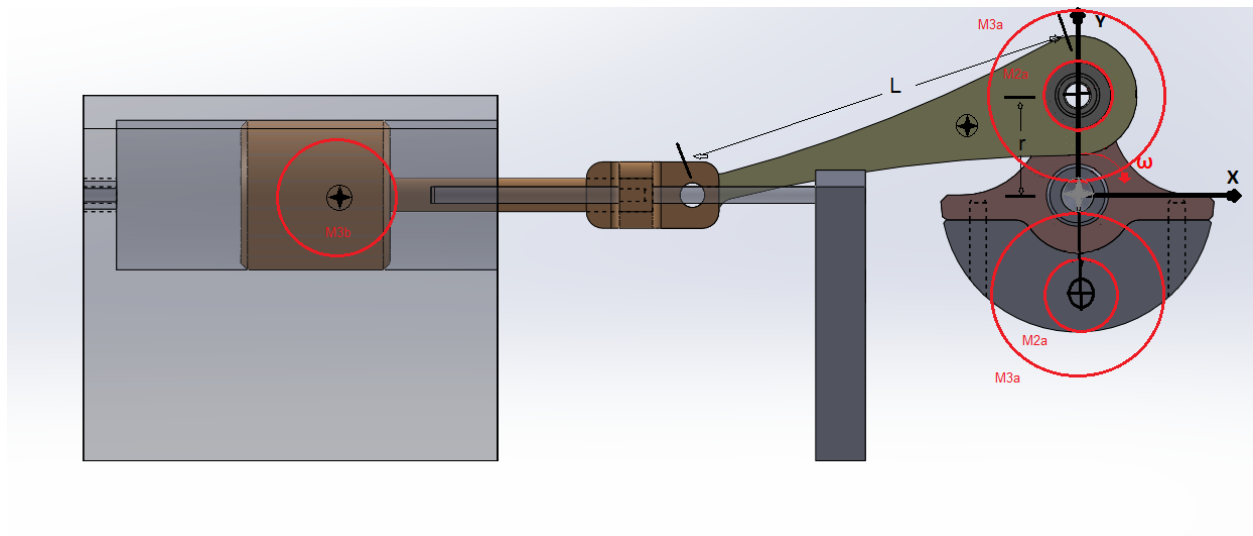


Figure 21: Statically balanced slider-crank model (see Norton Design of Machinery fig13-23 p. 632)

M2a has a mass*radius product equal to that of the unbalanced crank

M3a is equal to 2/3 the mass of the connecting rod

M3b is equal to 1/3 the mass of the connecting rod

$$M_a = M_{3a} + M_{2a}$$

$$M_a' = M_{3a}' + M_{2a}'$$

Effective mass at crank (lumped mass A)

- $M_a = M_a - M_a' = 0$

Effective mass at slider (lumped mass B)

- $M_b = M_{3b} + (\text{slider mass})$

$$F_{sx}(\theta) := -M_a \cdot (R \cdot \omega^2 \cdot \cos(\theta)) - M_b \cdot \left[R \cdot \omega^2 \left(\cos(\theta) + \frac{R}{L} \cdot \cos(2\theta) \right) \right]$$

Lumped Mass A

$$M_a := 0 \text{ kg}$$

$$F_{sy}(\theta) := -M_a \cdot (R \cdot \omega^2 \cdot \sin(\theta))$$

Lumped Mass B

$$M_b := 1.543 \text{ kg}$$

Slider – Crank Mechanism for Demonstration and Experimentation

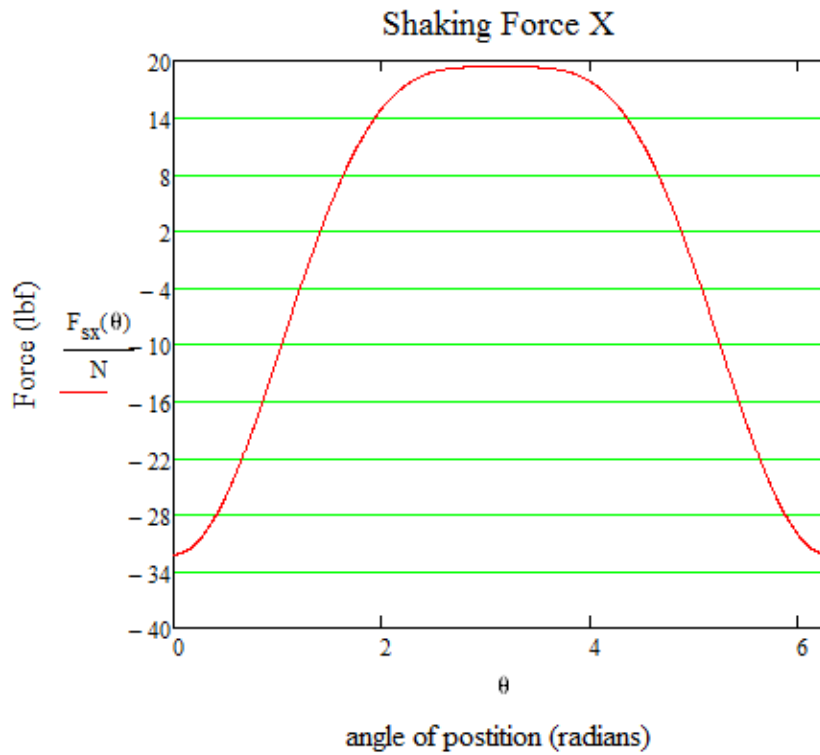


Figure 22: X-Component Shaking Force vs. Crank Angle (Statically Balanced)

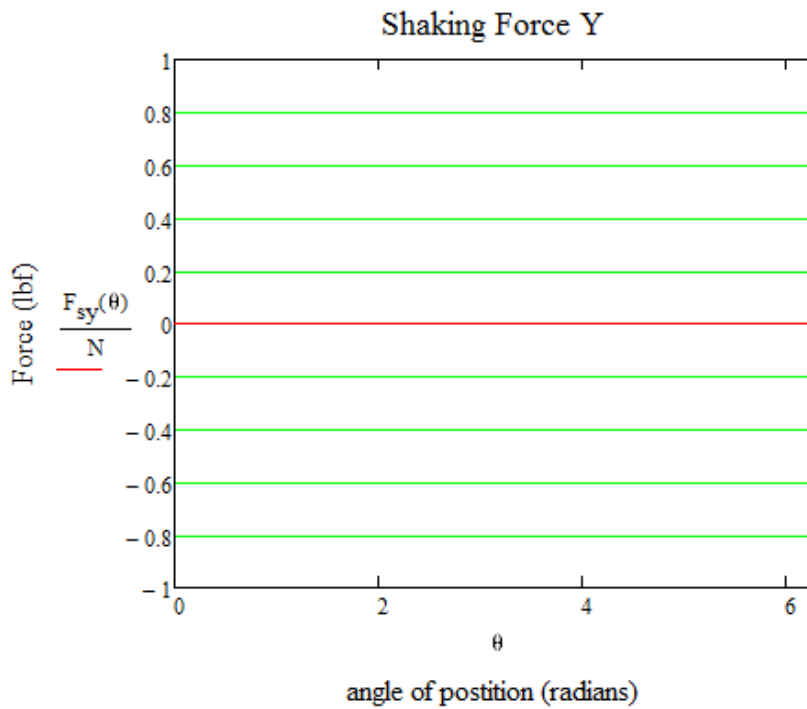


Figure 23: Y-Component Shaking Force vs. Crank Angle (Statically Balanced)

Slider – Crank Mechanism for Demonstration and Experimentation

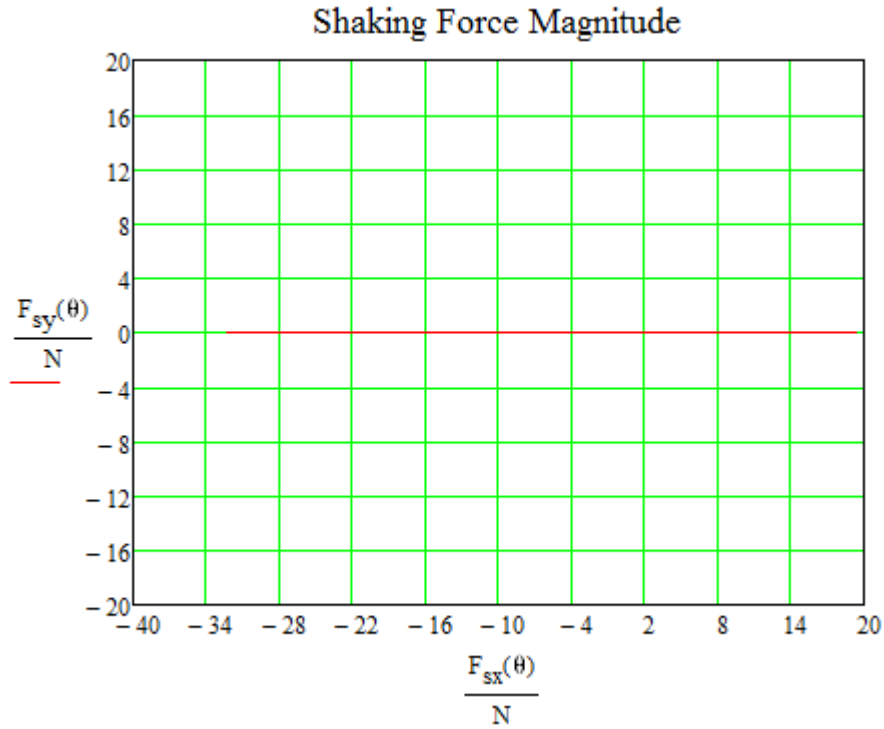


Figure 24: Total Magnitude Shaking Force (Statically Balanced)

Dynamically Balanced Configuration

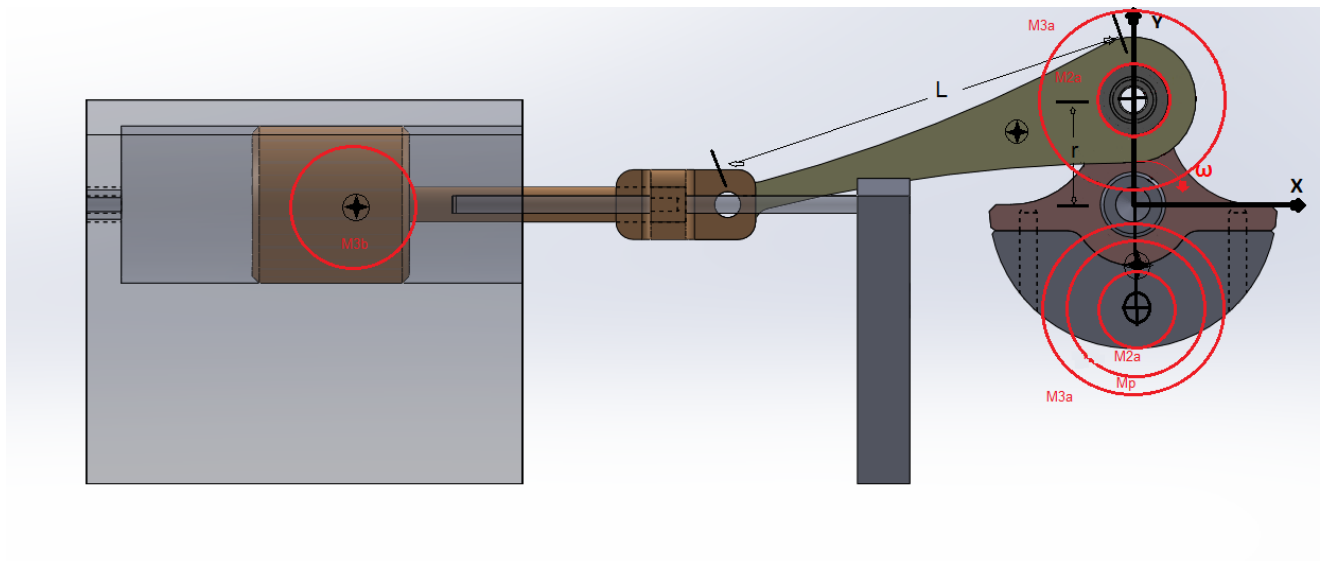


Figure 25: Dynamically Balanced Slider-Crank Model (see Norton Design of Machinery fig 13-23 p.632)

Slider – Crank Mechanism for Demonstration and Experimentation

M2a has a mass*radius product equal to that of the unbalanced crank

M3a is equal to 2/3 the mass of the connecting rod

M3b is equal to 1/3 the mass of the connecting rod

$M_a = M_{3a} + M_{2a}$

$M_{a'} = M_{3a'} + M_{2a'}$

$1/2 M_b \leq M_p \leq 2/3 M_b$ (the exact value depends upon the optimal operating speed)

Effective mass at crank (lumped mass A)

- $M_a = M_a - M_{a'} - M_p = -M_p$

Effective mass at slider (lumped mass B)

- $M_b = M_{3b} + (\text{slider mass})$

$$F_{sx}(\theta) := -M_a \cdot (R \cdot \omega^2 \cdot \cos(\theta)) - M_b \cdot \left[R \cdot \omega^2 \left(\cos(\theta) + \frac{R}{L} \cdot \cos(2\theta) \right) \right] \quad \begin{array}{l} \text{Lumped Mass A} \\ \text{Lumped Mass B} \end{array} \quad \begin{array}{l} M_a := -.7\text{kg} \\ M_b := 1.543\text{kg} \end{array}$$
$$F_{sy}(\theta) := -M_a \cdot (R \cdot \omega^2 \cdot \sin(\theta))$$

Slider – Crank Mechanism for Demonstration and Experimentation

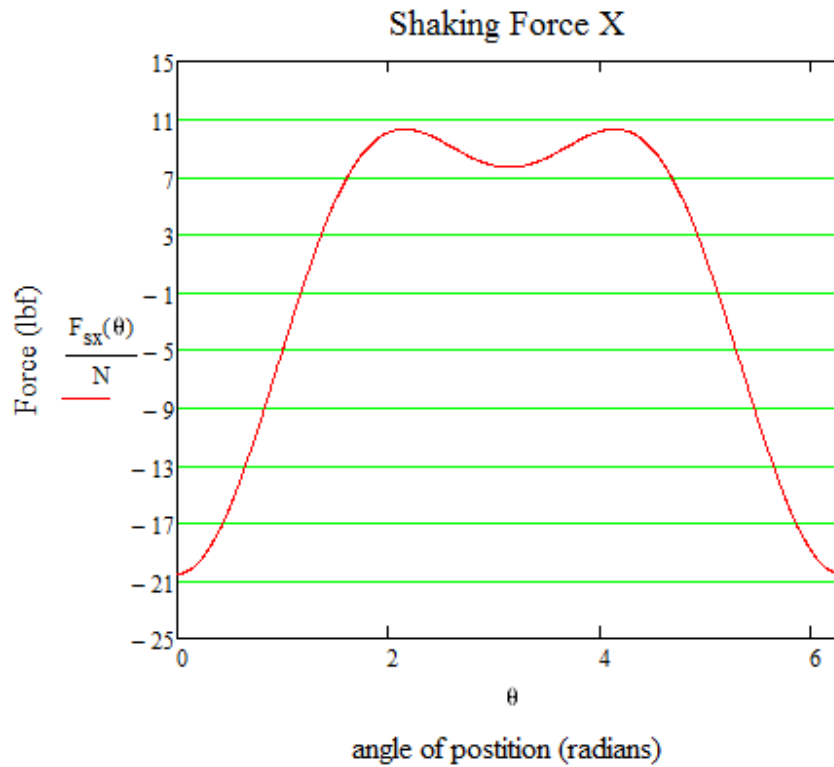


Figure 26: X-Component Shaking Force vs. Crank Angle (Dynamically Balanced)

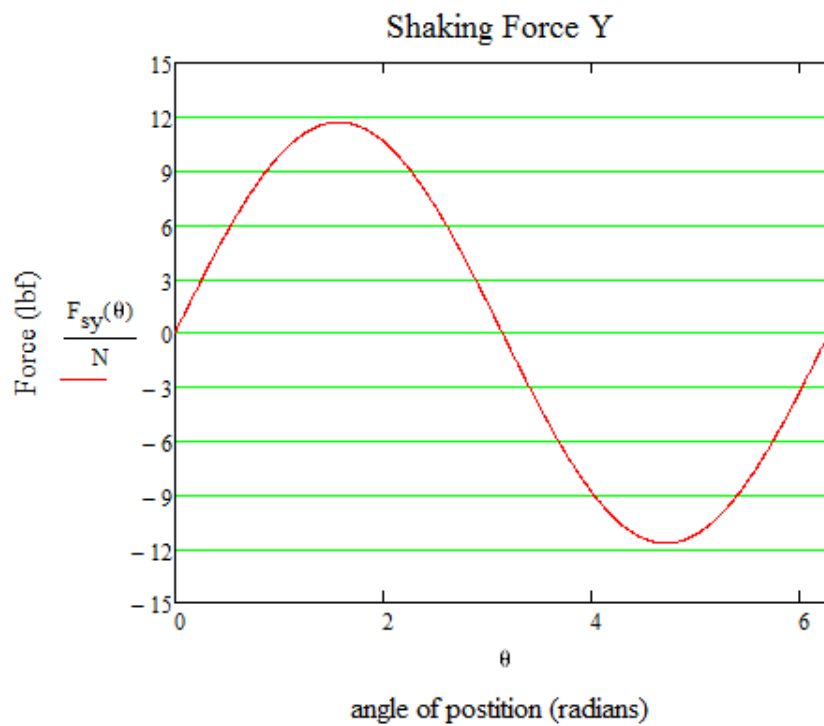


Figure 27: Y-Component Shaking Force vs. Crank Angle (Dynamically Balanced)

Slider – Crank Mechanism for Demonstration and Experimentation

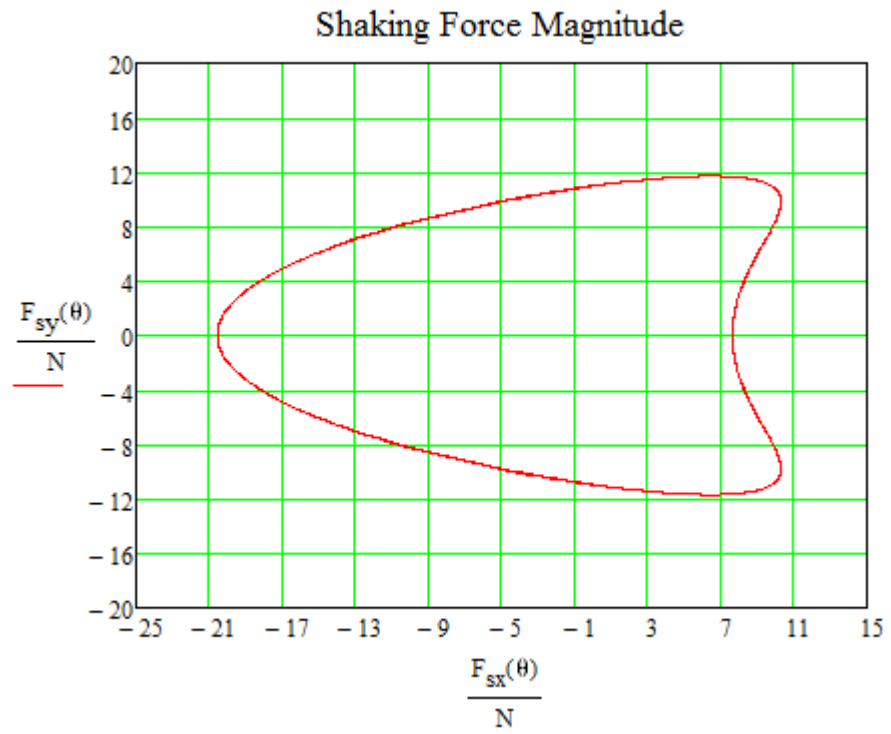


Figure 28: Total Magnitude Shaking Force vs. Crank Angle (Dynamically Balanced)

Slider – Crank Mechanism for Demonstration and Experimentation

Torsional Stress Analysis of Crankshaft

The engine's crankshaft rotates about the X axis as it is driven by the connecting rod. The geometry and loading of the crankshaft will produce significant torsional stress in the shaft, the maximum value of which must be evaluated. In order to represent a worst-case stress scenario, the assumption is made that one end of the shaft is fixed by the flywheel while the other is subjected to the torque generated by the device under maximum operational speed. The geometry and loading of the crankshaft will result in minimal bending so it will be neglected. A conservatively large value for maximum operational angular velocity is assumed to be $\omega = 500$ rpm (52.4 rad/s).



Figure 29: Crank-Shaft Fixtured for 4th Axis Machining

$$\text{Acceleration} \quad A(\theta) := \left[-R \cdot \omega^2 \left(\sin(\theta) + \frac{R}{L} \sin(2\theta) \right) \right]^2 = 110 \text{ m/s}^2$$

The primary shaking force calculated previously using the lump mass model is selected as the magnitude of force applied to the crankshaft through the connecting rod pin connection.

$$\text{Shaking force} \quad F_{sx}(\theta) := -M_a \cdot (R \cdot \omega^2 \cdot \cos(\theta)) - M_b \cdot \left[R \cdot \omega^2 \left(\cos(\theta) + \frac{R}{L} \cdot \cos(2\theta) \right) \right] = 185 \text{ N}$$

Slider – Crank Mechanism for Demonstration and Experimentation

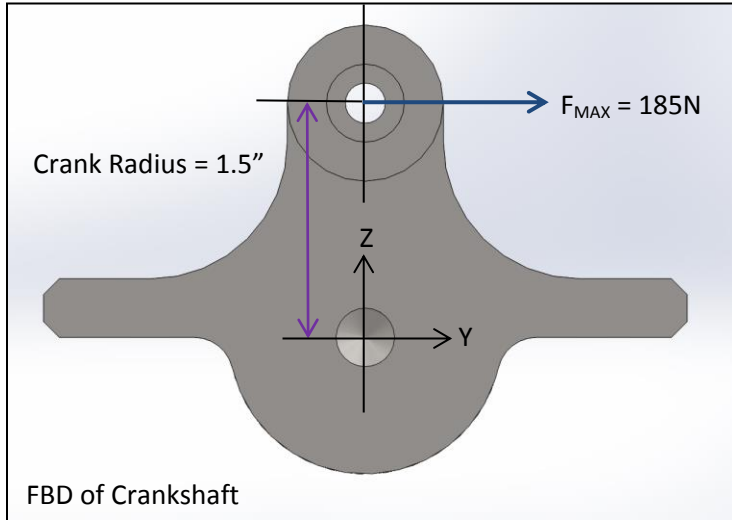


Figure 30: Free Body Diagram for Crankshaft Side View

Shaft torque $T = F \cdot r = 7.05 \text{ Nm}$

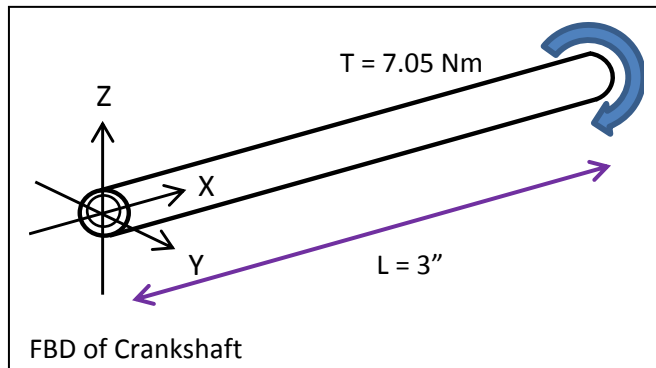


Figure 31: Free Body Diagram of Crankshaft Isometric View

The polar moment of inertia (J) of the crankshaft's cross section is approximated by assuming a uniform hollow shaft of outer diameter = 1.125", inner diameter = 0.375" and unsupported length $L = 3"$.

$$\text{Area moment of inertia } J = \frac{\pi}{32} (D_o^4 - D_i^4) = 6.48\text{E-}8 \text{ L}^4$$

A stress concentration factor (K) must be applied to approximate the amplification of stress caused by the non-uniform valves which cut into the shaft. The effect of these areas of stress concentration will be evaluated by applying empirical data from Walter Pilkey's *Peterson's Stress Concentration Factors*.

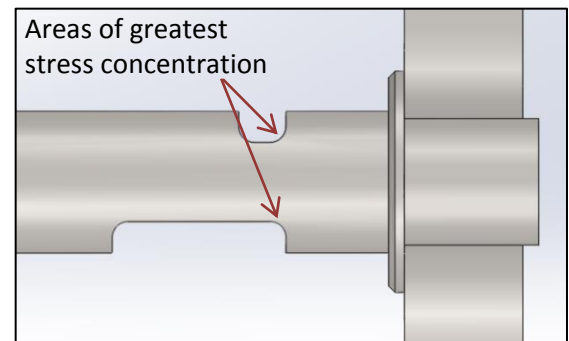


Figure 32: Stress Concentration Locations

Slider – Crank Mechanism for Demonstration and Experimentation

One scenario presented in Pilkey’s text resembles the crankshaft’s geometry and loading. The model is that of a hollow shaft undergoing torsion; an additional through hole exists perpendicular to the axis of rotation. Relevant empirical data is presented in the following chart.

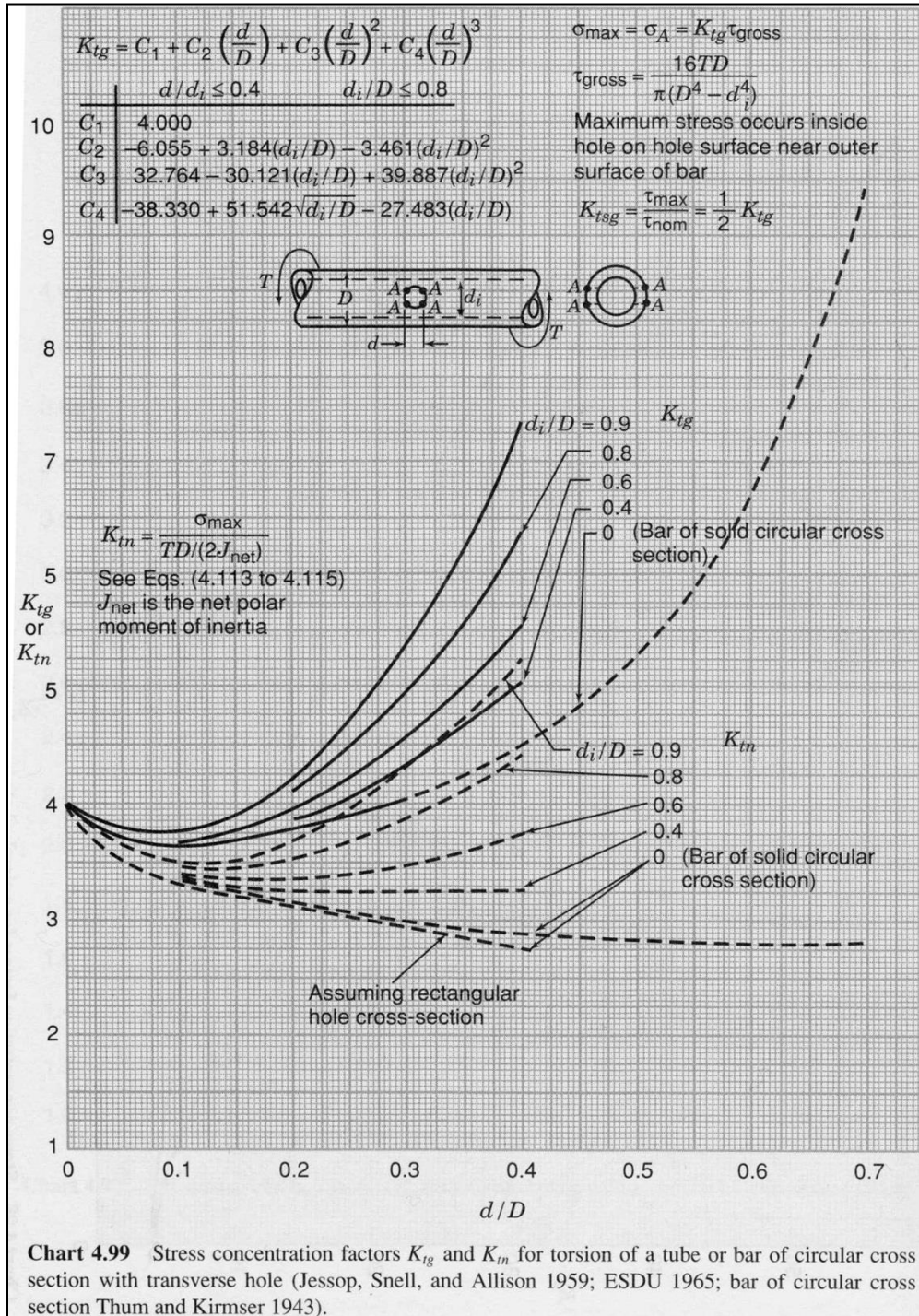


Figure 33: Stress Concentration Table

Slider – Crank Mechanism for Demonstration and Experimentation

The empirical data must be extrapolated slightly beyond the chart's limits. A conservative estimation of $K = 7$ will be incorporated into the calculation of torsional stress.

$$\text{Torsional stress } \tau = \frac{T \cdot r}{J} K = 10.9 \text{MPa}$$

The crankshaft is machined from 1018 carbon steel which possesses yield strength of 350MPa. Therefore a safety factor of 32 has been calculated for the condition of static failure due to torsion.

Excessive torsional deflection in the crankshaft (greater than 1°) must be avoided to preserve the relative location of the piston with respect to the valves.

$$\text{Torsional deflection } \theta = \frac{T \cdot L}{J \cdot G} = 0.006^\circ \text{ (with } G = 80.8 \text{GPa)}$$

Slider – Crank Mechanism for Demonstration and Experimentation

Finite Element Analysis of Crankshaft

The stress concentrations caused by the unusual geometry of the valves cut from the crankshaft may be better understood by applying numerical methods. Analysis using the finite element method will provide insight into the stress concentrators' magnitude and location.

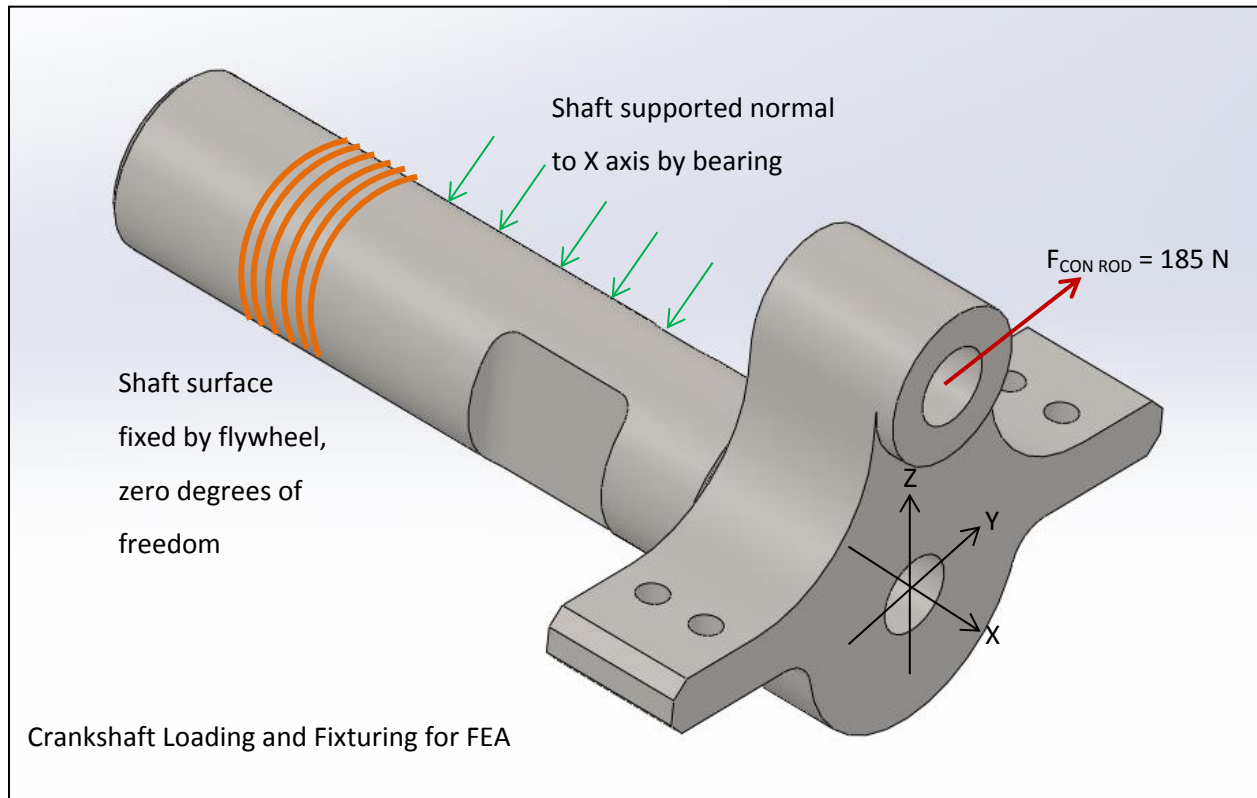


Figure 34: FEA Boundary Conditions for Crankshaft Analysis

A relatively fine mesh of triangular elements is applied to the crankshaft's solid model. The shaft is rigidly fixed by a portion of the outer surface corresponding to the location of the flywheel. It is supported along the portion of the shaft which contacts the bearing, normal and opposite of the applied force. The maximum force of 185N, as previously determined for an operational speed of 500rpm, is applied to the pin joint which connects the crank to the connecting rod.

Slider – Crank Mechanism for Demonstration and Experimentation

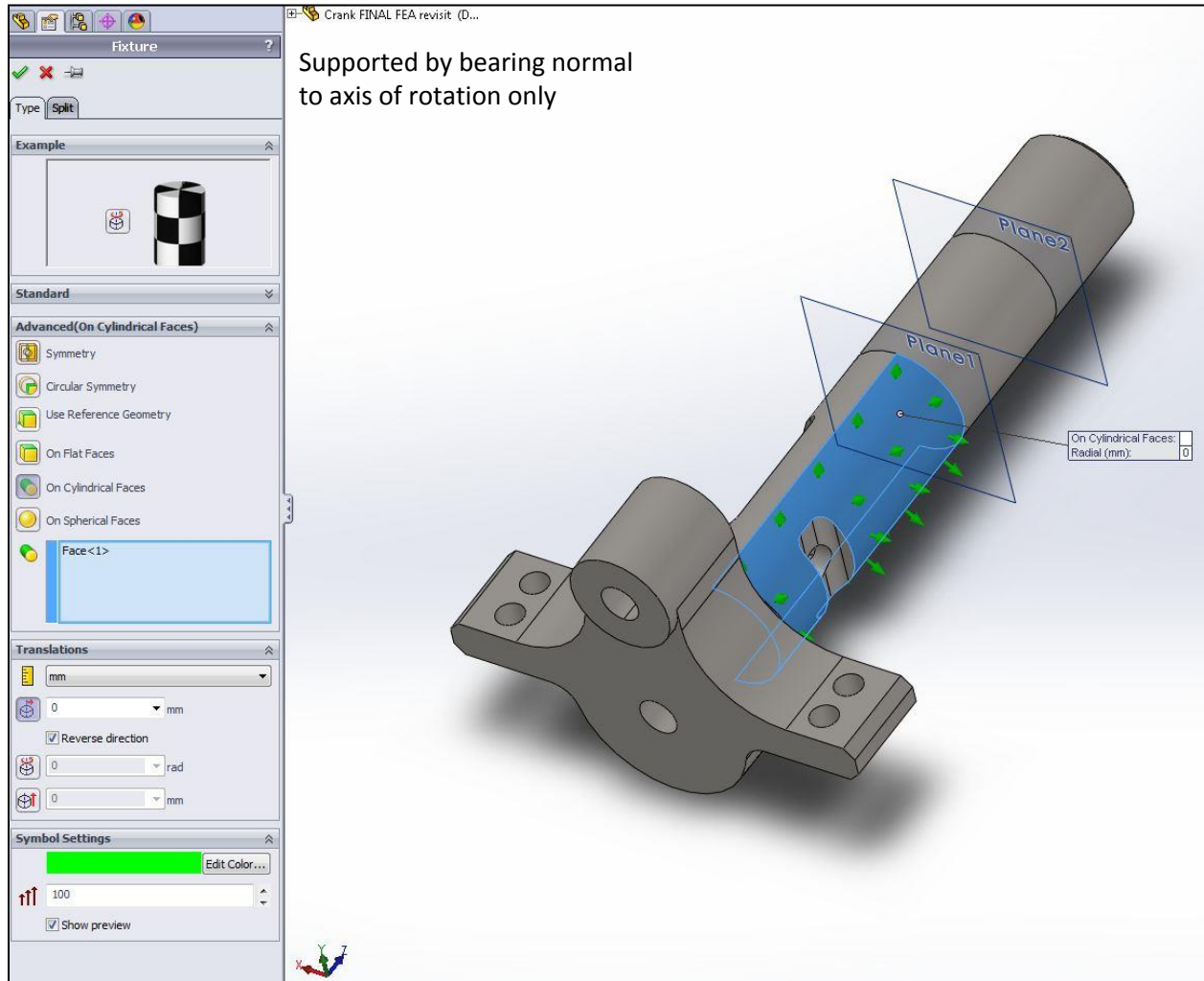


Figure 35: FEA Boundary Condition – Interaction with Bearing

Slider – Crank Mechanism for Demonstration and Experimentation

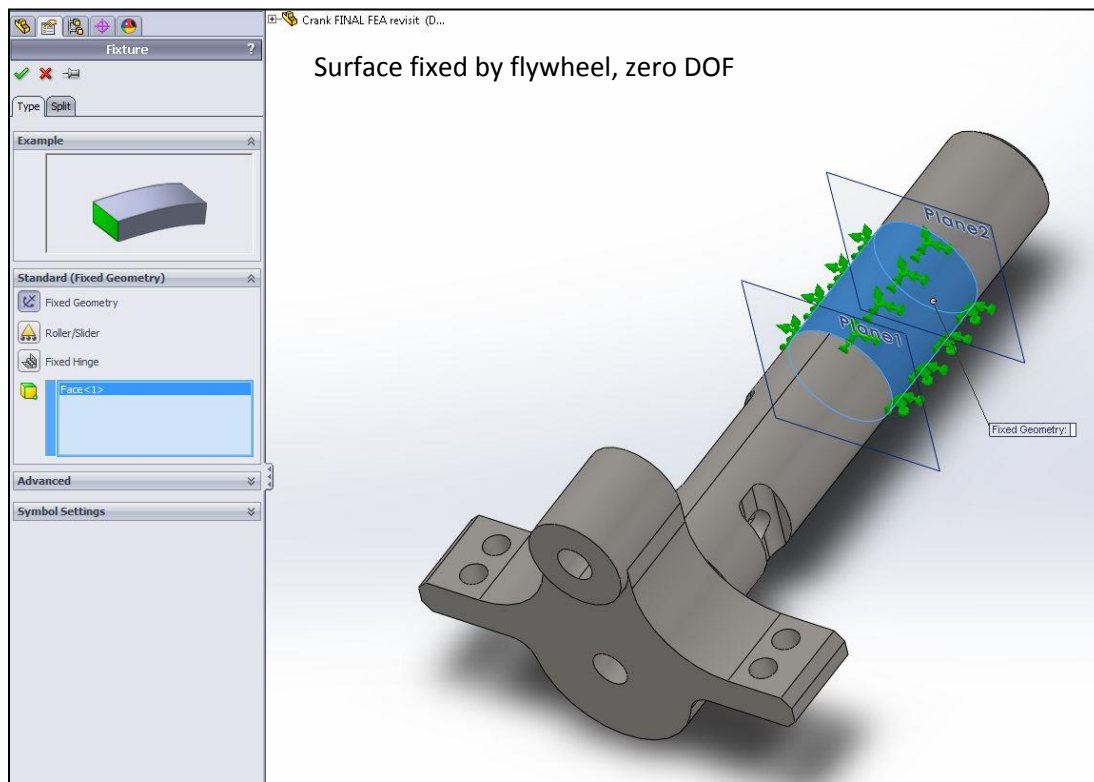


Figure 36: FEA Boundary Condition – Fixed by Flywheel

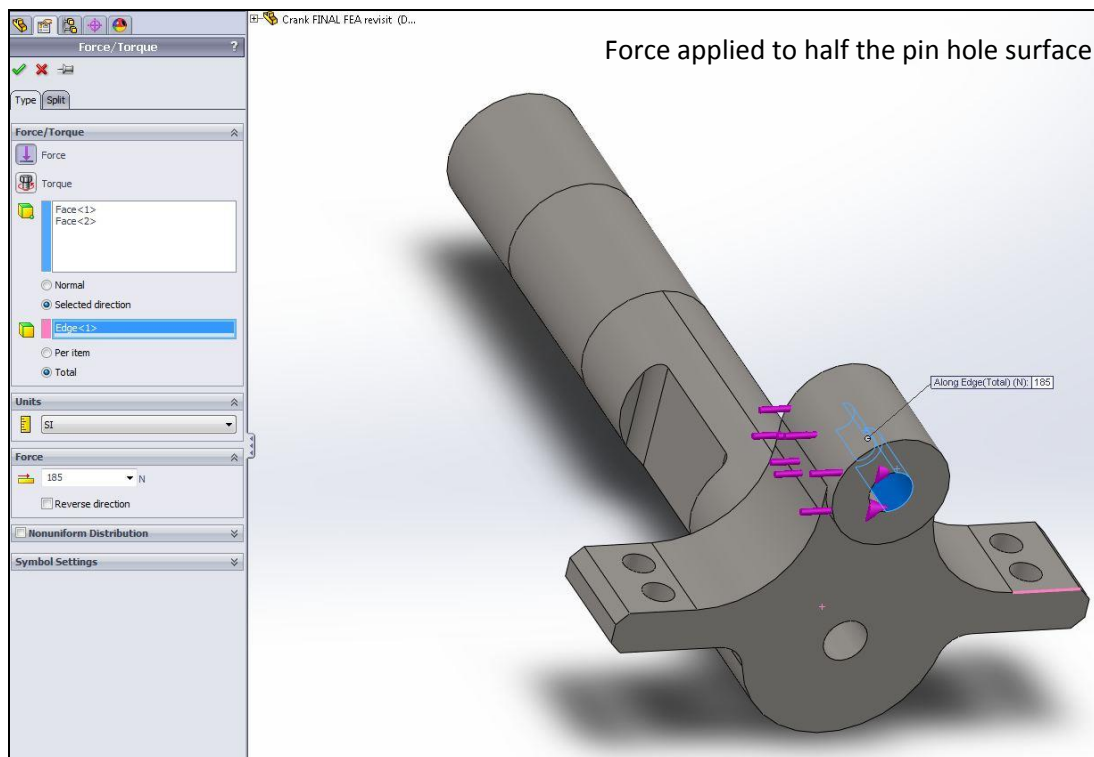


Figure 37: FEA Boundary Condition – Load Applied by Connecting Rod Pin Connection

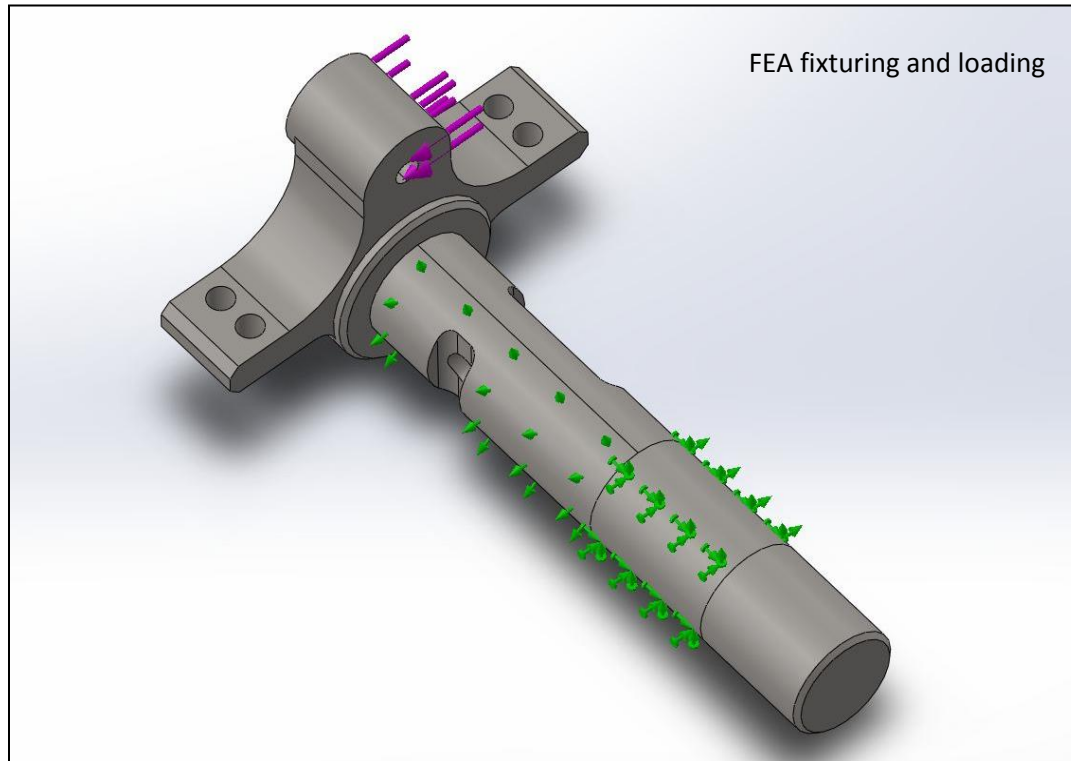


Figure 38: FEA Boundary Conditions

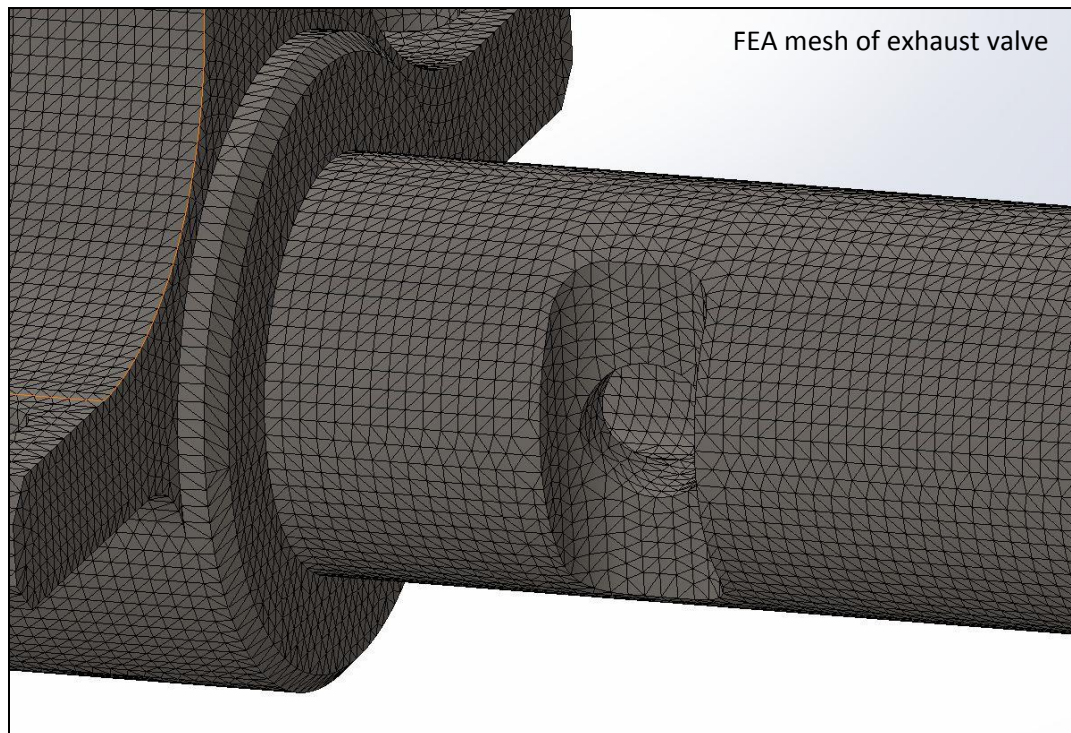


Figure 39: FEA Mesh

Slider – Crank Mechanism for Demonstration and Experimentation

The Von Mises Stress gradient determined by the analysis is displayed below graphically. Areas of greatest stress appear in red.

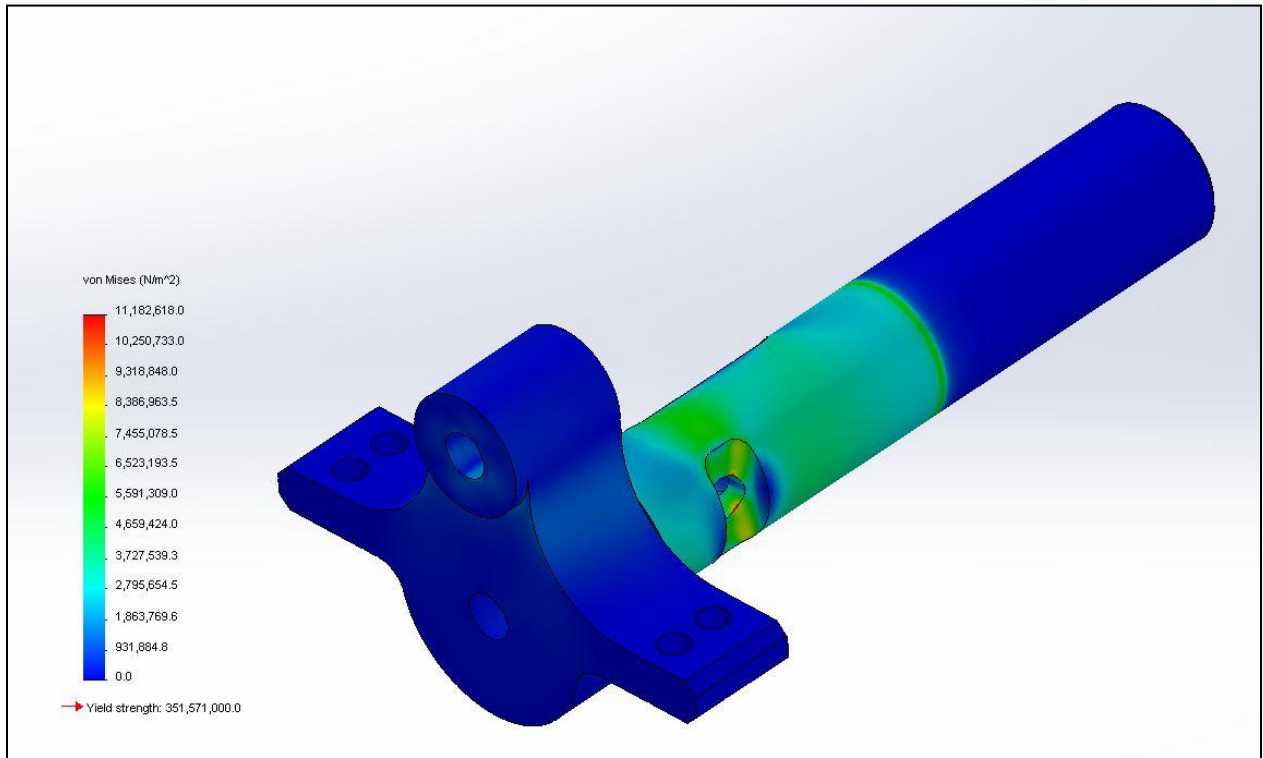


Figure 40: FEA Von Mises Stress Gradient Isometric View

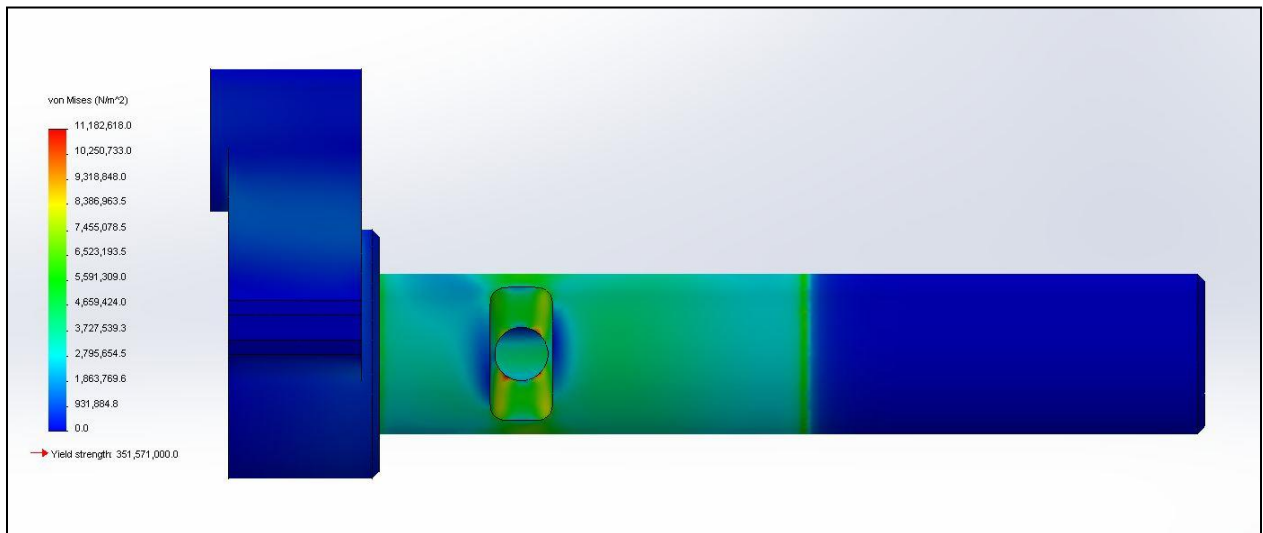


Figure 41: FEA Von Mises Stress Gradient Front View

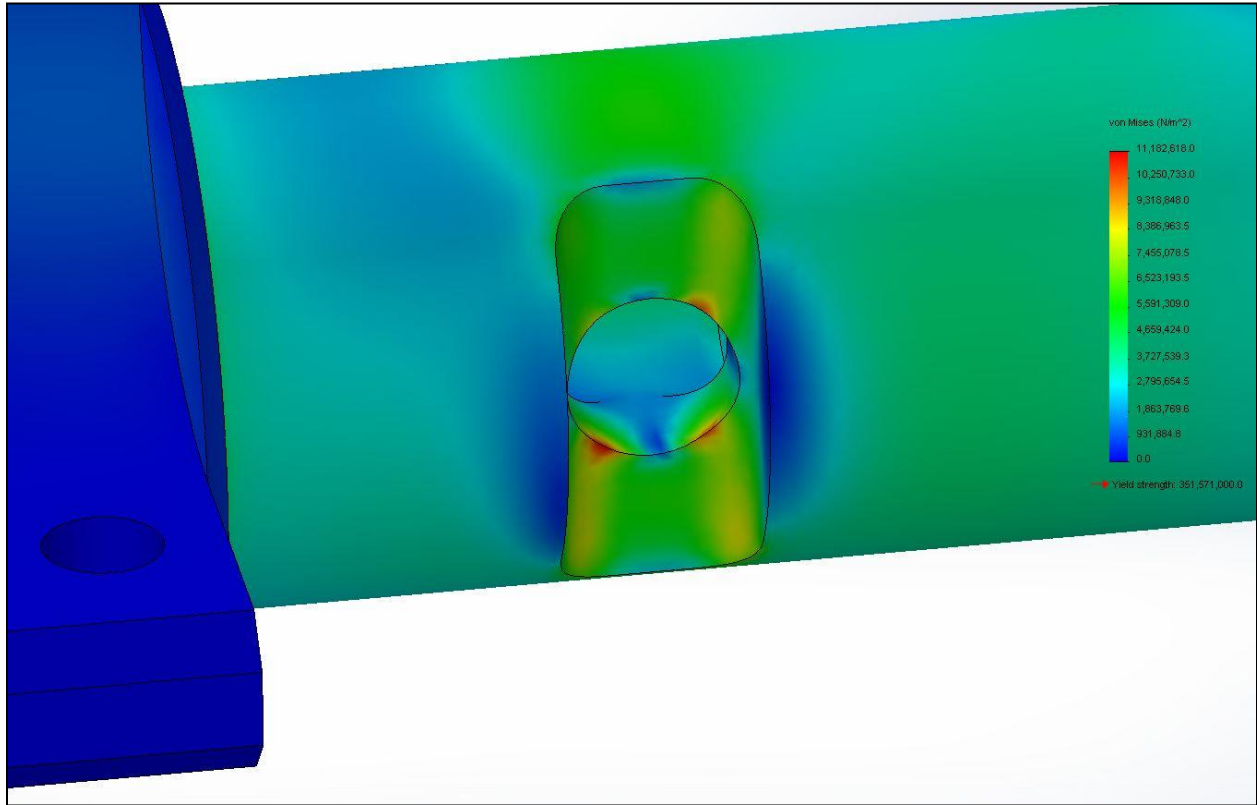


Figure 42: FEA Von Mises Stress Gradient Exhaust Port

As expected, the areas of highest stress concentration are located in the valves. The highest magnitude of stress occurs where the exhaust port passes through the valve.

Slider – Crank Mechanism for Demonstration and Experimentation

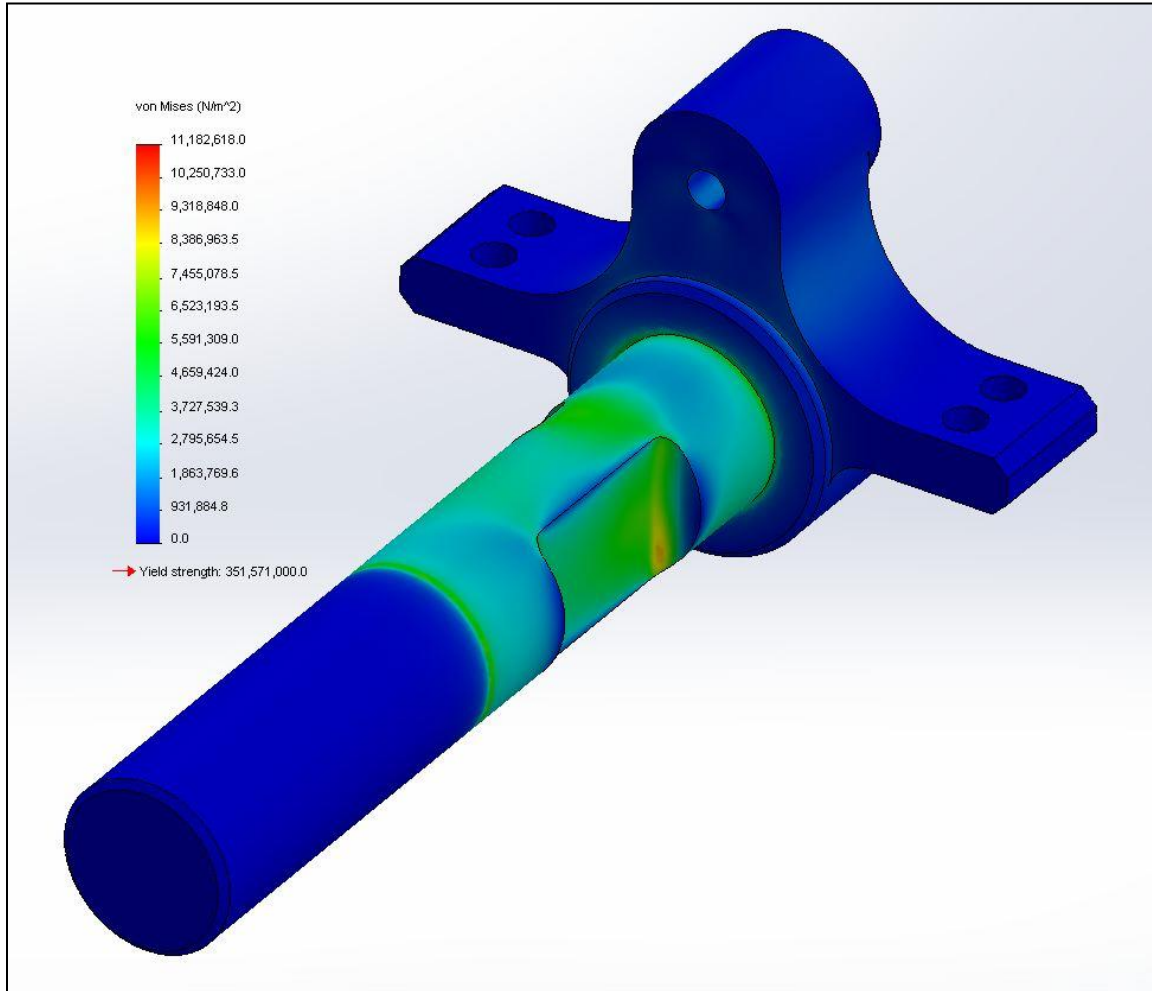


Figure 43: FEA Von Mises Stress Gradient

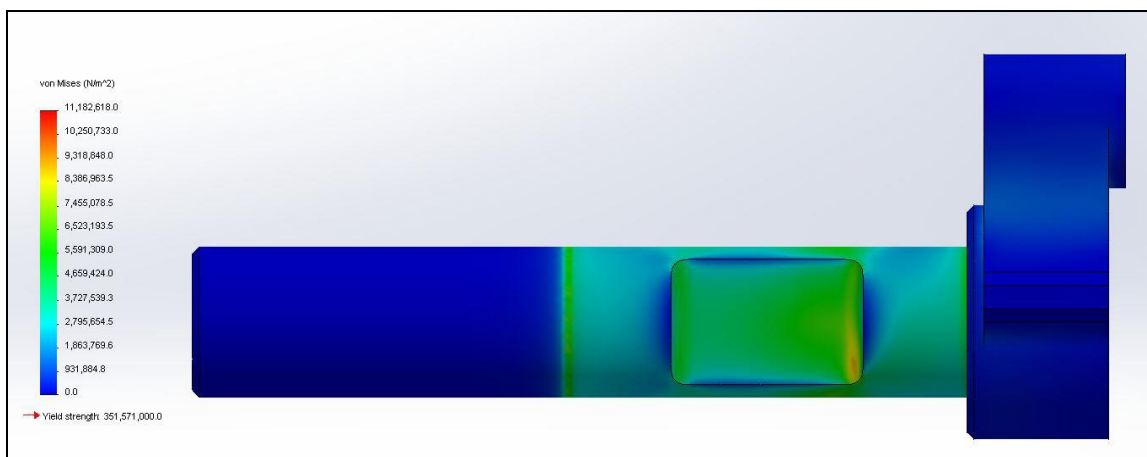


Figure 44: FEA Von Mises Stress Gradient with Intake Port Shown

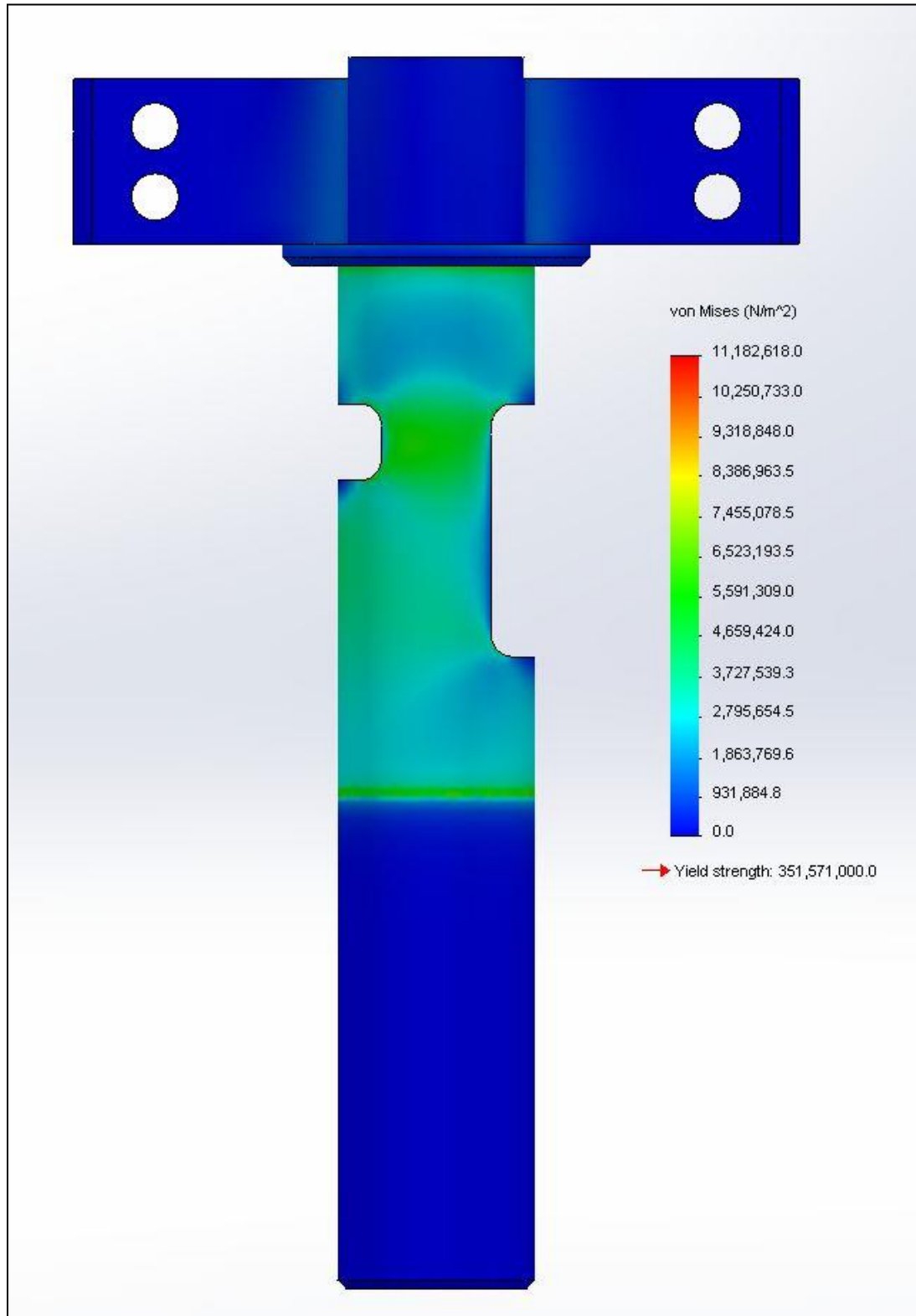


Figure 45: FEA Von Mises Stress Gradient Top View

Slider – Crank Mechanism for Demonstration and Experimentation

The maximum von Mises stress experienced by the crankshaft is just over 11MPa. The steel crankshaft possesses yield strength of over 350MPa. The finite element analysis thus suggests a safety factor of 31.4 exists for the same torsional scenario as was evaluated analytically. This result is reasonable and is supported closely by the analytical solution.

The highest concentrations of stress exist at the corners of the valve cuts. In anticipation of this, the crankshaft was designed with large radii in these corners. The stress concentrations would be much greater if these corners were sharp angles, as they are depicted in Elmer's original small scale steam engine blueprints.

The displacement gradient determined by the FEM analysis is displayed below.

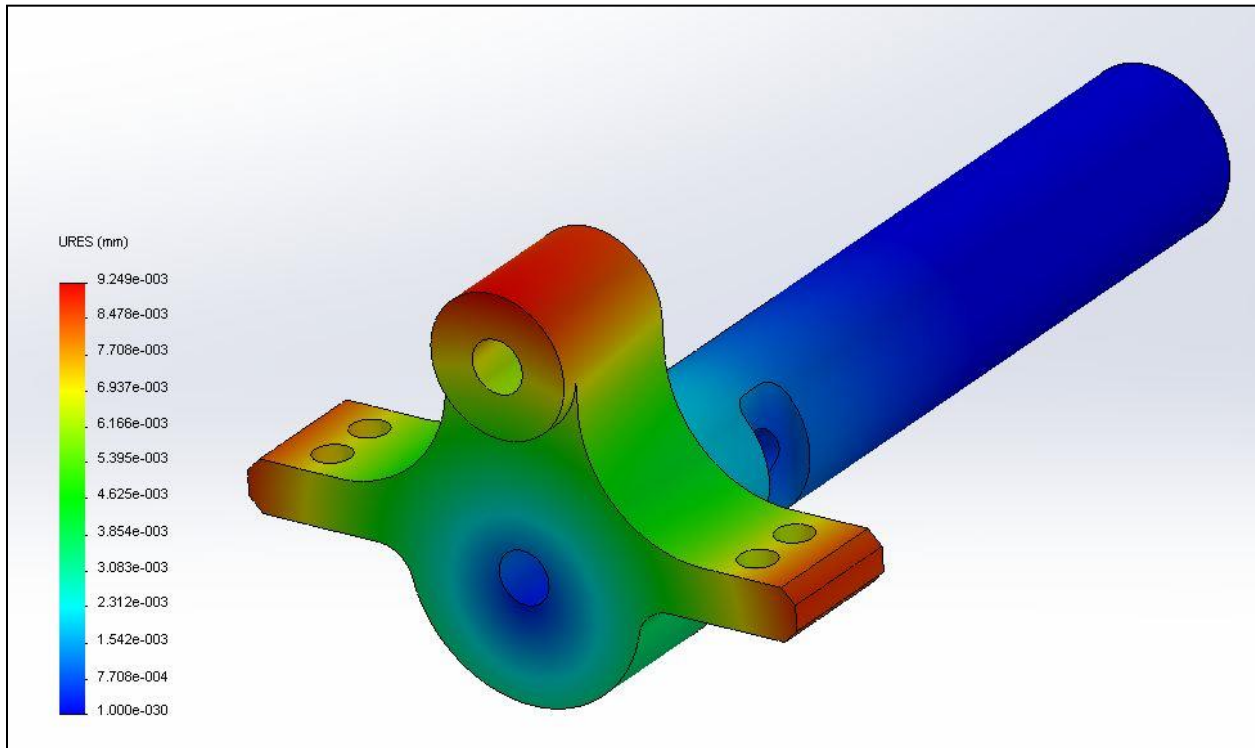


Figure 46: FEA Deflection Gradient

The maximum displacement of the crankshaft is 0.00925mm. This corresponds to an angular displacement of 0.01°, which is supported by the analytical solution.

Slider – Crank Mechanism for Demonstration and Experimentation

Torsional Vibration Analysis of Crankshaft

The torsional load that was previously evaluated is a result of the periodic piston motion. The load manifests as a pulse acting over half the full cycle. If the driven frequency approaches the shaft's torsional natural frequency, the condition of resonance will occur, inducing vibrations of unbounded amplitude. Thus the shaft's torsional natural frequency (ω_{nt}) must be evaluated. The crankshaft geometry will again be simplified by assuming a uniform hollow tube of outside diameter $D_o = 1.125''$ and inside diameter $D_i = 0.375''$.

Area moment of inertia $J = \frac{\pi}{32} (D_o^4 - D_i^4) = 6.48E-8 \text{ m}^4$

Torsional stiffness $k_t = \frac{GJ}{L} = 6.8E4 \text{ Nm}$ [with $G_{\text{steel}} = 80.8\text{GPa}$; $L = 3''$ (0.0762m)]

Centroidal Moment of Inertia $I_m = \frac{m(R_o^2 + r_i^2)}{2} = 5.68E-5 \text{ kgm}^2$ (with $m = 0.5\text{kg}$)

Torsional natural frequency $\omega_{nt} = \sqrt{\frac{k_t}{I_m}} = 3.4E4 \text{ rad/s}$ (3.3E5 rpm)

The torsional natural frequency of the crankshaft far exceeds the maximum achievable driving frequency and as such will not result in resonance during operation.

Slider – Crank Mechanism for Demonstration and Experimentation

Crosshead Guide Deflection Analysis

The engine's crosshead slides along two parallel shafts of length 4.75" and diameter 0.25". The rotational nature of the crank's motion produces a component of force orthogonal to the direction of the crosshead's translation. As such, the shafts will deflect to some extent during operation. Large deflections would result in misalignment, increasing friction and possibly causing the crosshead to bind or chatter as it travels along the guides. The magnitude of deflection must be evaluated.

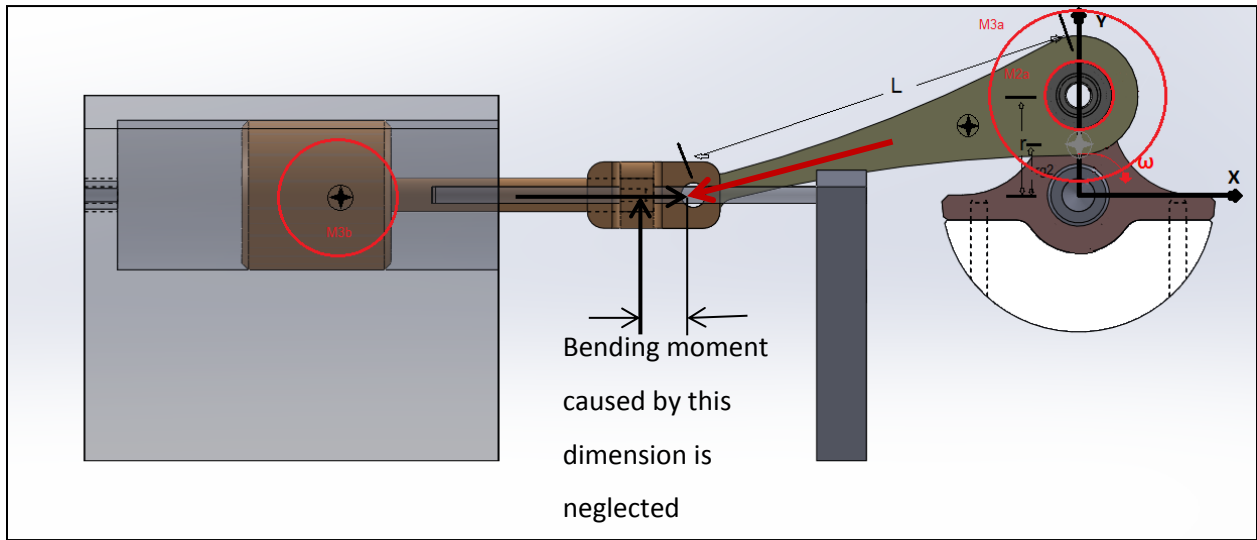


Figure 47: Free Body Diagram for Slider Crank

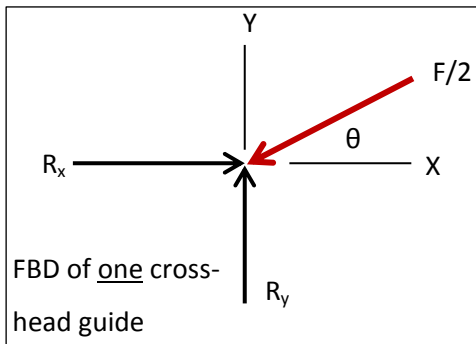


Figure 48: FBD Cross-head guide

To simplify the analysis, the crosshead is assumed to be a point with forces acting on it. The piston is fixed, while a conservatively high magnitude of force is applied to the crosshead by the connecting rod. The crosshead travels along the horizontal axis. The vertical reaction force is of interest.

This component of force is maximized when the angle θ is

maximum. Theta reaches an ultimate value of 14.5° during

operation. Assuming a conservatively high maximum cylinder

pressure of 60 psi (0.414 MPa), a value for the applied load can be derived from $F = P \cdot A = 840\text{N}$. It is important to note that this load is distributed over two crosshead guides.

Slider – Crank Mechanism for Demonstration and Experimentation

Sum of forces along y axis $\Sigma Fy = Ry - Fsin\theta = 0$

Vertical component of force $Ry = 210 \text{ N}$ (distributed over two shafts)

The y component of force applied to each crosshead guide is 105 N. The associated deflection is evaluated as a point load applied at the center of the shafts' 4.75" span. The crosshead guides are rigidly fixed on both ends. An equation describing the deflection of a simply supported beam may be used because the deflections in this scenario will exceed that of the fixed crosshead guides.

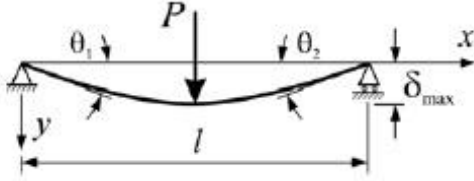
BEAM TYPE	MAXIMUM AND CENTER DEFLECTION
Beam Simply Supported at Ends – Concentrated load P at the center	
	$\delta_{\max} = \frac{Pl^3}{48EI}$

Figure 49: Diagram for Beam Deflection

Centroidal moment of Inertia $I = \frac{m \cdot L^2}{12} = 3.66\text{E-}5 \text{ kgm}^2$

Deflection $\delta_{\max} = \frac{Pl^3}{48EI} = 2.57\text{E-}10 \text{ m}$ (with $E_{\text{steel}} = 206 \text{ GPa}$)

The magnitude of deflection is quite low and should not pose any misalignment issues independently. To establish a sense of scale, the maximum deflection is approximately 0.0000041% of the shafts diameter, or 0.0004% of the thickness of a human hair.

Slider – Crank Mechanism for Demonstration and Experimentation

Crosshead Guide Natural Frequency Analysis

The amplitude of oscillations will increase dramatically if the oscillating frequency of the equivalent vertical point load approaches the crosshead guides' natural frequency.

For each rotation of the crank, this load is applied once along the positive y axis and once along the negative y axis. Therefore the driven frequency is equal to the operational frequency of the engine. For example, when the engine speed is 100 rpm, the driving frequency is 100 oscillations per minute, or 1.67Hz. The shaft stiffness (k) is derived from the deflection equation above, utilizing the relationship $F = k \cdot x$ and solving for k.

$$\text{Stiffness of crosshead guides } k = \frac{48EI}{L^3} = 2.04E11 \text{ N/m}$$

$$\text{Natural frequency } \omega_n = \sqrt{\frac{k}{m}} = 2.6E6 \text{ rad/s} = 2.5E7 \text{ rpm (with } m = 0.03 \text{ kg)}$$

The natural frequency of the crosshead guides is far greater than the maximum achievable driving frequency and as such will not pose any issues during operation.

Slider – Crank Mechanism for Demonstration and Experimentation

Damper Selection through Vibration Analysis

The engine is mounted to a rigid plate. This plate will experience vibrations during operation which correspond to the oscillating mass of the piston, crosshead, connecting rod and crankshaft. The shaking forces caused by these oscillating masses have been previously calculated using a lump mass approximation and are shown below for reference. Note that gravity is neglected in the following calculations.

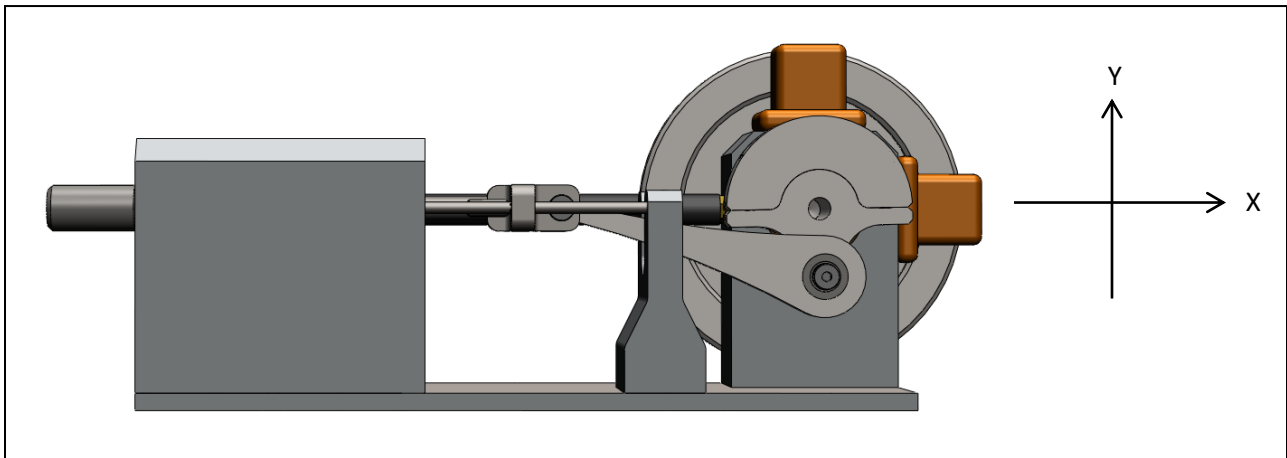


Figure 50: Solid Model for Engine with Axes Defined

Shaking force X component
$$F_{sx}(\theta) := -M_a \cdot (R \cdot \omega^2 \cdot \cos(\theta)) - M_b \cdot \left[R \cdot \omega^2 \left(\cos(\theta) + \frac{R}{L} \cdot \cos(2\theta) \right) \right] = 185 \text{ N}$$

Shaking force Y component
$$F_{sy}(\theta) := -M_a \cdot (R \cdot \omega^2 \cdot \sin(\theta)) = 50 \text{ N}$$

Compression type dampers will be utilized to isolate vibrations in both the x and y directions. Four dampers will be mounted along the x axis, isolating the x component of the shaking force. Four additional dampers will be mounted along the y axis, isolating the y component of the shaking force.

Slider – Crank Mechanism for Demonstration and Experimentation

Shape factor $K_T = 1 + \beta \left(\frac{S}{S'}\right)^2 = 1.22$

S = cross sectional area = 0.00107m

S' = nonload-carrying area = 0.00304m

β = nondimensional constant = 1.75

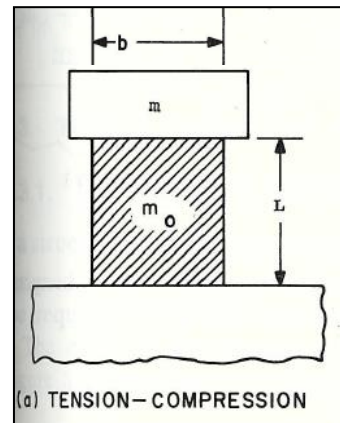


Figure 51: Damper Loading Conditions

Stiffness of tension-compression type damper $k = E \frac{S \cdot K_T}{L} = 3.7E5 \text{ Nm}$ (with $E = 7.2 \text{ MPa}$; $L = 0.0254 \text{ m}$)

Four dampers are positioned along the x and y axes, quadrupling the effective stiffness

Displacement along x axis $x = \frac{F_x}{4k} = 1.24E-4 \text{ m}$

Displacement along y axis $y = \frac{F_y}{4k} = 3.38E-5 \text{ m}$

The oscillating displacement caused by the engine's shaking force is quite low when compression type dampers are introduced. The maximum operational displacement is approximate 1/8 of a millimeter.

Slider – Crank Mechanism for Demonstration and Experimentation

Pin Stress Analysis

The maximum pin shear occurs at the maximum loading for both the crank and wrist pin. Both experience the same force of 185N in the x-direction as a maximum. These maxima occur 90° out of phase. The wrist pin's maximum occurs at the opening of the exhaust valve when the piston is at TDC. The maximum force applied to the crank pin occurs half way through the pistons stroke when the crank is vertical in z. The shear stress for both of these pins will be equal because they have the same applied force and the same cross sectional area and are described by the equation:

$$\tau = \frac{F_{max}}{A_{pin}} = \frac{F_{max}}{\pi r^2} = \frac{185N}{\pi * (0.00476m)} = 12371.29Pa = 12.371kPa$$

The maximum pin shear stress is 12.371 kPa which is significantly less than the yield.

Slider – Crank Mechanism for Demonstration and Experimentation

Preliminary Valve Design

Cylinder Pressurization Analysis

In order to determine if the engine would operate based on the inlet airline dimension as well as the valve geometry the group performed a simple calculation for required mass flow. Assuming that the pressure in the cylinder was constant throughout, and a pressure of 35psi (241.3650kPa) was required for the process it was possible to check the design dimensions for the inlet port and piping. The total volume for the inlet piping and cylinder at bottom dead center for the piston, (i.e. full expansion) was 0.0001927m^3 . Given that dry air at 35psi has a density determined by: $\rho = \frac{P}{R*T}$ where

$R=287.058 \text{ kJ/kg}\cdot\text{K}$ and T is absolute temperature assumed to be 300K (approximately room temperature). Given these parameters the density of air is 2.80274kg/m^3 . Given the volume of the chamber the total mass required to maintain this pressure is calculated by $m = \rho * V$, resulting in a total mass of $5.40*10^{-5} \text{ kg}$. This mass has to enter the cylinder through the inlet piping and valve within the open valve time which is determined by the angular velocity of the crankshaft. At 200RPM the valve which is ported for 80° on the crankshaft is open for 0.608sec. This means that in order for the cylinder to pressurize, the valve and port must be able to handle $8.88*10^{-5}\text{kg/sec}$ of dry air.

Experimental Evaluation of Mass Flow through System

Mass flow into the system is provided by a compressor, providing consistent air pressure of 100PSI. As the valve opens, pressurized air must flow through 14in of 0.375in inner diameter piping, ending with a 90° bend, before reaching the cylinder. An experiment was conducted to determine an approximate value for mass flow through this section of pipe. A tank of known volume was pressurized to 80PSI, resulting in air density of 7.74kg/m^3 . The total mass of air inside the tank was calculated to be 0.42kg. Piping of similar geometry to that used on the pneumatic engine was connected to the pressurized tank. A valve was rapidly opened and the time required for tank pressure to return within 90% of atmospheric pressure was recorded. The average depressurization time was 18.14s. This corresponds to an approximate average mass flow rate of 0.023kg/s, over 250 times the minimum amount required to pressurize the cylinder to 30PSI.

Slider – Crank Mechanism for Demonstration and Experimentation



Figure 52: Tank Pressurization Experiment

Some sources of error exist in this experiment. The air leaving the pressurized tank in this experiment is not encountering resistance from a piston like in the engine. However, the pressure in the tank is rapidly decreasing, unlike the more stable pressure of the compressor. Even so, the scale of the safety factor is sufficient to conclude that the piping does not inhibit the pressurization of the cylinder.

Slider – Crank Mechanism for Demonstration and Experimentation

Manufacturing

Limitations and Variations

When machining the parts it was vital to compensate for potential error in the machine, and verify that the final size would meet the requirements dictated by these fits. If there was variation from the desired size this had to be accounted for and the appropriate offsets adjusted in order to generate the desired dimension. This error came as a result of several factors including, variation in probe calibration, and accuracy, tool wear, tool deflection, and overall machine capability. Using measuring instruments from the Washburn shops including 0.0001 Outside Micrometers, Bore Gauges in conjunction with the Micrometers as well as Vernier Calipers the group was able to accurately measure and meet the design specified fits.

The critical dimensions as mentioned in the design for manufacturing section occurred where there was a press or sliding fit. In order to guarantee the desired tolerance was achieved, the group allowed and compensated for variation using the CAM software and machine offsets. Though the machined parts in some cases varied from the nominal values designated by the design, the clearance and interference values were maintained. The true values of the fits were measured with the use of telescoping bore gauges and a 0.0001" micrometer.

Slider – Crank Mechanism for Demonstration and Experimentation

Crankshaft Operations and Fourth Axis Machining

In order to manufacture each of the components for the project, the group utilized the CAM software Esprit. With this program it was possible to use the Solidworks model to generate the required tool-paths in order to physically produce the parts. Features were generated using existing geometry then operations from these features. The operations required that the group determine appropriate Surface footage per minute and feed-rates based on tool geometry and material as well as based on work-piece material. For the purpose of this report the focus of manufacturing will be placed on the Crank-shaft.

To manufacture the crank, a piece of 5" SAE-1018 Plain Carbon Steel stock material was required. The stock was first cut to the appropriate length (8.5") using a horizontal band-saw. The next operation required the stock be turned to a specific geometry which required the use of the HAAS SL20 CNC Lathe. In order to fixture the stock in the machine the group had to first bore the jaws (in a three jaw chuck) to the appropriate 5" diameter. This was accomplished using a $\frac{3}{4}$ " boring bar and the intuitive turning option available on the lathe. The next step was to face and chamfer each side of the stock so that the material both sat squarely in the chuck, and maintained concentricity in the machine. The stock was also center-drilled on one side so that the use of the tailstock and live center was possible for support of the stock. The stock was then turned down to the nominal fit required by the design tolerances. This allowed the group to compare the actual turned diameter with the expected output from the machine. The group found that the machined output for an Outer Diameter turning operation was 0.004" larger than was expected. Taking this variation from the expected output into account the group changed the tool offset within the machine in order to compensate for the deviation. The group also measured the bronze bearing in the same fashion when boring the inner diameter to compensate for the deviation in order to match the design tolerance specifications. With the offsets accounted for the final dimension of the crankshaft was 1.1292" and the inner diameter of the bearing was 1.1300". The clearance generated fell adequately in the range specified by the Class RC-3 Precision Sliding Fit. The diameter of the shaft and bore of the bearing were however oversized, because of initial difficulty in measurement and machine capabilities. The bearing's inner diameter was oversized by 0.004" when bored to the nominal size requiring that the crankshaft also be oversized to compensate. The CAM file simulation for the turning operation is as follows:

Slider – Crank Mechanism for Demonstration and Experimentation

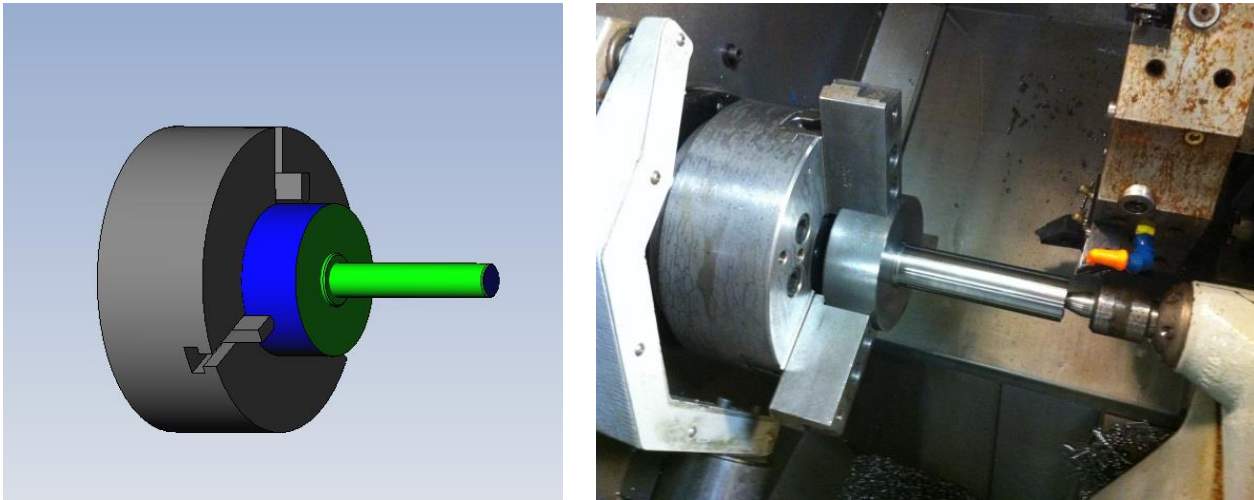


Figure 53: (Left) Esprit CAM Simulation for OD Turning of Crankshaft; (Right) Crankshaft OD Turning

Upon completion of the turning operation the group needed to mill off extra material that was used to hold the stock securely in the jaws during the turning. This required the use of a manual vertical three-jaw chuck for the HAAS VM3 milling machine. In order to fixture the crankshaft the group had to make aluminum soft-jaws which would be bored to the diameter of the shaft. Once the jaws were machined the piece was fixtured in the chuck as follows.

The chuck was bolted into the table and the group used the HAAS VM3 to mill the excess material off of the top of the crank portion of the crankshaft so that the thickness of the crank-section was correct. The group then used the same fixture to mill out the profile of the crank section and drill out the exhaust port in the center of the crankshaft. The result appears as follows.



Figure 54: Three Jaw Rotary Chuck Fixture for Crankshaft Milling

Slider – Crank Mechanism for Demonstration and Experimentation



Figure 55: Crankshaft Profile Milling

The final operation on the crank included milling the valve grooves in the shaft as well as drilling the clearance holes for the balance weights on the flats of the crank profile and the exhaust port from the exhaust valve groove. This operation required the use of the fourth-axis rotary chuck in the HAAS VM3. In order to fixture the shaft inside of the rotary chuck without marring the critical surface of the shaft, the group machined a clamp collar to hold the steel shaft in the hardened steel jaws. The clamp collar made of aluminum was machined to the correct inner diameter to match the outer diameter of the shaft and was turned down to have a wall thickness of 0.125". A vertical cut was made on one side of the collar and thus when the jaws closed on the collar it would clamp to the shaft. The fixture for the fourth-axis is shown below.



Figure 56: Rotary Fixture with Clamp Collar for 4th Axis Milling

Slider – Crank Mechanism for Demonstration and Experimentation

The next step was to mount the 4th axis rotary and tail-stock into the HAAS VM3 Milling machine, and check that the two components were properly squared on the table in the machine. The group used dowel pins as a backstop for the rotary chuck and made adjustments while using a dial indicator to ensure that the chuck was square in the machine. The same process was repeated for the tailstock and finally for the part to ensure the work-piece was aligned properly within the machine.

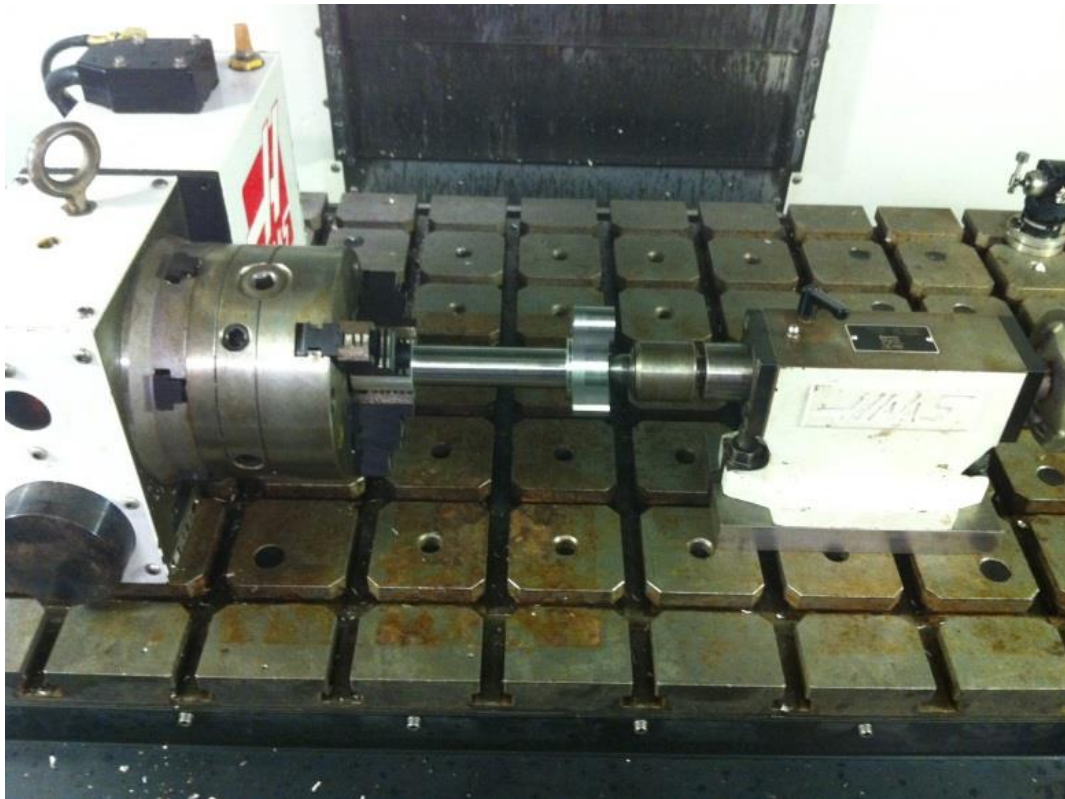


Figure 57: Crankshaft Fixtured For 4th Axis Milling

Once the part was securely mounted in the machine the rotary had to be correctly zeroed to match the orientation of the part in the CAM software. The group rotated the 4th axis and measured, using a dial indicator, the flat surfaces of the crankshaft until they were perfectly level and parallel with the x and y axes of the table. Once the machine setup was complete the group ran the program generated in Esprit to drill and groove the shaft. The finished shaft in the machine is shown below.

Slider – Crank Mechanism for Demonstration and Experimentation



Figure 58: Finished Crankshaft

All of the Esprit CAM files can be found in the appendix. The tooling used for the steel crankshaft were produced by Kenametal™ and the turning inserts for the steel were 55° Polycarbonate Diamond while the milling operations used DHEC coated carbide end-mills. The drilling was done using high speed steel uncoated twist drills.

Slider – Crank Mechanism for Demonstration and Experimentation

Machining Images

Results of the machining process are depicted below for several of the pneumatic engine's components.

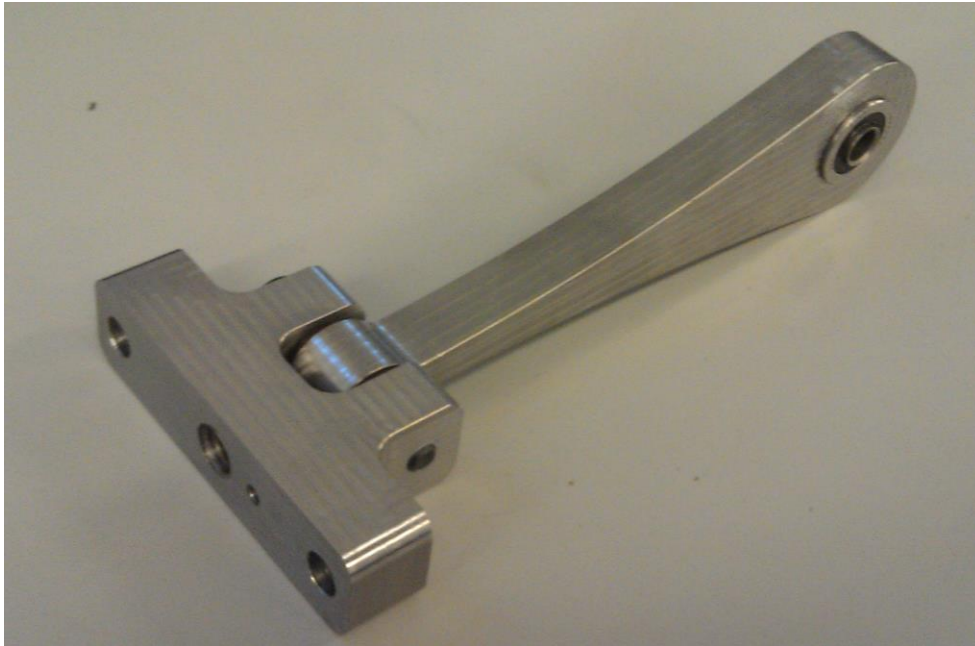


Figure 59: Finished Connecting Rod and Cross-head

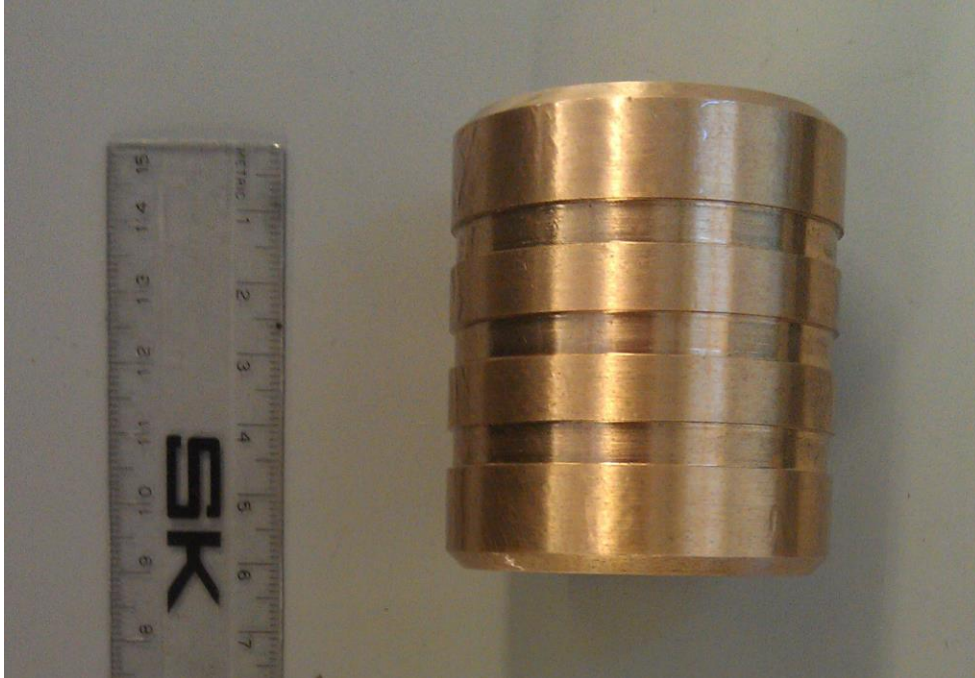


Figure 60: Finished Piston



Figure 61: Sleeve ID boring with 1.5" Boring Bar

Slider – Crank Mechanism for Demonstration and Experimentation



Figure 62: Piston inside Sleeve Demonstrating Airtight Seal

Slider – Crank Mechanism for Demonstration and Experimentation

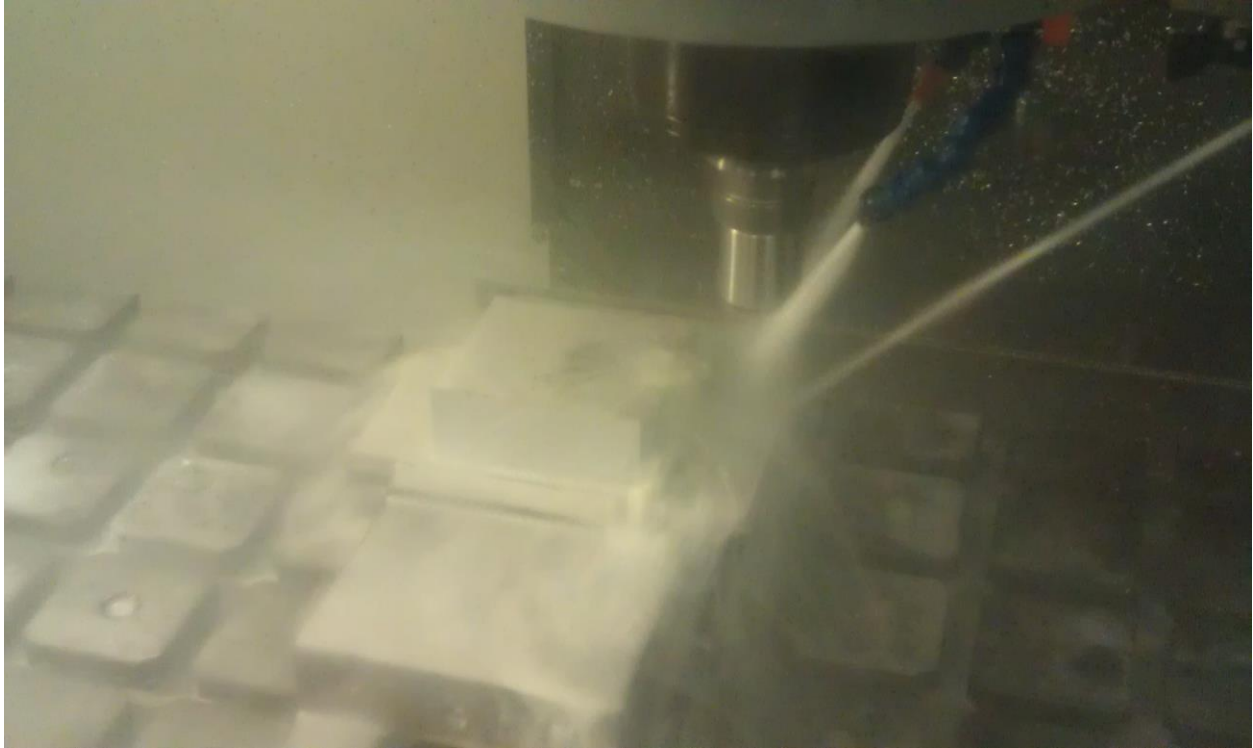


Figure 63: Cylinder Block Machining

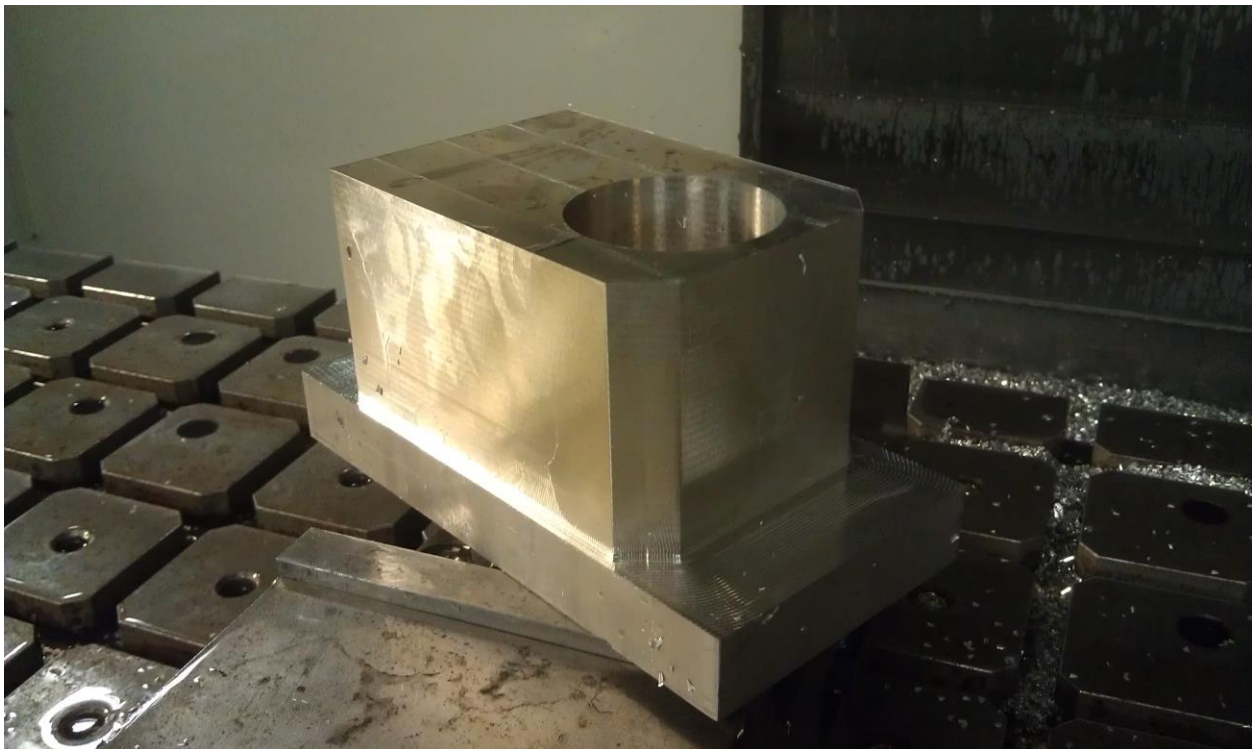


Figure 64: Cylinder Block mid-operation

Slider – Crank Mechanism for Demonstration and Experimentation

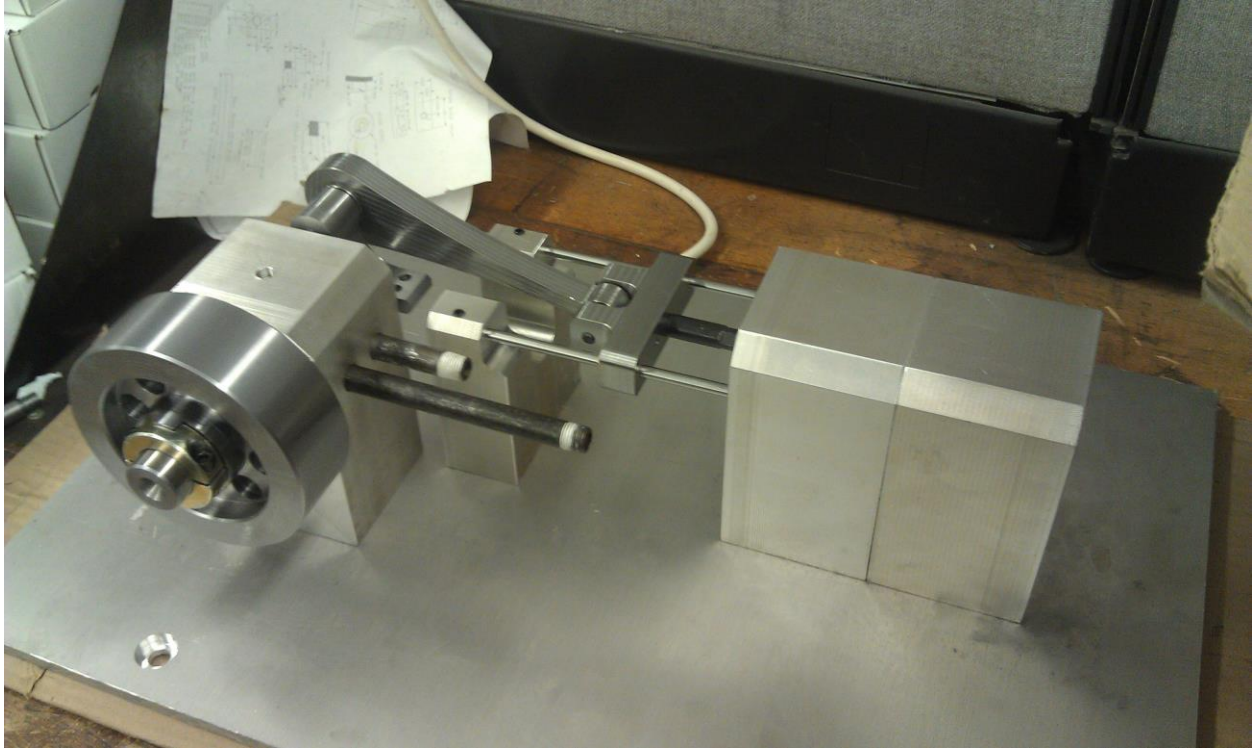


Figure 65: Initial Engine Assembly

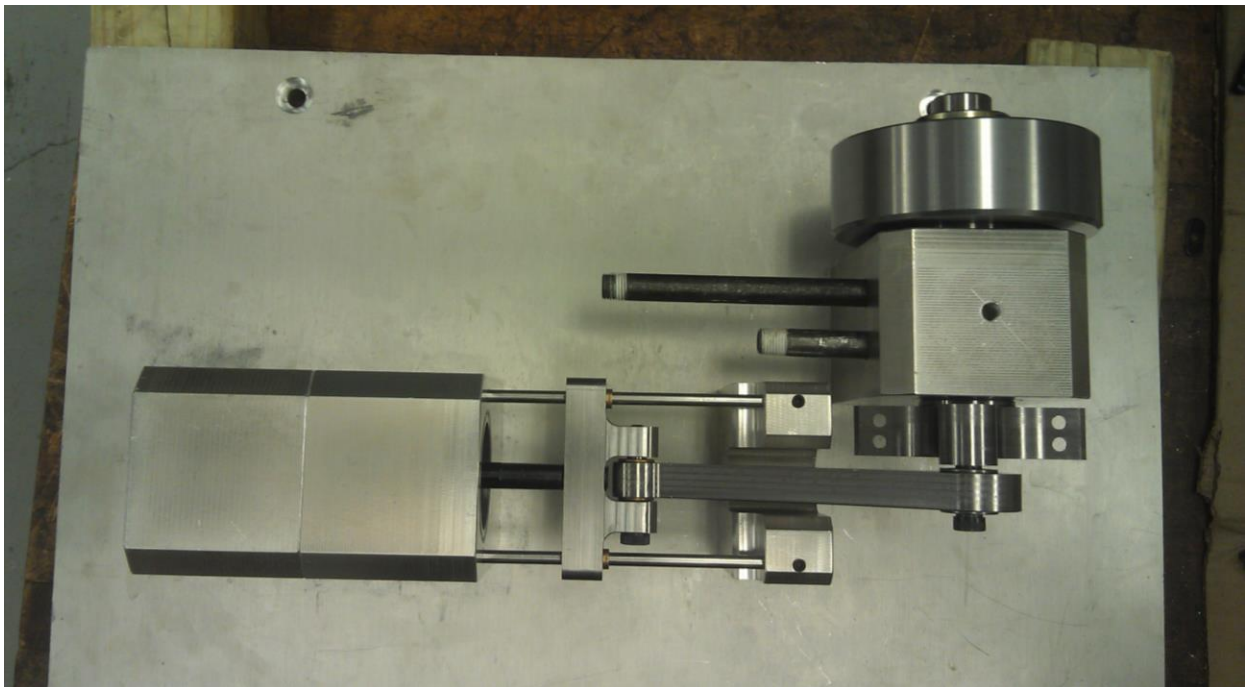


Figure 66: Top View Initial Engine Assembly

Slider – Crank Mechanism for Demonstration and Experimentation

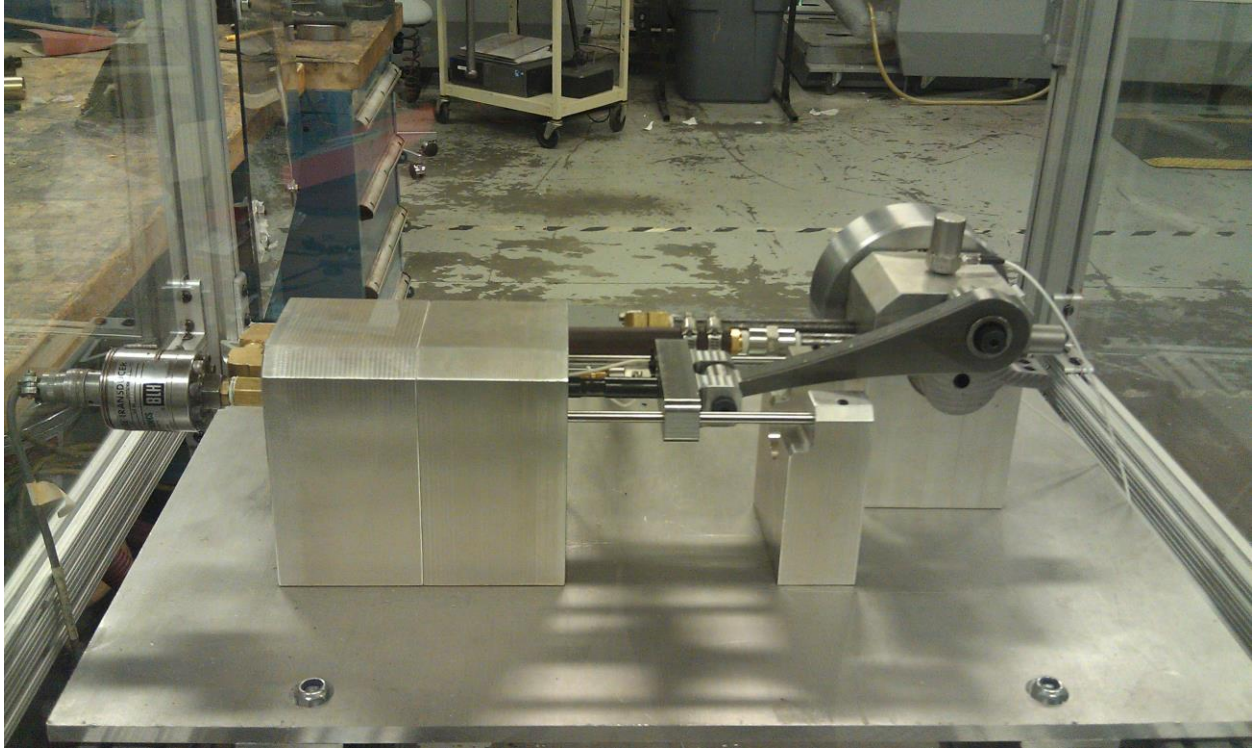


Figure 67: Finished Engine Assembly

Results of Initial Testing

Slider Acceleration and Cylinder Pressure

Unbalanced Configuration

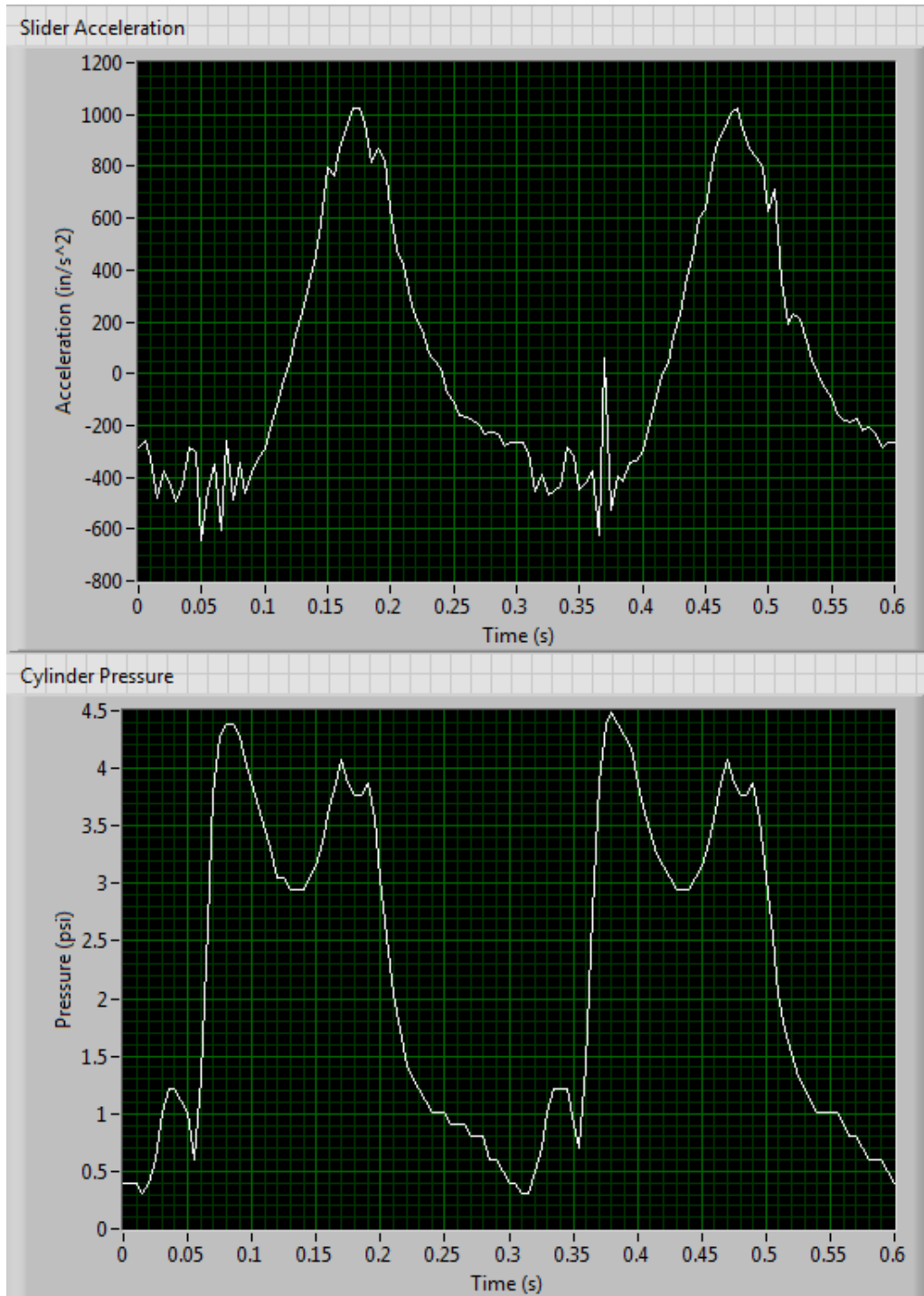


Figure 68: Slider Acceleration and Cylinder Pressure for Unbalanced Configuration

Slider – Crank Mechanism for Demonstration and Experimentation

Statically Balanced Configuration

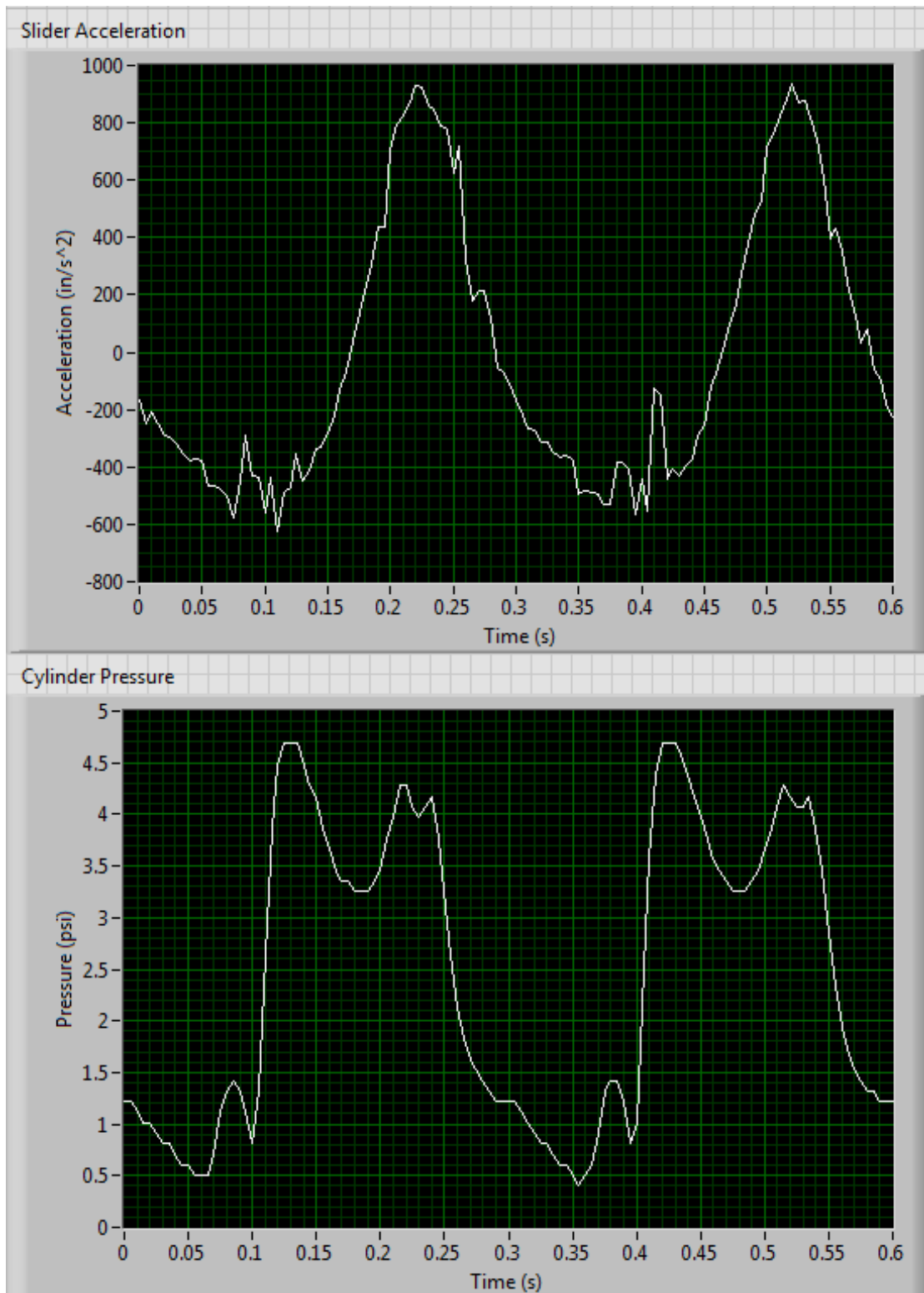


Figure 69: Slider Acceleration and Cylinder Pressure for Statically Balanced Configuration

Slider – Crank Mechanism for Demonstration and Experimentation

Dynamically Balanced Configuration

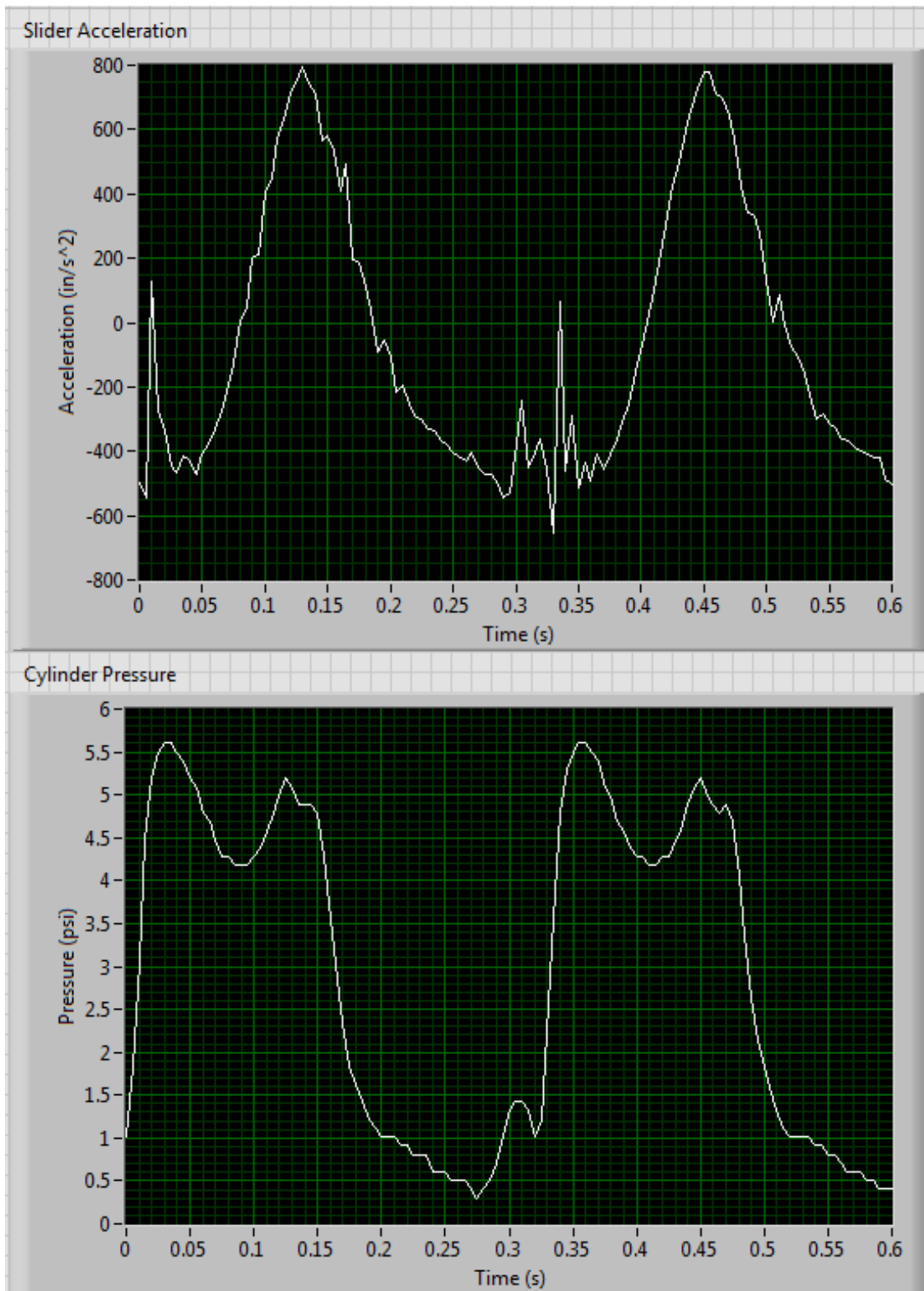


Figure 70: Slider Acceleration and Cylinder Pressure for Dynamically Balanced Configuration

Shaking Forces

Unbalanced Configuration

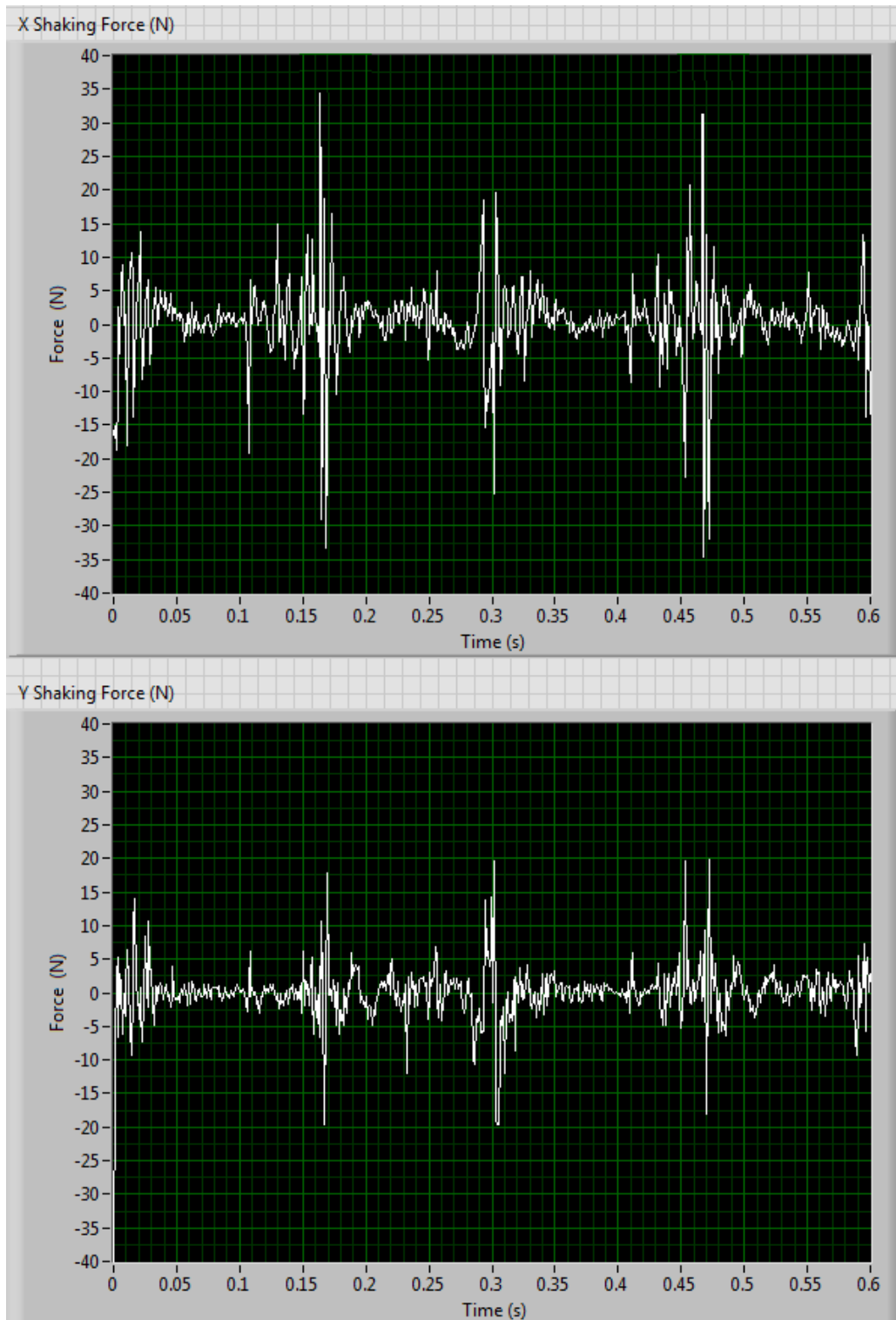


Figure 71: Shaking Forces in X and Y for Unbalanced Configuration

Slider – Crank Mechanism for Demonstration and Experimentation

Statically Balanced Configuration

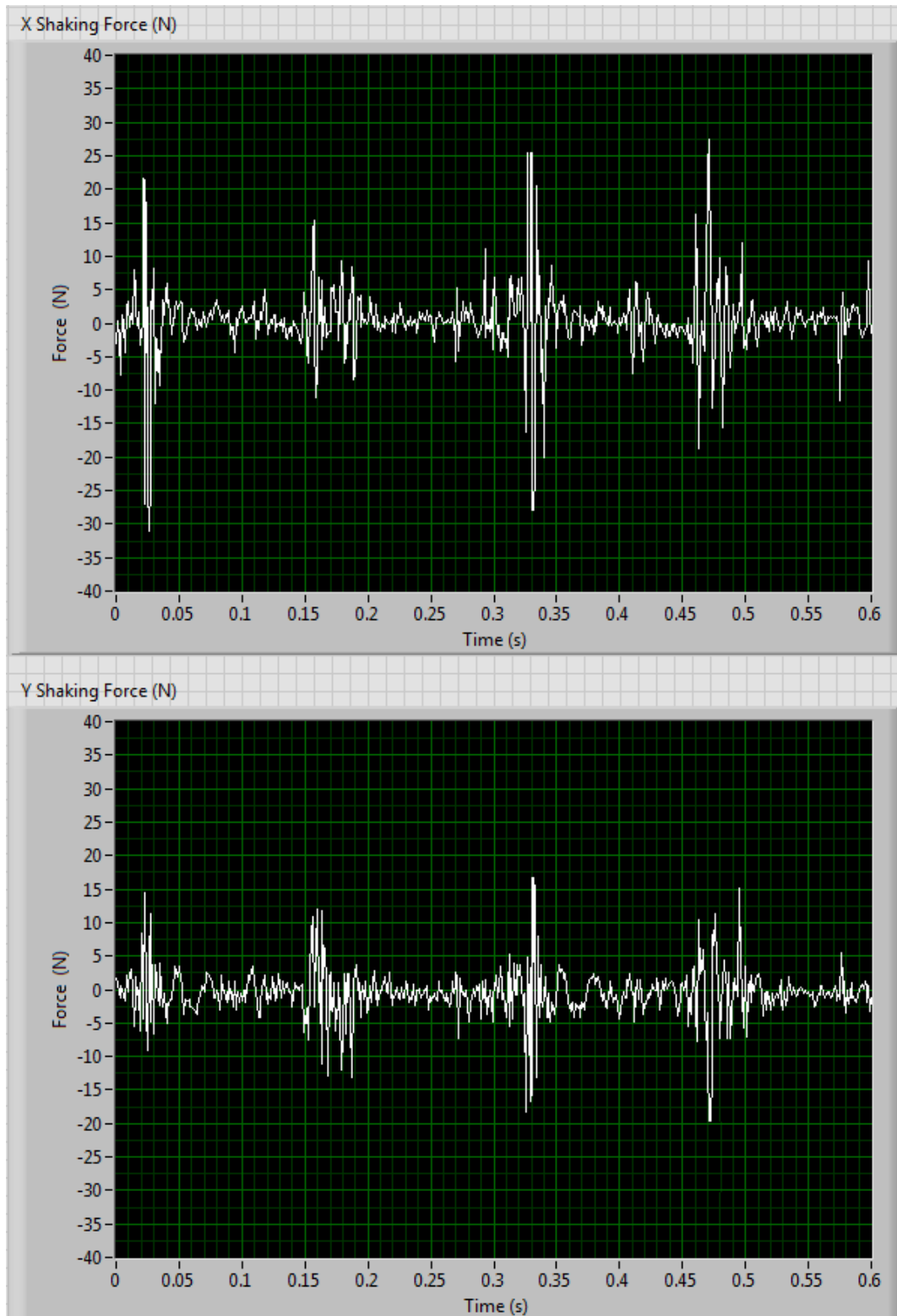


Figure 72: Shaking Forces in X and Y for Statically Balanced Configuration

Slider – Crank Mechanism for Demonstration and Experimentation

Dynamically Balanced Configuration

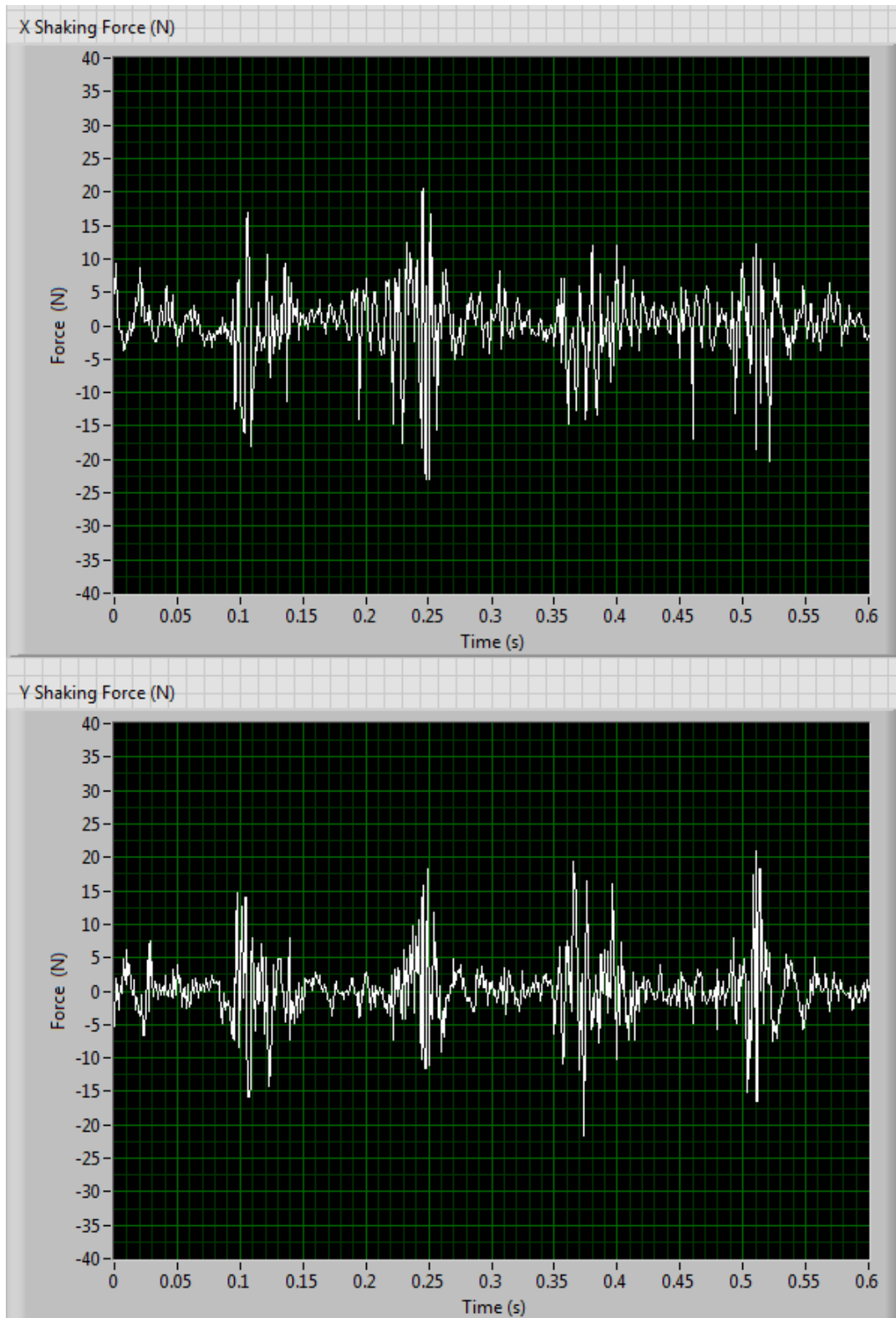


Figure 73: Shaking Forces in X and Y for Dynamically Balanced Configuration

Slider – Crank Mechanism for Demonstration and Experimentation

Comparison of Analytical and Experimental Results

In General, the experimental results compared well with the analytical results. There were some inconsistencies due to differences in real world operation versus theoretical operation, as well as some degree of error introduced by the instrumentation methods and the fixturing of the engine.

The first results analyzed were the pressure data for the cylinder. The expected calculated values for pressure data resembles a pseudo-sinusoidal curve, with peak values matching that of the inlet pressure and minimum value being zero when the valve is closed. The actual measured results were somewhat different. Although the general form of the pseudo-sinusoidal curve is visible with peak pressure only about 2 psi below input pressure, there are also some local extremum values that were not expected. These are likely results of the shock wave experienced in the long tube between the crank-valve and the cylinder. Since air is a compressible fluid, shock waves are formed during the pressurization of the cylinder. The local extremums become larger with higher input pressure which further supports this hypothesis.

In comparing the results of the real slider accelerations to the analytical results, some interesting trends were observed. The peak maximum and minimum slider accelerations were determined to be (+/- 720 in/sec²) for operation at 200 rpm with constant angular velocity. In actuality, the engine does not operate with constant angular velocity. The engine acceleration is much greater on the power stroke than on the return stroke, since it is only single acting. This fluctuation in acceleration is larger in the unbalanced and statically balanced states than the dynamically balanced state. In the dynamically balanced state, the slider acceleration matches the analytical results most closely. In all cases, the acceleration curve resembled the analytical curve quite closely, but with some level of noise. The peak acceleration values for all 3 balance cases investigated are shown next.

1. Unbalanced
Max acceleration: 1010 in/sec²
Min acceleration: -700 in/sec²
2. Statically Balanced
Max acceleration: 980 in/sec²
Min acceleration: -610 in/sec²
3. Dynamically Balanced
Max acceleration: 800 in/sec²
Min acceleration: -610 in/sec²

Slider – Crank Mechanism for Demonstration and Experimentation

The vibrational analysis yielded results that were quite noisy but still resembled the analytical results. The vibration was measured using two accelerometers mounted on the crank bearing support, and can be seen in any of the images of the engine. These accelerations were then multiplied by the mass of the engine block to calculate the shaking force in Newtons. The analytical values for the shaking force were obtained using the lumped mass engine model, and this procedure is described in the results section. Unfortunately, the method of obtaining shaking force measurements introduces a large amount of error. The slight noise present in the acceleration measurements is made more apparent when these values are multiplied by mass. Furthermore, the fact that the engine is mounted in a movable enclosure introduces reverberated shaking in the system. As a result of this, there is a large amount of noise present in the experimental data. The peak values for the vibrational results are as follows.

Balance State (200 RPM)		Measured Results (N)		Analytical Results (N)	
		X	Y	X	Y
Unbalanced	Max	35	20	28	7.9
	Min	-35	-20	-40	-7.9
Statically Balanced	Max	30	15	20	0
	Min	-30	-15	-32	0
Dynamically Balanced	Max	20	15	10	12
	Min	-20	-15	-21	-12

Figure 74: Shaking Force Comparison Between Balance States

Although the measured results do not always match the analytical values completely, they do bear a close resemblance, and the differences between the two can be explained. The pressure measurements vary due to the fact that air is a compressible fluid. Slider acceleration varies from the analytical values because the engine doesn't actually operate at constant angular velocity which the analytical calculation assumes. The high noise level present in the vibration measurement is mainly due to the fact that the results are measured using accelerometers and multiplied by the engine block mass. However, in general, the values do correlate well with the analytical data.

Slider – Crank Mechanism for Demonstration and Experimentation

Conclusion

The production of the slider-crank mechanism was successful, with minimal variation from the original design required. Specified tolerances of interfacing parts were met and functioned as intended. Assembly was conducted through a procedure that allowed for incremental adjustments, minimizing system friction. Satisfactory operation of the engine was achieved with minimal tuning. The engine is capable of operating at angular velocities ranging from 80 to 330 rpm, using a balancing weight optimized for 200rpm. A wider range of operational speeds could be achieved with alternative balancing weights. Motion is achievable with cylinder pressures as low as 4.5psi, with a loss of only 2 psi in the crankshaft-bearing interface. The reduction in shaking force achieved through use of the balance weights is apparent both visually and in recorded data. Values recorded by the accelerometer and pressure transducer, mounted to the slider and cylinder respectively, provide insight into the operational characteristics of piston driven engines. All experimental values were reasonable when compared with analytical calculations.

Slider – Crank Mechanism for Demonstration and Experimentation

Discussion

During the project the group encountered difficulties as a result of factors such as machine and tooling limitations, time constraints and budgetary constraints. The major limitation in the project from the beginning was lack of adequate funding for the raw materials and required tooling for the machine shop. This limited budget made it necessary to purchase larger wholesale pieces of stock (cut-offs) which required significantly more time to both cut to size and to machine.

In addition to the greater required cycle times, the lack of budget for specialty tooling also significantly increased the manufacturing time. The available tooling in the machine shop was better suited for smaller geometries than that required for the project. In order to complete several of the parts it was necessary to run multiple operations using different tooling in order to achieve the desired output. Adjustments such as these increased the total time required to machine these parts. The increased time required for machining changed the group's timeline for the project limiting the available time for experimentation.

The group also encountered challenges in achieving all of the desired outputs because of the strict timeframe of the project. The time required to fabricate the final design was much greater than was anticipated at the beginning of the project. The increased time spent on machining and assembly of the engine reduced the available time for experimentation of the engine. Though the group was able to extract useful data from the project, interpretation and analysis of the data was limited due to the limited available time. Had the group continued, filters may have been generated in order to remove noise and to produce a clearer representation of the output.

Slider – Crank Mechanism for Demonstration and Experimentation

Recommendations for Future MQPs

The group considered doing many additional things to the project but due to a combination of time and budgetary constraints not all of these tasks could be completed. There are a number of additional things that could be incorporated into the project which could encompass an entire new MQP. Some important things to add to the slider-crank device would be a data acquisition system and computer. Since these two things would far exceed the budget for the project they could not be incorporated into it, and instead had to be borrowed for the duration of the project. Keeping a DAQ system and computer with the device would make it much easier to set up for demonstrations. These items would need to be incorporated into the device in such a way that they would not be affected or damaged by the shaking of the mechanism. There are also a number of things that could be added to the project in order to acquire better data for assessment. These include force sensors, a shaft encoder, and a driver motor.

Currently, the shaking forces of the engine are measured using accelerometers, but if force transducers were incorporated into the system, they would provide more accurate and more detailed results. It may be possible to incorporate force transducers into the damper system that supports the engine, in order to directly monitor shaking forces.

A shaft encoder could be attached to the end of the crankshaft to monitor engine speed. A shaft encoder is a device that is used to measure rate of rotation per unit time on a shaft. This device could be used to monitor the rpm of the engine, as well as the angular velocity and corresponding coefficient of fluctuation. Since it is known that the engine does not operate with constant angular velocity, it would be important to know the rate at which this value fluctuates throughout the engine stroke. The fluctuation corresponds directly to the resulting slider accelerations and shaking force.

A driver motor could also be incorporated into the slider-crank system. Using a driver motor to drive the mechanism as opposed to compressed air would yield very different results for measured shaking force and slider acceleration. This is because with a driver motor, the engine would operate with a constant angular velocity, as opposed to the fluctuating angular velocity of the pneumatically driven configuration.

The next recommendations involve serious research and engineering and could be incorporated into a future MQP. This includes the design and incorporation of an adjustable dynamic counter-balance and adjustable flywheel. Design of these two items would be complicated but the basic goal would be

Slider – Crank Mechanism for Demonstration and Experimentation

to have a balance with an adjustable center of gravity, and a flywheel with an adjustable mass-radius product. The adjustment could be facilitated by mechanical means or by a servo-driven system. By having an adjustable counterbalance, the balance conditions could be changed so that the engine can operate dynamically balanced at any speed. An adjustable flywheel could be used to change the coefficient of fluctuation of the engine throughout the power stroke. Such items would require time for research and design, but the end product could yield informative results.

Slider – Crank Mechanism for Demonstration and Experimentation

Figures

Figure 1: Decision Matrix used to rank proposed designs.....	5
Figure 2: Elmer's Standby Model Engine	6
Figure 3: Isometric View Solid Model of Slider Crank Mechanism	7
Figure 4: Top View Solid Model of Slider Crank Mechanism	7
Figure 5: Assembly Drawing for Slider Crank Mechanism	8
Figure 6: (Left) Solid Model of Crankshaft Top View; (Right) Solid Model of Crankshaft Isometric View....	8
Figure 7: Slider Position vs. Crank Angle	13
Figure 8: Crankshaft X Displacement vs. Crank Angle	14
Figure 9: Crank Y Displacement vs. Crank Angle.....	14
Figure 10: Slider Velocity vs. Crank Angle	15
Figure 11: X Component of Crank Velocity vs. Crank Angle	16
Figure 12: Y Component of Crank Velocity vs. Crank Angle.....	16
Figure 13: Slider Acceleration vs. Crank Angle.....	17
Figure 14: X-Component of Crank Acceleration vs. Crank Angle.....	18
Figure 15: Y-Component of Crank Acceleration vs. Crank Angle	18
Figure 16: Slider-Crank Coordinate System and Variables	19
Figure 17: Unbalanced Slider-Crank model (see Norton Design of Machinery fig. 13-12 p.618).....	19
Figure 18: X-Component Shaking Force vs. Crank Angle (Unbalanced)	20
Figure 19: Y-Component Shaking Force vs. Crank Angle (Unbalanced).....	21
Figure 20: Total Magnitude of Shaking Force (Unbalanced)	21
Figure 21: Statically balanced slider-crank model (see Norton Design of Machinery fig13-23 p. 632).....	22
Figure 22: X-Component Shaking Force vs. Crank Angle (Statically Balanced).....	23
Figure 23: Y-Component Shaking Force vs. Crank Angle (Statically Balanced).....	23
Figure 24: Total Magnitude Shaking Force (Statically Balanced).....	24
Figure 25: Dynamically Balanced Slider-Crank Model (see Norton Design of Machinery fig 13-23 p.632)	24
Figure 26: X-Component Shaking Force vs. Crank Angle (Dynamically Balanced).....	26
Figure 27: Y-Component Shaking Force vs. Crank Angle (Dynamically Balanced).....	26
Figure 28: Total Magnitude Shaking Force vs. Crank Angle (Dynamically Balanced)	27
Figure 29: Crank-Shaft Fixtured for 4th Axis Machining	28
Figure 30: Free Body Diagram for Crankshaft Side View	29

Slider – Crank Mechanism for Demonstration and Experimentation

Figure 31: Free Body Diagram of Crankshaft Isometric View	29
Figure 32: Stress Concentration Locations	29
Figure 33: Stress Concentration Table	30
Figure 34: FEA Boundary Conditions for Crankshaft Analysis.....	32
Figure 35: FEA Boundary Condition – Interaction with Bearing	33
Figure 36: FEA Boundary Condition – Fixed by Flywheel.....	34
Figure 37: FEA Boundary Condition – Load Applied by Connecting Rod Pin Connection.....	34
Figure 38: FEA Boundary Conditions.....	35
Figure 39: FEA Mesh	35
Figure 40: FEA Von Mises Stress Gradient Isometric View	36
Figure 41: FEA Von Mises Stress Gradient Front View	36
Figure 42: FEA Von Mises Stress Gradient Exhaust Port.....	37
Figure 43: FEA Von Mises Stress Gradient	38
Figure 44: FEA Von Mises Stress Gradient with Intake Port Shown	38
Figure 45: FEA Von Mises Stress Gradient Top View	39
Figure 46: FEA Deflection Gradient.....	40
Figure 47: Free Body Diagram for Slider Crank.....	42
Figure 48: FBD Cross-head guide	42
Figure 49: Diagram for Beam Deflection	43
Figure 50: Solid Model for Engine with Axes Defined.....	45
Figure 51: Damper Loading Conditions.....	46
Figure 52: Tank Pressurization Experiment	49
Figure 53: (Left) Esprit CAM Simulation for OD Turning of Crankshaft; (Right) Crankshaft OD Turning	52
Figure 54: Three Jaw Rotary Chuck Fixture for Crankshaft Milling.....	52
Figure 55: Crankshaft Profile Milling.....	53
Figure 56: Rotary Fixture with Clamp Collar for 4th Axis Milling.....	53
Figure 57: Crankshaft Fixtured For 4th Axis Milling.....	54
Figure 58: Finished Crankshaft.....	55
Figure 59: Finished Connecting Rod and Cross-head.....	56
Figure 60: Finished Piston	56
Figure 61: Sleeve ID boring with 1.5" Boring Bar	57
Figure 62: Piston inside Sleeve Demonstrating Airtight Seal.....	58

Slider – Crank Mechanism for Demonstration and Experimentation

Figure 63: Cylinder Block Machining.....	59
Figure 64: Cylinder Block mid-operation	59
Figure 65: Initial Engine Assembly	60
Figure 66: Top View Initial Engine Assembly	60
Figure 67: Finished Engine Assembly.....	61
Figure 68: Slider Acceleration and Cylinder Pressure for Unbalanced Configuration	62
Figure 69: Slider Acceleration and Cylinder Pressure for Statically Balanced Configuration	63
Figure 70: Slider Acceleration and Cylinder Pressure for Dynamically Balanced Configuration	64
Figure 71: Shaking Forces in X and Y for Unbalanced Configuration	65
Figure 72: Shaking Forces in X and Y for Statically Balanced Configuration	66
Figure 73: Shaking Forces in X and Y for Dynamically Balanced Configuration	67
Figure 74: Shaking Force Comparison Between Balance States	69

Slider – Crank Mechanism for Demonstration and Experimentation

Bibliography

Erik, Oberg. *Machinery's Handbook Toolbox Edition*. Diss. Industrial Press, 2008.

Norton, Robert L. *Design of machinery: an introduction to the synthesis and analysis of mechanisms and machines*. WCB McGraw-Hill, 1999.

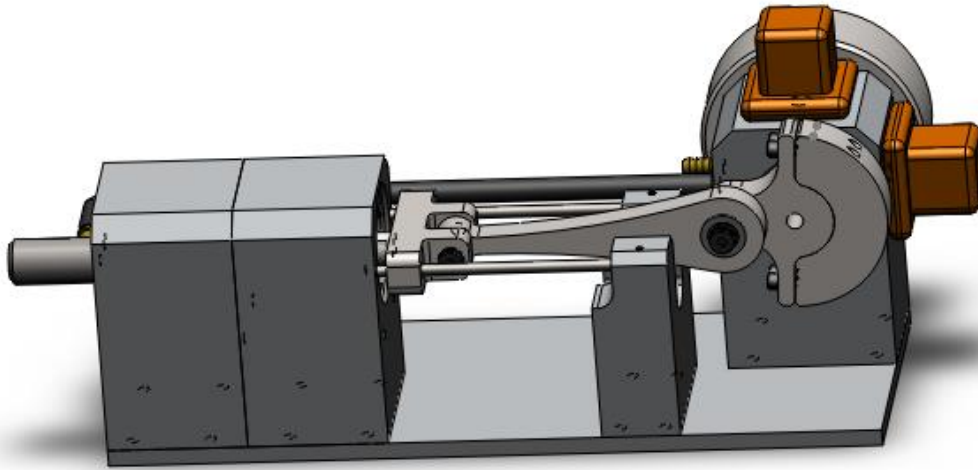
Norton, Robert L. *Machine Design: An Integrated Approach, 2/E*. Pearson Education India, 2000.

Verburg, Elmer. *Elmer's Engines*. Old Orchard Pub. Service, 1988.

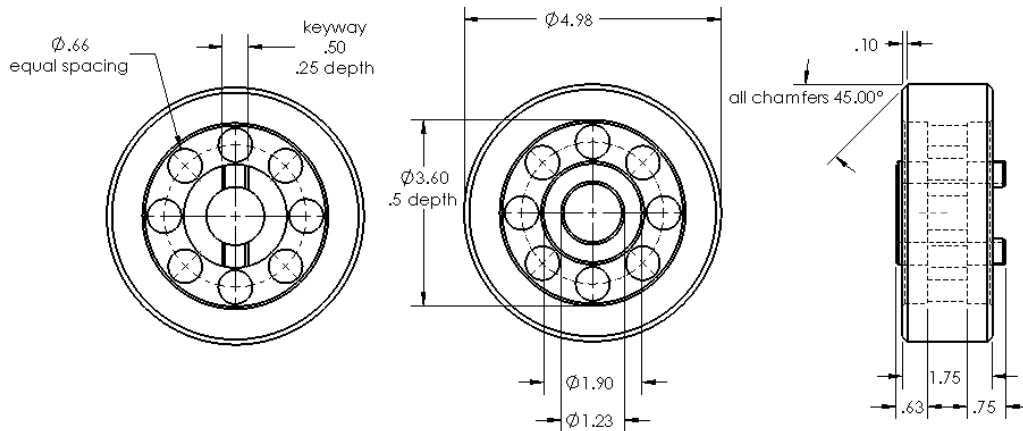
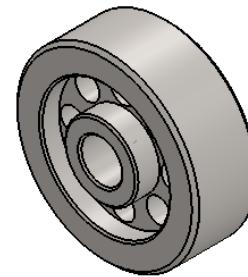
Slider – Crank Mechanism for Demonstration and Experimentation

Appendices

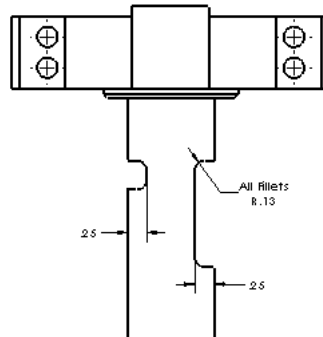
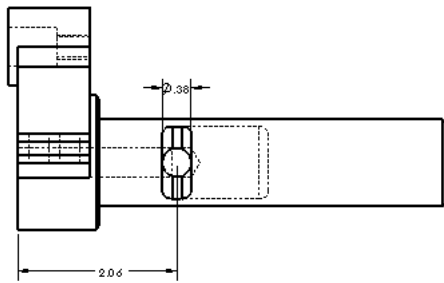
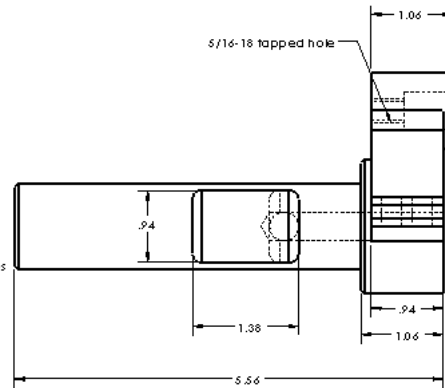
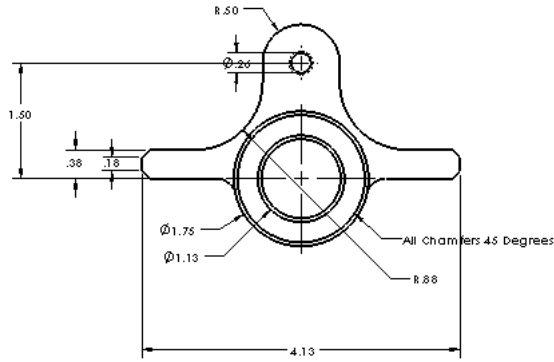
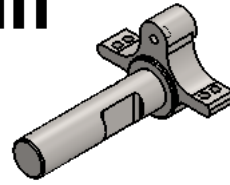
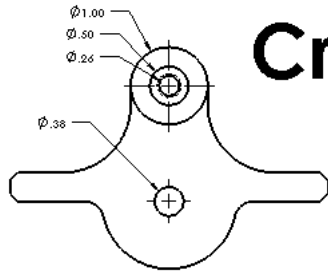
Drawings of Major Components:



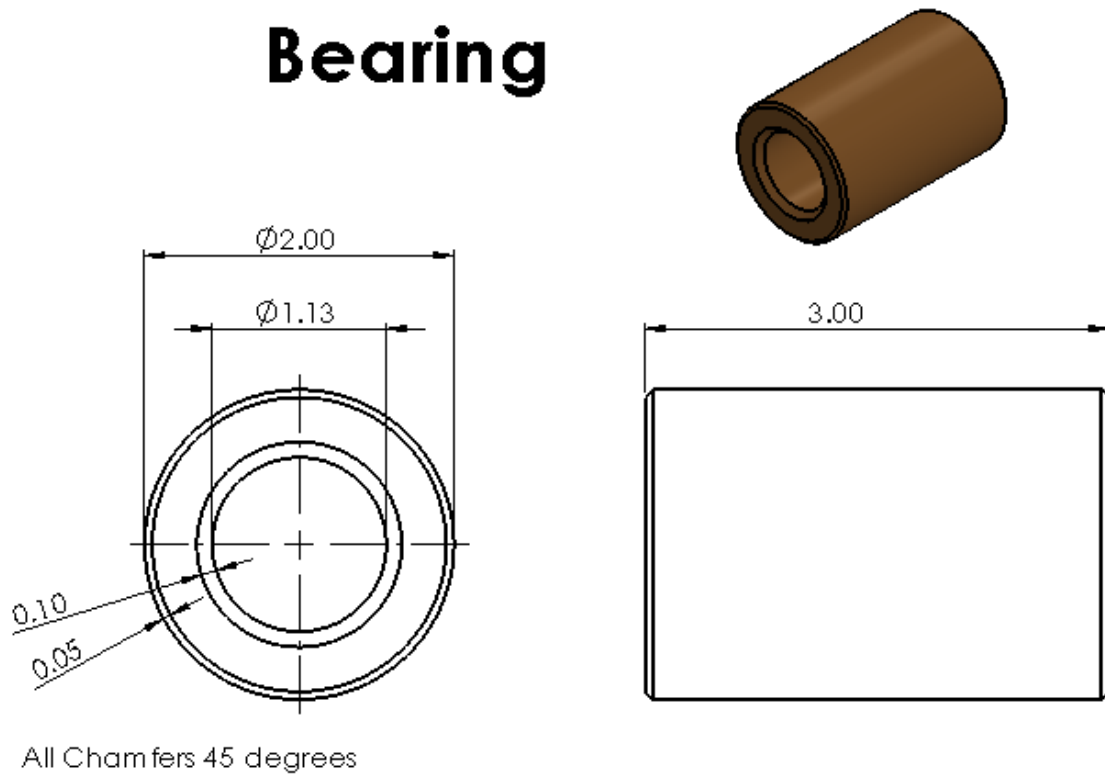
Flywheel



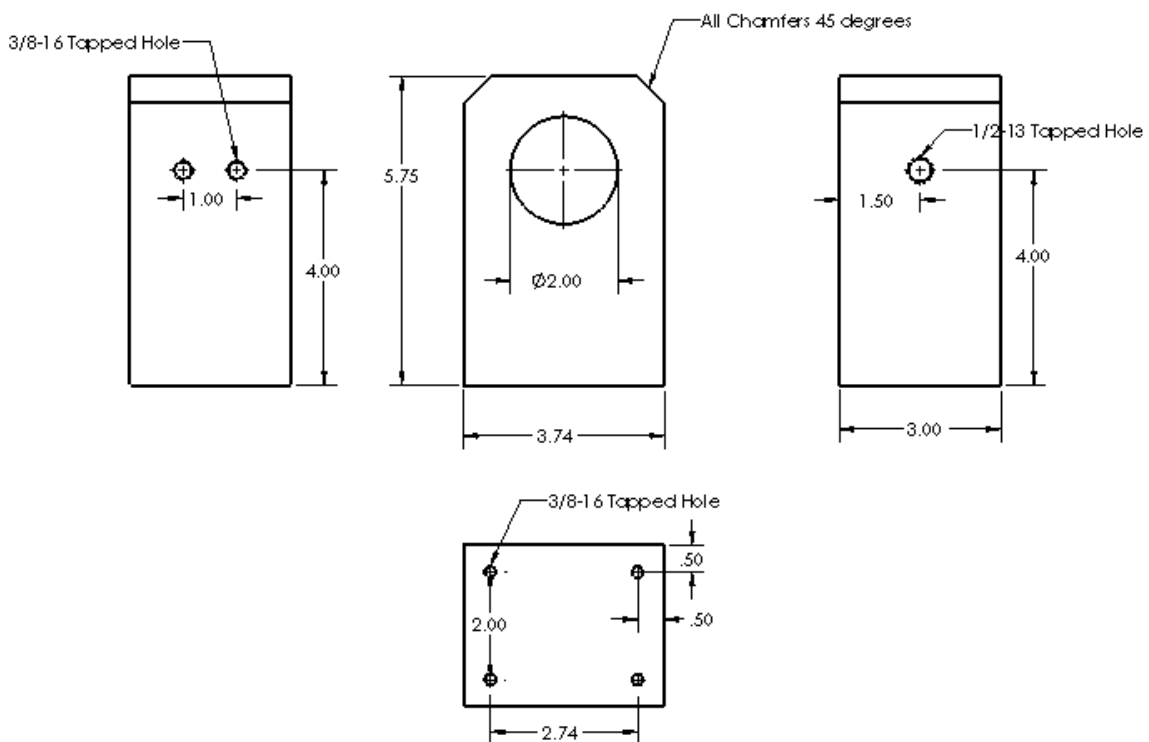
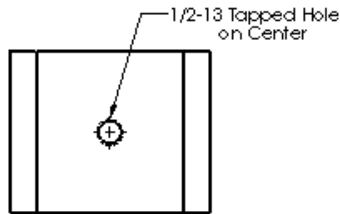
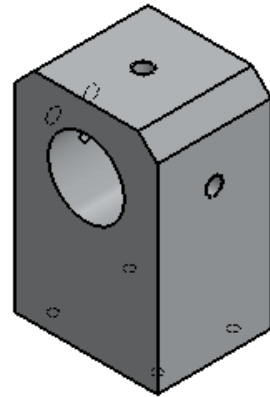
Crankshaft



Bearing

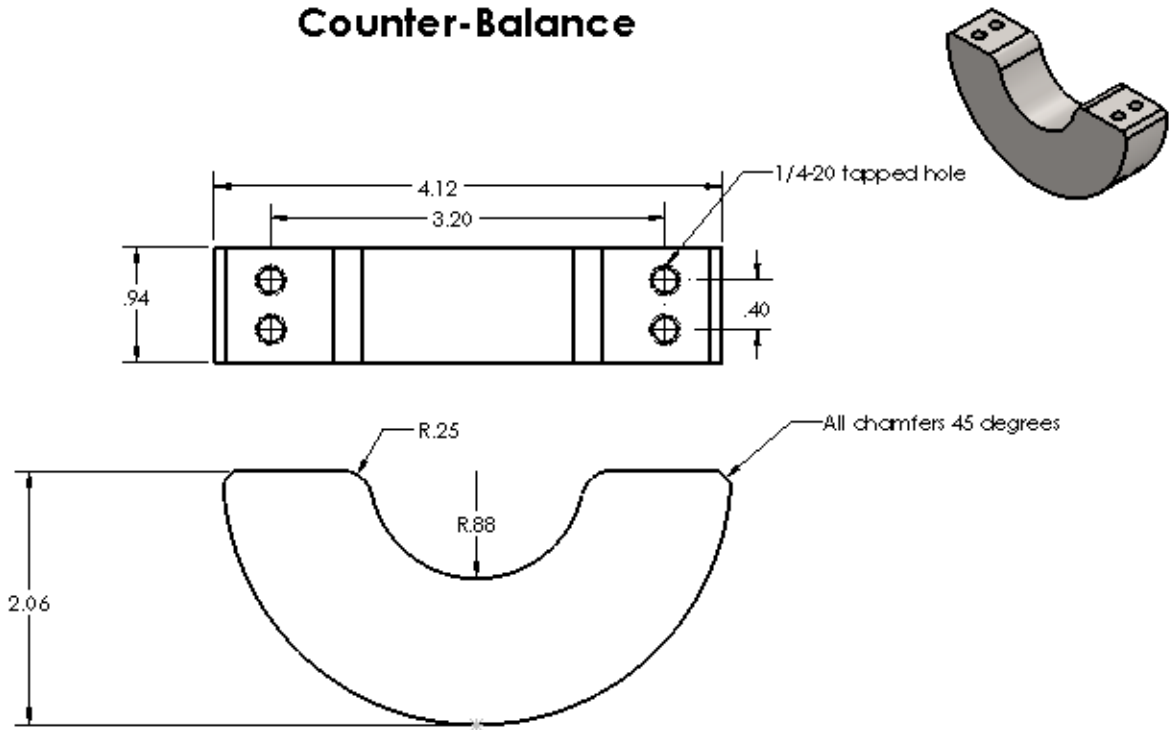


Crankshaft Support

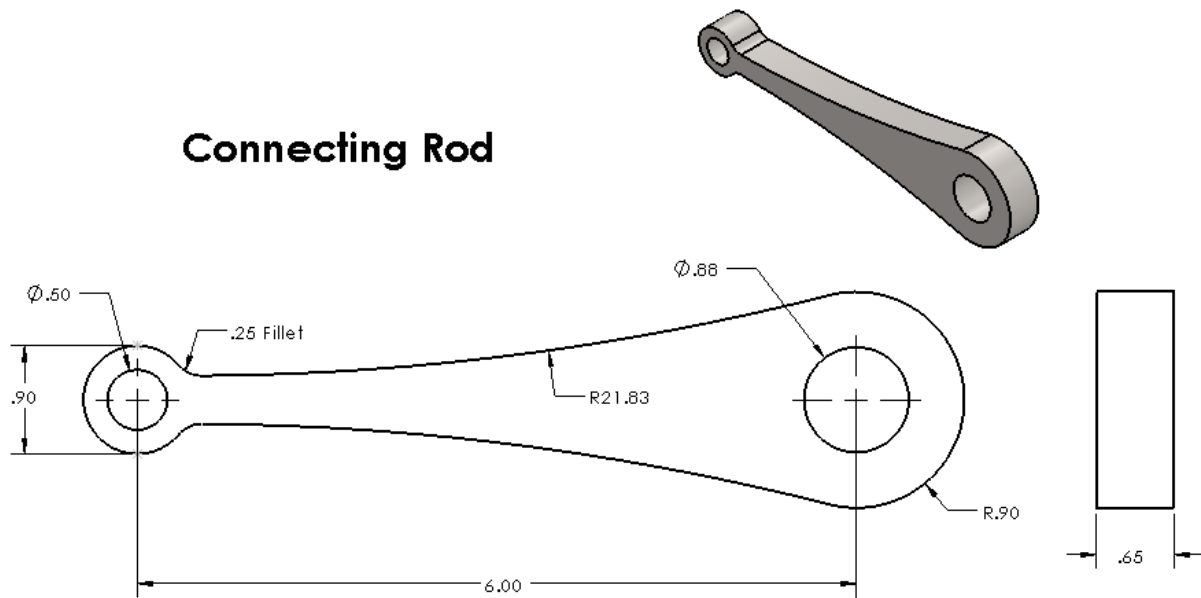


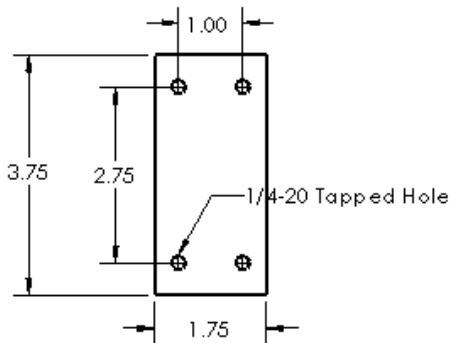
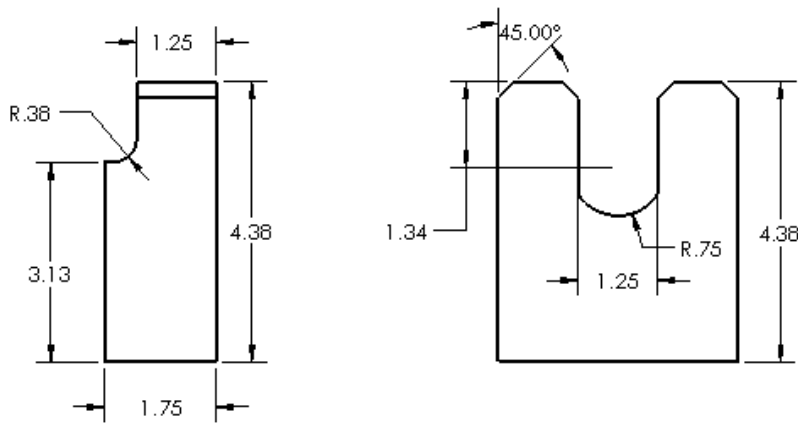
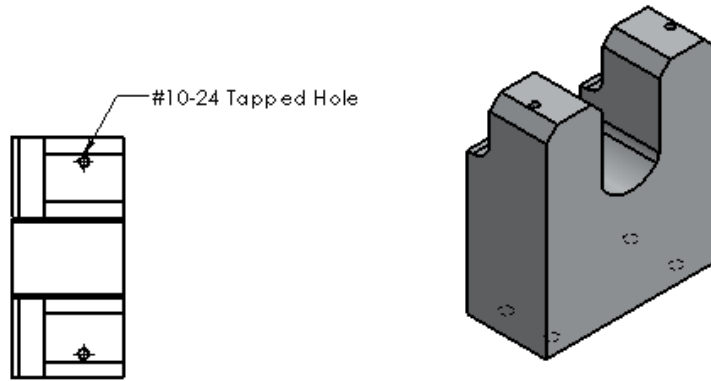
Slider – Crank Mechanism for Demonstration and Experimentation

Counter-Balance



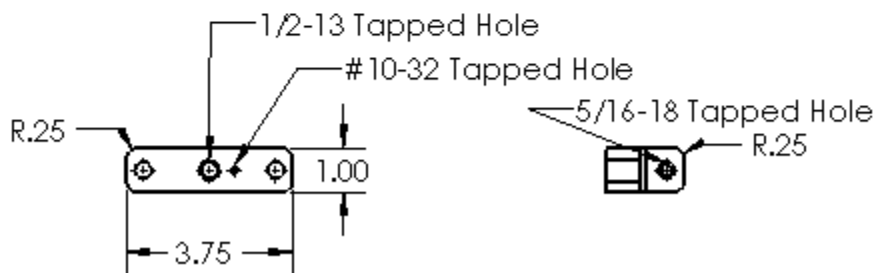
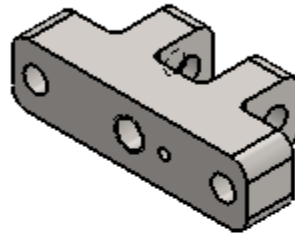
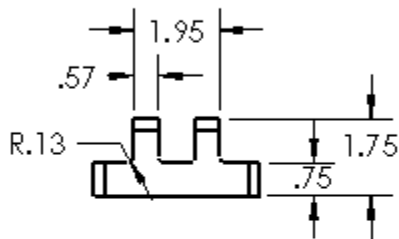
Connecting Rod



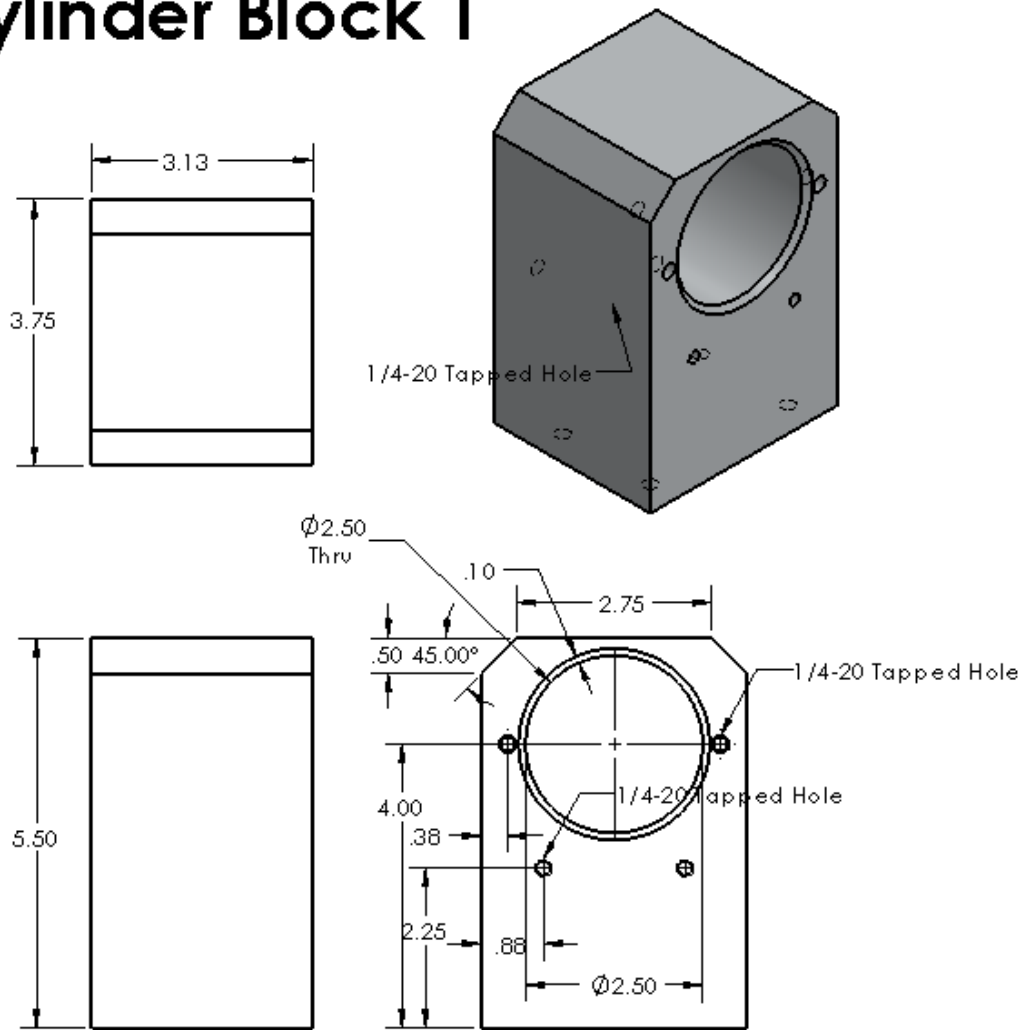


Guide Support

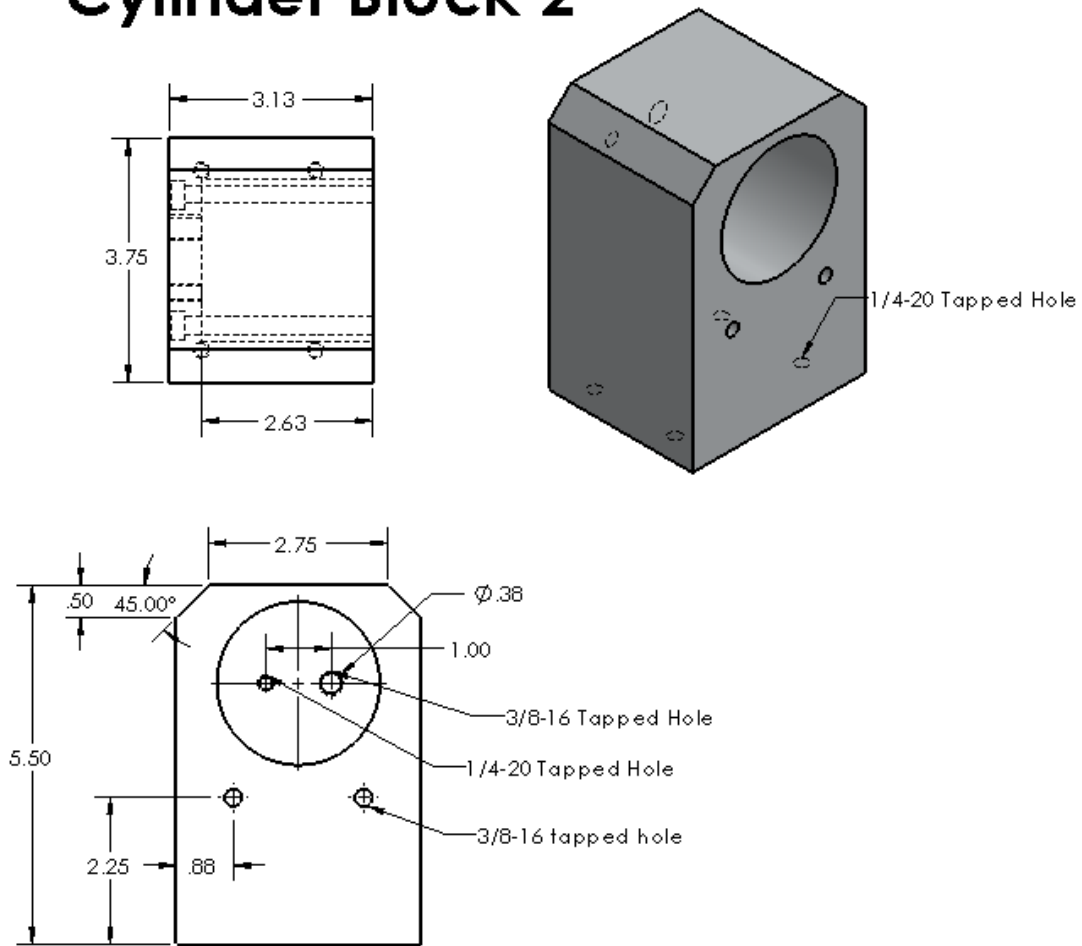
Guide



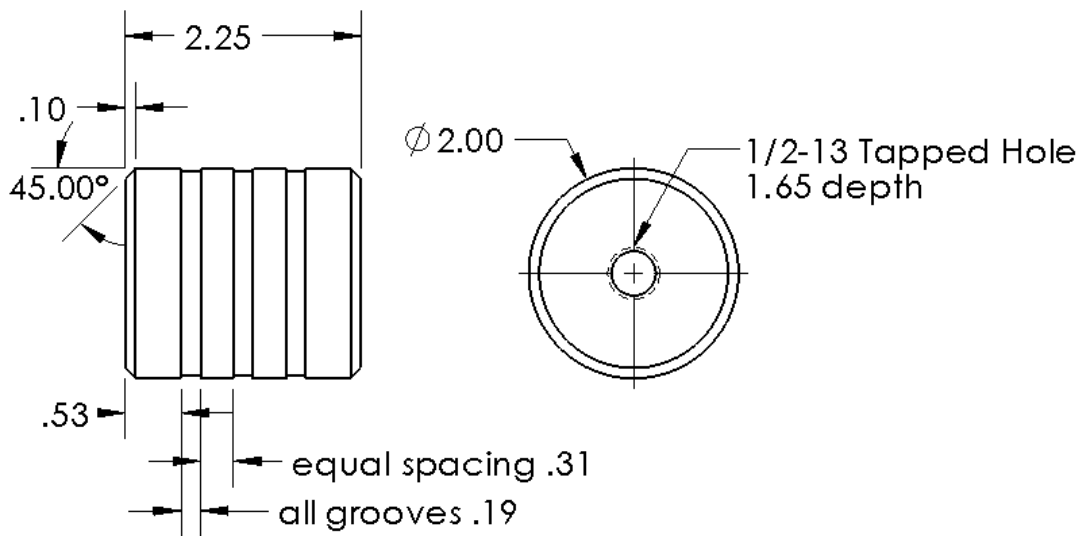
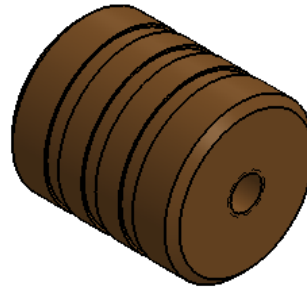
Cylinder Block 1



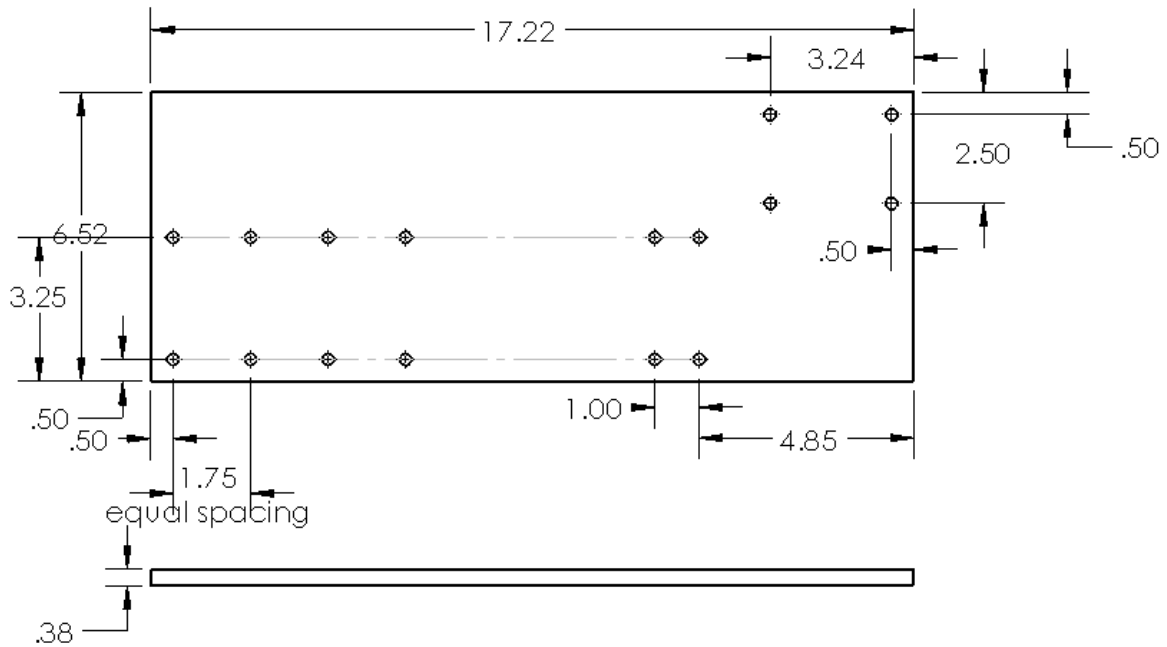
Cylinder Block 2



Piston

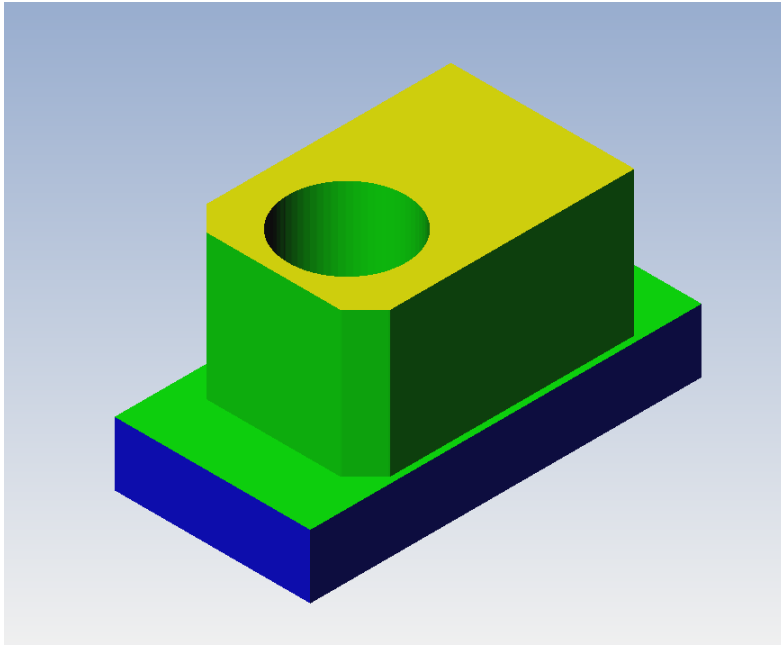


Base Plate

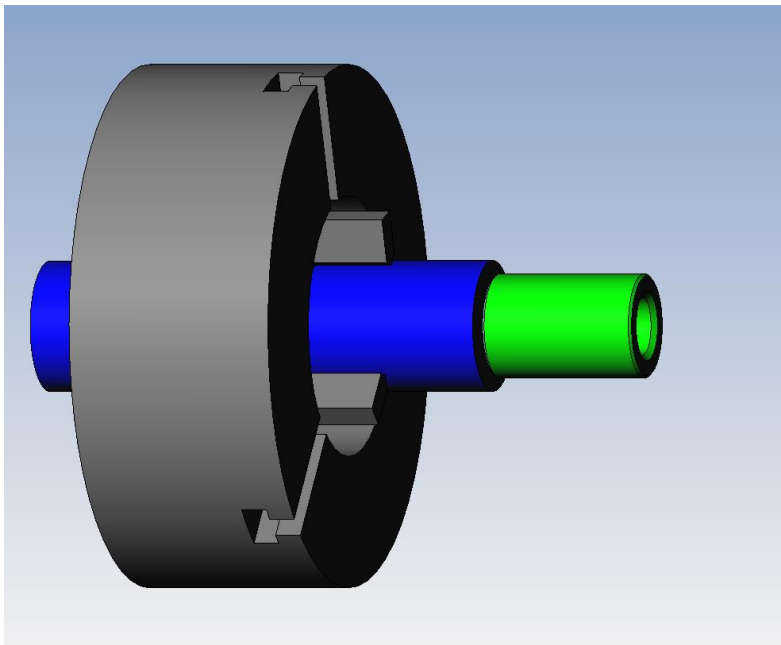


Slider – Crank Mechanism for Demonstration and Experimentation

CAM Simulation Cylinder Block Operation 1:

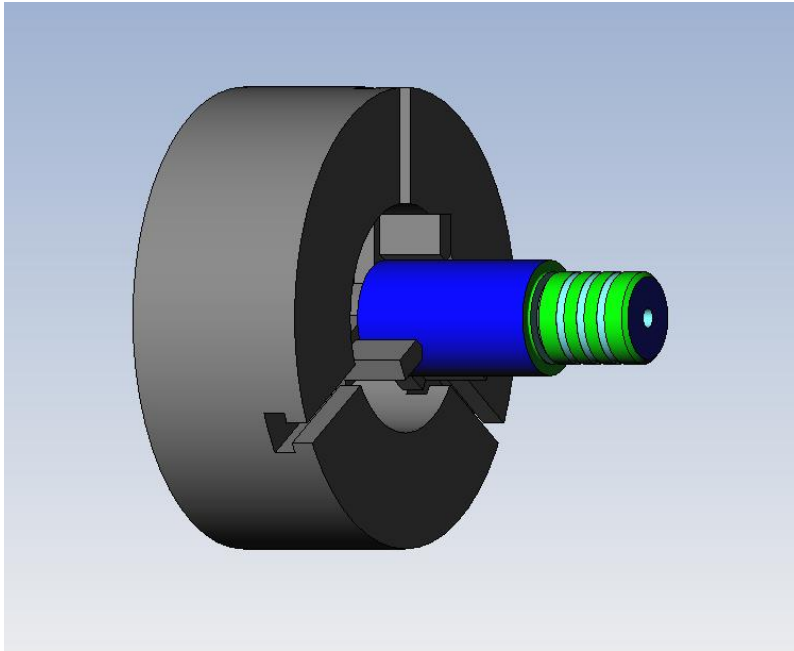


CAM Software Simulation Crankshaft Bearing:

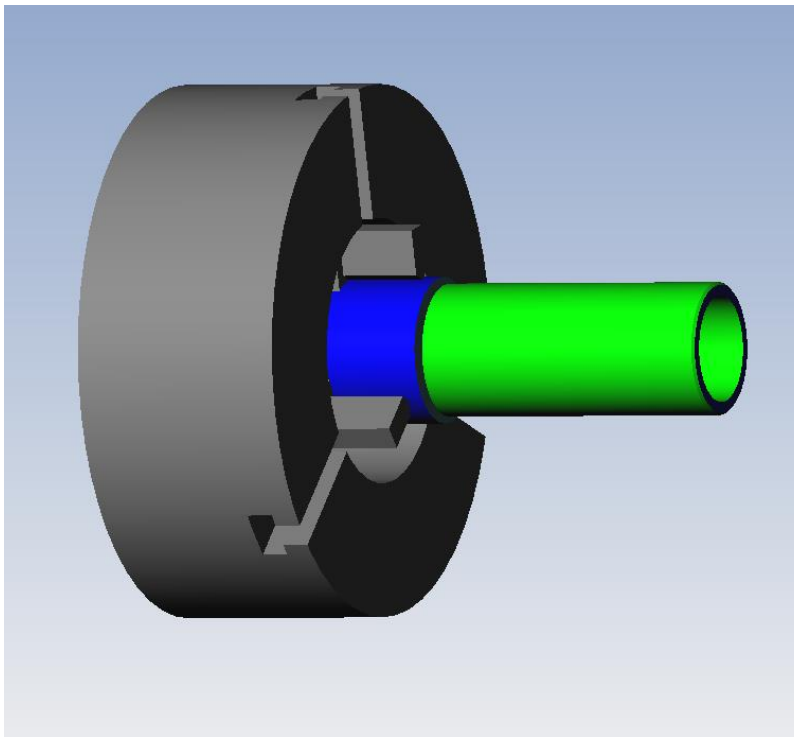


Slider – Crank Mechanism for Demonstration and Experimentation

CAM Software Simulation Piston Turning:

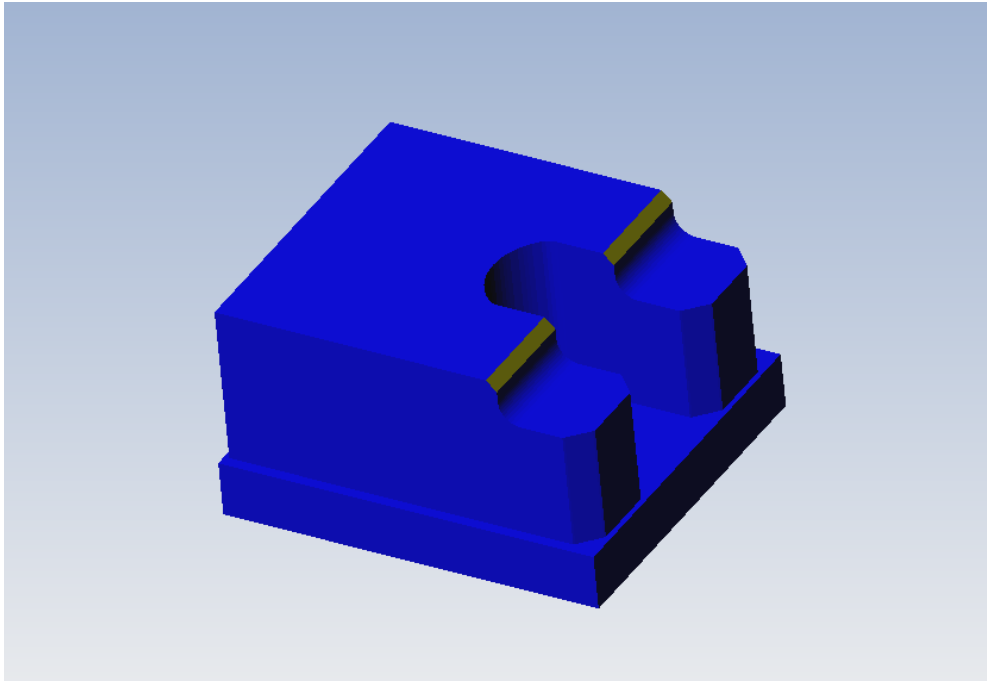


CAM Software Simulation Cylinder Sleeve:



Slider – Crank Mechanism for Demonstration and Experimentation

CAM Software Simulation Slider Stand:



CAM Software Simulation Cross-Head Operation 1:

